

POLITECNICO DI MILANO

Facoltà di Ingegneria dei Sistemi

Corso di Laurea in

Ingegneria Biomedica



Validation and tuning of a novel algorithm for the
analysis of galvanic skin conductance signals

Relatore: Prof. Luca MAINARDI

Co-relatore: Ing. Riccardo BARBIERI

Tesi di Laurea di:

Carlo CERIOTTI

765531

Anno Accademico 2012/2013

1 Sommario

Introduzione

Le variazioni nei segnali di skin conductance (SC) sono state proposte come misure di eccitazione neurofisiologica ed indicatori di attività del sistema nervoso simpatico (Wallin, 1981). Quando si verifica un burst sudomotorio (risultato della sommazione spaziale e temporale di spikes innescati da un nervo sudomotorio) ne consegue un processo di sudorazione causato dall'attività delle cellule sudoripare (per la maggior parte eccrine) e una risposta elettrodermica (skin conductance response o SCR) visibile nel segnale di SC. Un aumento della frequenza (o ampiezza) di tali SCR viene interpretato come un aumento del livello di attività del sistema nervoso simpatico (Lidberg, et al., 1981) poichè le cellule sudoripare eccrine sono controllate esclusivamente da tale sistema. Il segnale sudomotorio scatenante SCR è composto da bursts discreti, separati e temporalmente brevi ma le conseguenti SCR rilevate sulla cute spesso non sono più distinguibili per via di un problema di sovrapposizione, avendo una dinamica più lenta rispetto ai bursts. Esempi di algoritmi in letteratura che propongono una soluzione a tale problema sono, per citare i principali (Lim, et al., 1997), (Alexander, et al., 2005), (Benedek, et al., 2010) (with Ledalab software) nei quali comun denominatore è la tecnica deconvolutiva. Tale tecnica fa affidamento sull'esistenza di una risposta all'impulso stereotipata, attraverso cui è possibile stimare l'ampiezza e l'occorrenza dei bursts sudomotori generati dal nervo sudomotorio.

In questo elaborato di tesi descriviamo un metodo tuttora non pubblicato (Barbieri Citi o BC) sviluppato presso MIT di Boston capace di risolvere il problema di sovrapposizione di SCR senza affidarsi alla tecnica deconvolutiva quindi senza la necessità di conoscere la risposta all'impulso.

Dopo aver descritto come tarare adeguatamente l'algoritmo BC ottimizzando le sue prestazioni tramite segnali SC simulati, le sue prestazioni nell'identificare bursts sudomotori sono state confrontate con quelle di Ledalab. Infine BC è stato applicato a segnali SC reali per studiare gli effetti prodotti da differenti emozioni (rabbia, paura, gioia, tristezza) su 35 soggetti sani.

Materiali e metodi

Taratura di BC e confronto tra algoritmi - Metodo

Abbiamo generato 78 segnali realistici SC servendoci di un modello originale appositamente sviluppato per questa tesi: esso convolve una sequenza di spikes (impulsi) con una funzione risposta all'impulso (IRF) (Equazione 1- (Lim, et al., 1997)). Gli spikes simulano l'occorrenza e l'ampiezza dei bursts sudomotori e la IRF descrive la risposta elettrotermica (SCR) rilevabile nel segnale SC a seguito di un burst sudomotorio. Precisamente, data una documentata variabilità inter ed intrasoggettiva della risposta all'impulso

(Breault, et al., 1993), (Edelberg, et al., 1981), (Janes, et al., 1985), ogni spike è stato convoluto, per la sola creazione della componente fasica del segnale, utilizzando l'equazione proposta da Lim variando di volta in volta i parametri che la governano secondo una distribuzione Gaussiana. La Figura 1-1 mostra un esempio di 100 risposte all'impulso.

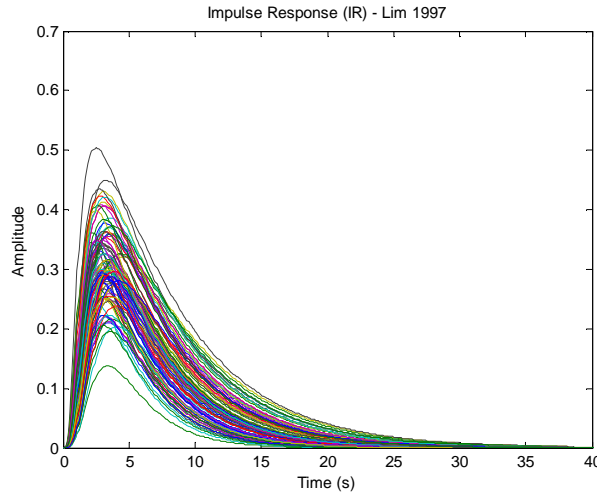


Figura 1-1: Esempio di 100 risposte all'impulso

La componente tonica e fasica sono generate separatamente entrambe con tecniche di convoluzione, utilizzando per la parte tonica l'equazione proposta da Lim ma con parametri fissi. L'occorrenza temporale degli spikes e la loro ampiezza nelle sequenze sono state rispettivamente generate secondo una curva Gaussiana Inversa (dimostratasi empiricamente come la miglior approssimazione) e una distribuzione Gaussiana. Al fine di rendere i segnali più realistici abbiamo aggiunto un rumore (flicker noise) la cui natura del rumore è stata determinata empiricamente da segnali SC reali.

Abbiamo generato diversi 4 dataset composti da 78 segnali simulati, ognuno con un rapporto S/N di 10^6 , 10^5 , 10^4 , 10^3 .

$$f_{s1} = \frac{g_1^{-((t-T_{os1})/t_d)}}{\{1 + [(t - T_{os1})/t_r]^{-2}\}^2}$$

Equazione 1: Risposta all'impulso (Lim)

Analizzando i segnali simulati con Ledalab e BC abbiamo ottenuto le sequenze di spikes che successivamente abbiamo confrontato con gli spikes usati per la generazione degli stessi segnali simulati. In questo processo possiamo distinguere i tre casi mostrati in Figura 1-2 da cui abbiamo ottenuto la sensibilità (SE) e il valore predittivo positivo (VPP) per la costruzione delle curve ROC per ogni rapporto S/N. Le curve ROC quantificano le prestazioni di detezione degli spikes di entrambi i softwares, dove però

ogni coppia SE-VPP è stata ottenuta variando diversi parametri: per Ledalab variando la minima soglia di ampiezza ammessa per gli spikes forniti mentre per BC variando i due parametri interni all'algoritmo che determinano le frequenze di Cut-off dei filtri (S_w e B_w). Avendo così un quadro completo delle prestazioni al variare dei parametri per i due software, possiamo tarare BC scegliendo la coppia S_w e B_w . In Figura 1-3 due esempi di curve ROC per il dataset di con rapporto S/N di 10^5 .

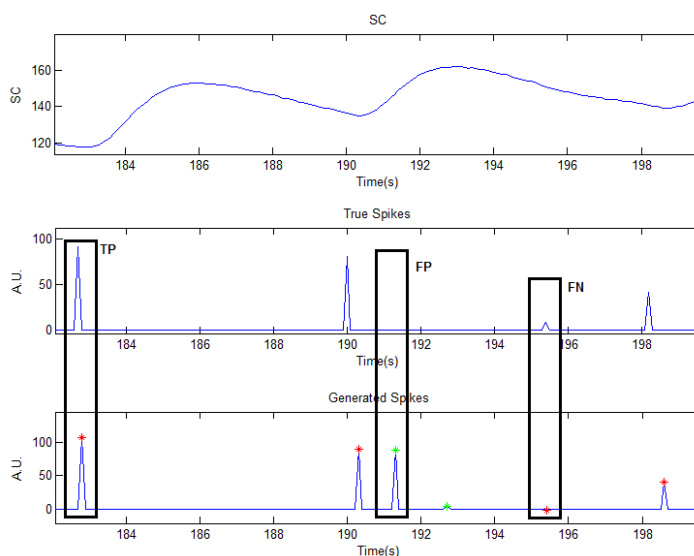


Figura 1-2: Veri positive (FP), Falsi negativi (FN) e Falsi Positivi (TP)

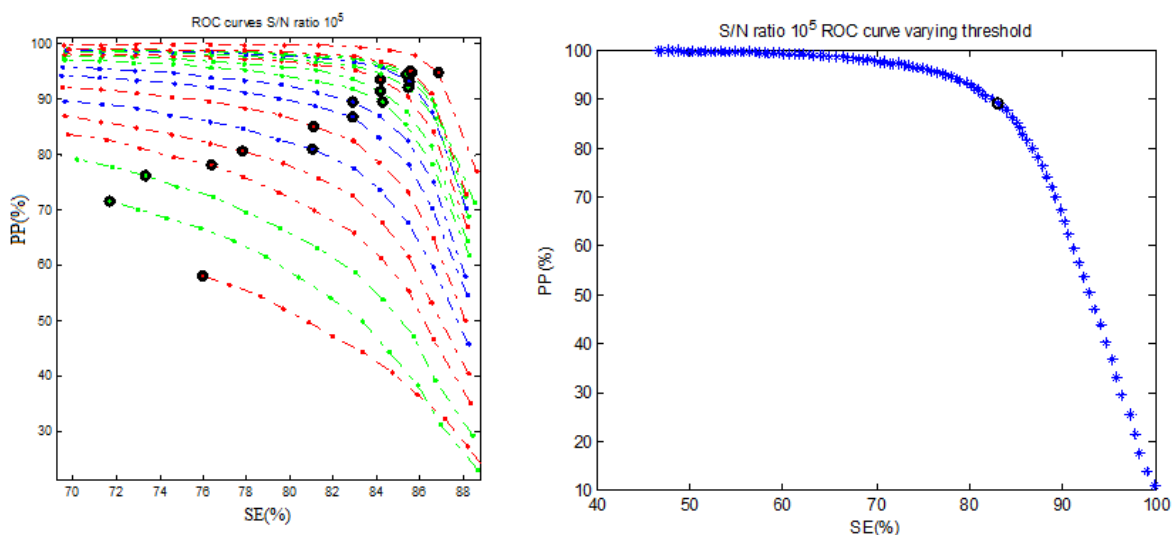


Figura 1-3: (Sinistra) Curve ROC di BC per livello S/N di 10^5 ottenute variando S_w e B_w

(Destra) Curve ROC per Ledalab con livello S/N di 10^5 variando la soglia di ampiezza degli spikes

I cerchi neri indicano i punti di massima performance per ogni ROC

Dataset Emozioni - Metodo

I segnali SC sono stati acquisiti con Flexcomp Infinity™ encoder (Thought Technology Ltd.; Montreal, Canada). I segnali, dapprima acquisiti con una frequenza di campionamento di 2048 Hz sono stati poi sottocampionati a 256 Hz. L'acquisizione della SC è avvenuta posizionando due elettrodi su indice e anulare con metodo esosomatico (exosomatic).

Ai soggetti non è permesso assumere sostanze stimolanti (caffè, the o altro) il giorno dell'acquisizione così come il giorno precedente per non alterare il sistema simpatico. 35 soggetti sani sono stati volontariamente reclutati dal corpo studentesco dell'università IULM (Milano). Presso il Behaviour and Brain Lab i soggetti vengono intervistati da uno psicologo al quale sono stati invitati a raccontare con ricchezza di particolari due recenti episodi relativi ad ognuna delle 4 emozioni target (Gioia, Paura, Rabbia, Tristezza). I soggetti non in grado di rievocare tutti gli episodi sono stati scartati dall'esperimento. Lo psicologo, dopo aver annotato con dovizia di particolari gli episodi, ha scelto un solo episodio per ogni emozione, giudicato più intenso, ricco di stimoli e vivido nella memoria del soggetto. E' quindi fissato un secondo appuntamento dove il soggetto, firmata la liberatoria, viene fatto sedere, posizionati i sensori e l'acquisizione ha inizio.

Dopo una fase di relax (*baseline*) della durata di 3 minuti nel quale viene invitato il rilassamento fisico e mentale, lo psicologo, privatamente con il soggetto, rievoca verbalmente un episodio descritto durante l'intervista; in questa fase il soggetto deve ascoltare attentamente e cercare di rivivere più intensamente possibile l'emozione (fase di *Listening*). La durata delle fasi di *Listening* è dipendente dal particolare episodio evocato. Al termine il soggetto, in silenzio, deve continuare a focalizzarsi cercando il massimo coinvolgimento per la durata continuativa di 3 minuti (fase di *Focusing*). Successivamente è prevista una fase di *recovery* prima di reiniziare con la seguente emozione. La sequenza delle emozioni rievocate è casuale per ogni soggetto permettendo così di non introdurre polarizzazioni nei risultati. La sessione di acquisizione dura dai 30 ai 50 minuti.

Dalle sequenze di spikes ottenute con l'algoritmo BC (opportunamente tarato) abbiamo calcolato l'ampiezza media degli spikes, la frequenza media degli spikes (Hz) e l'area sottesa (AS) dalla curva di attività integrata (CAI) (indice continuo che condensa l'informazione di frequenza e ampiezza degli spikes) ottenuta sommando l'ampiezza degli spikes compresi in una finestra della lunghezza di 2 secondi che slitta, secondo dopo secondo sull'intera sequenza di spikes. Tali parametri sono stati calcolati per l'ultimo minuto della fase di *Listening* (*List*), per ognuno dei 3 minuti che compongono la fase di *Focusing* (*Foc1*, *Foc2*, *Foc3* riepisttivamente) e per il minuto centrale della fase di *Baseline* (*Bl*).

Per evidenziare possibili differenze statistiche esistenti un ANOVA a una via è stato eseguito considerando tutte le fasi per ogni parametro e successivamente dei t-tests: tra *Bl* e le successive *List*, *Foc1*, *Foc2*, *Foc3* per ogni emozione, tra *List*, *Foc1*, *Foc2*, *Foc3* e ognuno con se stesso in ogni emozione. Avendo effettuato t-test multipli, il livello di significatività è stato corretto con la correzione di Bonferroni, passando da 0.05 a α_{Bonf} stimato secondo la formula $0.05/n$ dove n è il numero di confronti che abbiamo effettuato, nel nostro caso 40, ottenendo un α_{Bonf} di 0.0013.

Risultati

Taratura di BC e Confronto

L'algoritmo BC offre le sue massime performance eliminando, per ognuno dei 4 rapporti S/N, il filtro governato dal parametro B_w mentre S_w è 0.1, 0.2, 0.5, 0.9 rispettivamente per rapporti S/N di 10^6 , 10^5 , 10^4 , 10^3 . Per Ledalab invece le soglie ottimali per le massime performances sono 3.60 uS, 6.20 uS, 11 uS, 12.80 uS rispettivamente per rapporti S/N di 10^6 , 10^5 , 10^4 , 10^3 .

In definitiva, l'algoritmo BC offre migliori performances (con la sola eccezione del rapporto S/N di 10^6) rispetto al metodo CDA di Ledalab come mostrato in Figura 1-4.

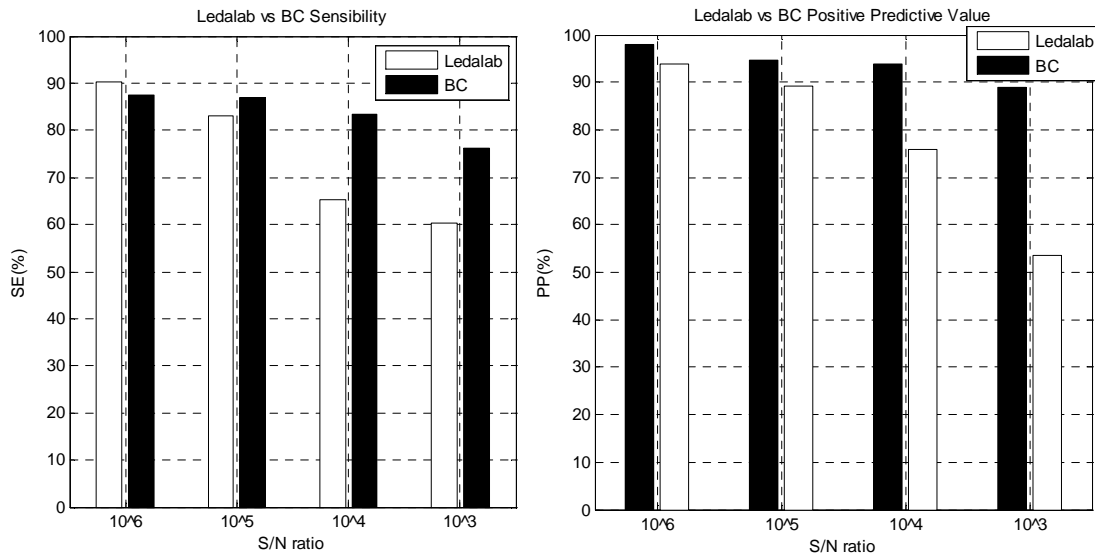


Figura 1-4: Ledalab and BC comparison

DataSet Emozioni - Risultati

ANOVA	P-Value	F (16,34)
M.S.Ampl.	9,442E-11 ^(*)	5,3916
AUC	2,22E-16 ^(*)	7,568
M. Spike Freq	2,22E-16 ^(*)	7,593

$\alpha_{Anova}=0.05$ ^(*)

Tabella 1: Risultati di ANOVA a una via

T-Test	Bas_HappList	Bas_HappFoc1	Bas_HappFoc2	Bas_HappFoc3	Bas_FearList	Bas_FearFoc1	Bas_FearFoc2	Bas_FearFoc3
M.S.Ampl.	1,57*10 ⁻⁸ ^(*)	0,0010 ^(*)	0,0317	0,0036	1,9647*10 ⁻⁷ ^(*)	2,84*10 ⁻⁵ ^(*)	6,12*10 ⁻⁵ ^(*)	0,0019
AUC	1,12*10 ⁻⁷ ^(*)	5.3*10 ⁻⁴ ^(*)	0,0229	0,0044	9,2335*10 ⁻⁸ ^(*)	2,4*10 ⁻⁴ ^(*)	5,6*10 ⁻⁴ ^(*)	8,2*10 ⁻⁴ ^(*)
M Spike Freq	1,42*10 ⁻⁸ ^(*)	0,1020	0,2724	0,1329	2,5032*10 ⁻⁷ ^(*)	9,9*10 ⁻⁴ ^(*)	0,0120	0,0211

T-Test	Bas_RageList	Bas_RageFoc1	Bas_RageFoc2	Bas_RageFoc3	Bas_SadList	Bas_SadFoc1	Bas_SadFoc2	Bas_SadFoc3
M.S.Ampl.	2,34*10 ⁻⁹ ^(*)	8,87*10 ⁻⁶ ^(*)	0,0011 ^(*)	4,6*10 ⁻⁴ ^(*)	2,9387*10 ⁻⁸ ^(*)	0,0164	0,0249	0,0445
AUC	1,38*10 ⁻⁸ ^(*)	2,03*10 ⁻⁶ ^(*)	1,1*10 ⁻⁴ ^(*)	5,97*10 ⁻⁵ ^(*)	5,7321*10 ⁻⁹ ^(*)	0,0118	0,028	0,0875
M Spike Freq	1,47*10 ⁻⁸ ^(*)	9,6*10 ⁻⁴ ^(*)	1,6*10 ⁻⁴ ^(*)	5,6*10 ⁻⁴ ^(*)	8,3476*10 ⁻⁸ ^(*)	0,2111	0,1188	0,1391

$\alpha_{Bonf}=0.0013$ ^(*)

Tabella 2: Risultati T-Test tra *Bl* e le rimanenti fasi

La Tabella 1 riporta i risultati del test ANOVA a una via dove abbiamo evidenziato le significatività. La Tabella 2 riporta invece i risultati dei t-test tra *Bl* e le rimanenti fasi. Possiamo evidenziare differenze significative tra le fasi di *Baseline* e *Listening* per tutte le emozioni, dimostrando così che lo psicologo ha operato efficacemente riuscendo a coinvolgere emotivamente i soggetti.

La Paura e la Rabbia, ma anche solo parzialmente la Gioia, sono emozioni in grado di attivare il soggetto per un tempo più lungo a differenza della Tristezza dove le 3 fasi di *focusing* non sono significative. Rabbia, Paura, Gioia e Tristezza sono elencate in quest'ordine da quella più attivante alla meno attivante in termini temporali. Probabilmente la ragione di questo risultato coinvolge innati istinti di sopravvivenza poiché Paura e Rabbia, al contrario di Tristezza e Gioia, sono emozioni idonee a favorire l'adattamento del soggetto in un ambiente ostile ed infatti il semplice pensiero (*Focusing*) di queste emozioni innalza il livello di allerta del soggetto facilitando meccanismi di "Flight or Fight" strettamente connessi alla sopravvivenza. Diversamente da Rabbia e Paura, la Tristezza tende ad essere meno coinvolgente e persistente nel soggetto, forse un meccanismo inconscio con lo scopo di allontanare nel soggetto

sensazioni dolorose. La Gioia è più attivante della Tristezza, forse per favorire la socializzazione tra individui diversi. Non ci sono differenze significative tra fasi di *Listening* e *Focusing* confrontate con loro stesse (risultati non mostrati).

2 Abstract

Introduction

Changes in skin conductance signals (SC) were proposed as neurophysiologic arousal measures and as indexes of sympathetic nervous system activity (Wallin, 1981). When

When an outgoing sympathetic nervous burst occurs, resulting from temporal and spatial summation of spikes triggered by sudomotor nerve, a skin conductance responses (SCR) follow: an increase of the frequency or amplitudes in SC signal is interpreted as an increase of sympathetic nervous system activity level (Lidberg, et al., 1981). The underlying sudomotor signal triggering SCRs is composed by separate, discrete and temporally short bursts whereas the resulting SCRs recorded on skin surface often are not anymore individually distinguishable due to overlapping problem. Examples of algorithms solving overlapping problem can be found, to cite main papers, by (Lim, et al., 1997), (Alexander, et al., 2005), (Benedek, et al., 2010) (with Ledalab software) in which deconvolution technique is a common tool. Deconvolution relies on the precondition that there exists a stereotyped and stable impulse response function (IRF) thanks to they can estimate underlying bursts in sudomotor signal.

In the present thesis work we described a novel method (BC) still unpublished developed at MIT (Boston) able to solve overlapping SCRs estimating sudomotor bursts not relying on deconvolution techniques so without any IRF knowledge. After properly tuned up BC algorithm, its performances in identifying sudomotor burst were compared to Ledalab performances. In conclusion BC was applied to real SC signals in order to study the effects of 4 different emotions (Rage, Fear, Happiness, Sadness) on 35 healthy young subjects.

Materials and Methods

BC Tuning and algorithm comparison – Method

We generated 78 realistic SC signals through an original model ad hoc for this thesis: this model convolves spike sequences (simulating sudomotor bursts sequences) with an IRF (Equation 1– from (Lim, et al., 1997)). More precisely, because of a well known inter and intra subjective variability of IRF (Breault, et al., 1993), (Edelberg, et al., 1981), (Janes, et al., 1985), each spike was convolved, for phasic signal component creation, using Lim equation (Equation 1) but varying from time to time the governing parameters. Figure 2-1 depicts a group of 100 IRFs.

The tonic (slow varying) and phasic (fast varying) part of SC signals were generated separately both with convolution techniques.

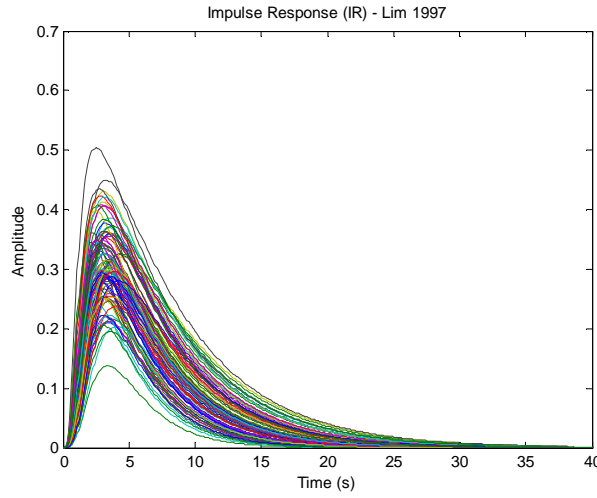


Figure 2-1: Group of 100 IRF

The temporal spike occurrences and amplitudes in the sequences were respectively generated according to an Inverse Gaussian Distribution (empirically proved to be the best approximation) and a Gaussian Distribution. In order to make the signals more realistic we added noise (flicker noise). This noise type was determined empirically from the mean spectra from 10 real SC signals. We generated 4 datasets each composed by 78 simulated signals, each one with S/N ratio level of 10^6 , 10^5 , 10^4 , 10^3 .

$$f_{s1} = \frac{g_1^{-((t-T_{os1})/t_d)}}{\{1 + [(t - T_{os1})/t_r]^{-2}\}^2}$$

Equation 1: IRF proposed by Lim

By analyzing the simulated signals with Ledalab and BC we obtained the spike sequences which at a later stage we compared to the spike sequences used to generate selfsame SC signals. In this process we can distinguish three cases depicted in Figure 2-2. Thanks to them we determined Sensibility (SE) and Positive Predictive Value (PP) used to generate ROC curves for each S/N ratio level considered. The ROC curves quantify spike detection performances of both Ledalab and BC algorithms in which coordinates SE-PP was obtained by changing different parameters in the algorithms: by varying the minimum spike amplitude threshold to output spike sequences for Ledalab whereas varying internal algorithm parameters (S_w e B_w) which determine filters cut-off frequencies for BC.

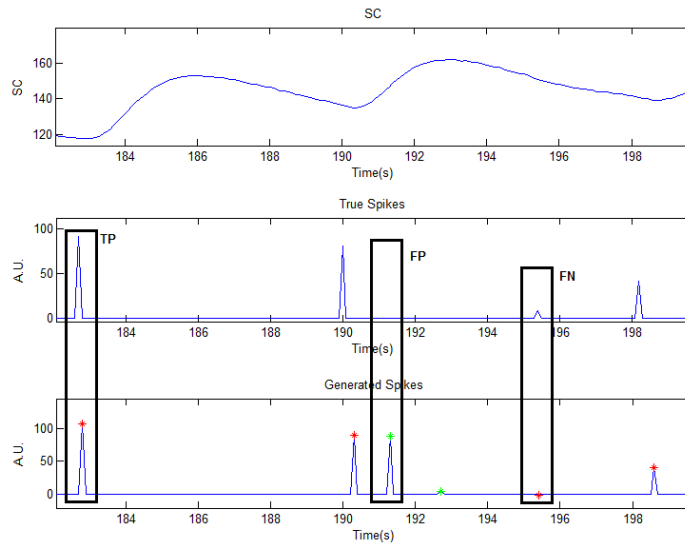


Figure 2-2: True Positive (FP), False Negative (FN) and False Positive (FP)

Figure 2-3 depicts BC ROC curves (more than 1 because by varying 2 parameters) and Ledalab ROC curve for the 78 simulated signals from dataset with S/N ratio level 10^5 .

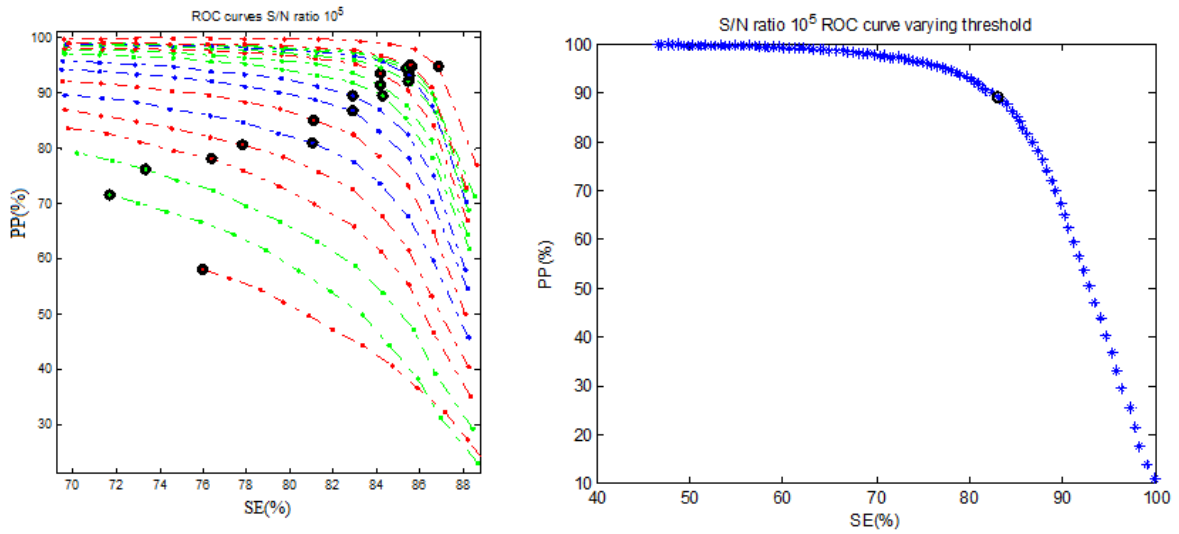


Figure 2-3: (Left) ROC curves from BC for S/N ratio level of 10^5 obtained by varying S_w and B_w (Right) ROC curves from Ledalab for S/N ratio level of 10^5 varying minimum spike amplitude threshold.

Black circles indicate best performances for each ROC

Emotion dataset - Method

SC signals were recorded continuously using Flexcomp Infinity™ encoder (Thought Technology Ltd.; Montreal, Canada) with a sampling rate of 2048 Hz, while subjects sitting; then it was resampled at 256 Hz. SC was recorded using two electrodes placed on different fingers of a hand (forefinger and ringfinger) using the exosomatic method.

It was not allowed for the subjects to drink coffee, tea or other stimulating substances on the recording day as well as the day before in order not to alter the sympathetic system. 35 normal healthy subjects were voluntarily recruited from the student body of IULM University of Milan. Students were scheduled to come at the Behavior and Brain Lab for an interview where they had to let the researcher know whether they could recall two recent episodes where they felt each of the 4 target emotions: joy, sadness, rage and fear. If positive, the researchers asked them to recall verbally while a psychologist took notes about all the episodes. After the psychologist chose the most vivid and intense episodes between the two, they were scheduled for a second appointment to participate to the recording session. All the people who could not recall a vivid recent episode for each of the four emotions were asked not to participate in the research. Once subjects came at the lab for the experiment, they were asked to fill in a consent form, and sit down. Then a researcher located all the sensors, and the recording started. After a *baseline* (relax) period of 3 minutes, the psychologist privately with the subject helped him to recall the episode he/she described in the interview while he/she is supposed to listen and focus on the emotion (*listening phase*). The duration of each of those is variable depending on the episode evoked. Once subject felt the emotion, the researcher asked to stay silent and try to focus intensely on the emotion without moving for 3 minutes (*focusing phase*). After the emotion recall, a rest of 3 minutes (*recovery time*) was provided before re-starting with the next emotion. The sequence of emotion recalled was randomly assigned for each subject in order not to bias the results. The recording sessions lasted approximately from 30 to 50 minutes. On the obtained spikes sequences we calculated mean spike amplitude, mean spike frequency (Number of spikes / s = Hz) and area under “Integrated Activity Curve (IAC)” curve (AUC) (continuous index comprising frequency and amplitude information of spikes) obtained by sliding a 2 seconds window second by second over the spike sequence summing spike amplitudes within it.

The 3 parameters were obtained for *listening phases* last minute (*List*), for each of the 3 minutes composing the *focusing phases* (*Foc1*, *Foc2* and *Foc3* respectively) and the central minute of *baseline* (*Bl*). To investigate whether existed statistical differences t-tests were performed between *Bl* and successive *List*, *Foc1*, *Foc2*, *Foc3* of each emotion as well as for *List*, *Foc1*, *Foc2*, *Foc3* and each one with itself for the four emotions. Because of multiple comparisons are performed, the significance level was corrected with

Bonferroni correction, passing from 0.05 to α_{Bonf} calculated according to $0.05/n$ where in our case parameter n is the number of all considered comparisons, precisely 40. α_{Bonf} is 0.0013 which will be considered as new significant level.

Results

BC Tuning and Comparison

We found that maximized performances is obtained eliminating, for all S/N levels, the filter governed by B_w whereas S_w should be 0.1 , 0.2 , 0.5 or 0.9 respectively for S/N levels of 10^6 , 10^5 , 10^4 , 10^3 . Ledalab minimum threshold to be applied to output spike sequences is 3.60 uS, 6.20 uS, 11 uS, 12.80 uS respectively for S/N levels of 10^6 , 10^5 , 10^4 , 10^3 .

The BC algorithm shows better performances (only exception SE for S/N level 10^6) compared to CDA method by Ledalab as depicted in Figure 2-4 where best sensibility and positive predictive values are shown varying S/N level.

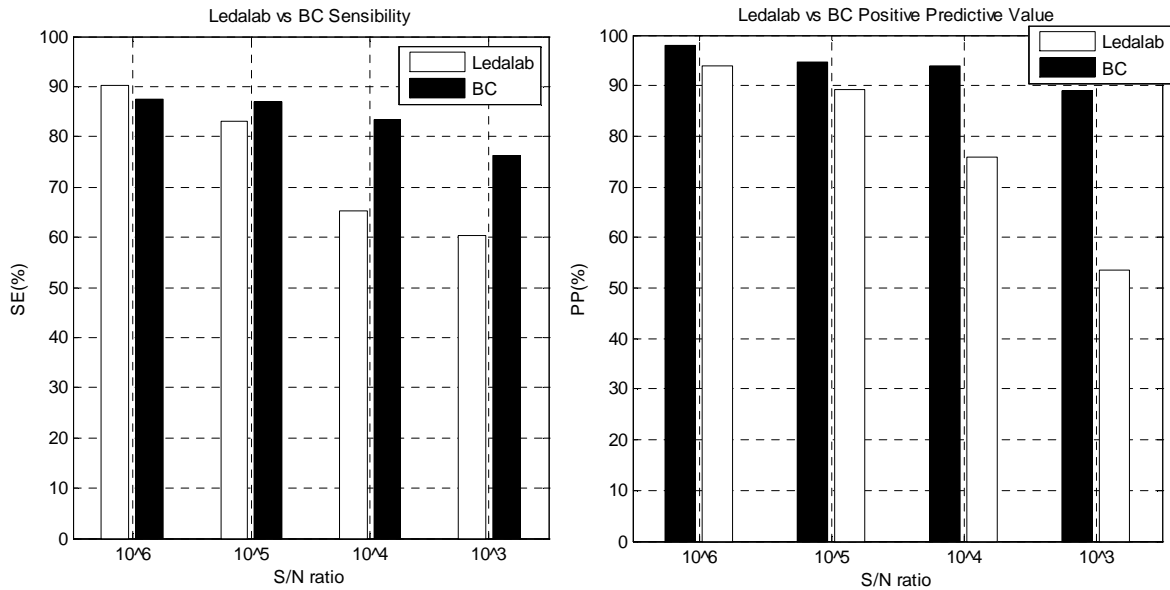


Figure 2-4: Ledalab and BC comparison

Emotion dataset - Results

ANOVA	P-Value	F (16,34)
M.S.Ampl.	9,442E-11 ^(*)	5,3916
AUC	2,22E-16 ^(*)	7,568
M. Spike Freq	2,22E-16 ^(*)	7,593

$$\alpha_{Anova}=0.05^{(*)}$$

Table 2-1: ANOVA results

T-Test	Bas_HappList	Bas_HappFoc1	Bas_HappFoc2	Bas_HappFoc3	Bas_FearList	Bas_FearFoc1	Bas_FearFoc2	Bas_FearFoc3
M.S.Ampl.	1,57*10 ⁻⁸ ^(*)	0,0010 ^(*)	0,0317	0,0036	1,9647*10 ⁻⁷ ^(*)	2,84*10 ⁻⁵ ^(*)	6,12*10 ⁻⁵ ^(*)	0,0019
AUC	1,12*10 ⁻⁷ ^(*)	5,3*10 ⁻⁴ ^(*)	0,0229	0,0044	9,2335*10 ⁻⁸ ^(*)	2,4*10 ⁻⁴ ^(*)	5,6*10 ⁻⁴ ^(*)	8,2*10 ⁻⁴ ^(*)
M Spike Freq	1,42*10 ⁻⁸ ^(*)	0,1020	0,2724	0,1329	2,5032*10 ⁻⁷ ^(*)	9,9*10 ⁻⁴ ^(*)	0,0120	0,0211

T-Test	Bas_RageList	Bas_RageFoc1	Bas_RageFoc2	Bas_RageFoc3	Bas_SadList	Bas_SadFoc1	Bas_SadFoc2	Bas_SadFoc3
M.S.Ampl.	2,34*10 ⁻⁹ ^(*)	8,87*10 ⁻⁶ ^(*)	0,0011 ^(*)	4,6*10 ⁻⁴ ^(*)	2,9387*10 ⁻⁸ ^(*)	0,0164	0,0249	0,0445
AUC	1,38*10 ⁻⁸ ^(*)	2,03*10 ⁻⁶ ^(*)	1,1*10 ⁻⁴ ^(*)	5,97*10 ⁻⁵ ^(*)	5,7321*10 ⁻⁹ ^(*)	0,0118	0,028	0,0875
M Spike Freq	1,47*10 ⁻⁸ ^(*)	9,6*10 ⁻⁴ ^(*)	1,6*10 ⁻⁴ ^(*)	5,6*10 ⁻⁴ ^(*)	8,3476*10 ⁻⁸ ^(*)	0,2111	0,1188	0,1391

$$\alpha_{Bonf}=0.0013^{(*)}$$

Table 2-2: T-Test results Baseline versus all remaining phases

Table 2-2 reports significant differences between Baseline and Listening phases for all emotions, so it is demonstrated that the psychologist’s goal was successfully reached managing to involve emotionally the subjects; moreover we can observe that Fear, Rage and only partially Happiness activate the subjects for longer time whereas Sadness is not significant for any of Focusing phases. Rage, Fear, Happiness and Sadness, in this order, are listed from the most activating to least activating emotion. Probably the reason involves innate survival instincts since rage and fear, opposed to sadness and happiness are more appropriate to promote subject adaptation to hostile environment so only focusing on memories involving those feelings increase the alertness level facilitating survival mechanisms. Only Rage and Fear create a more lasting alertness state in the subjects. Sadness tends to be the most short lasting emotion (being significant only Listening phase); the subject behave in this way probably due to psychological mechanisms

that aims to avoid painful or stressful memories. Happiness is less activating than rage and fear but more than sadness: it may be that this emotion facilitates socialization being useful for human survival as well.

There are no significant difference between Listening and Focusing phases with themselves (data not shown).

Contents

1	Sommario.....	2
2	Abstract.....	9
	Contents	16
	List of figures.....	19
	List of Tables	22
	List of equations.....	22
3	The Galvanic Skin Conductance.....	24
3.1	Historical frame	25
3.2	Physiology	26
3.2.1	Skin	26
3.3	Sweat glands.....	27
3.3.1	Apocrine sweat glands.....	27
3.3.2	Eccrine sweat glands	28
3.4	Neurology	29
3.4.1	Brain areas.....	29
3.4.2	Periferal innervations	30
3.4.3	Sweat Secretion Mechanism.....	31
3.4.4	Sudomotor nerve bursts.....	33
3.5	EDA elicitation	36
3.6	GSR signal.....	38
3.6.1	Tonic and Phasic	40

3.6.2	SCR – Specific and non-specific responses	41
3.6.3	Phasic SC parameters	41
3.6.3.1	Amplitude.....	42
3.6.3.2	Latency time.....	43
3.6.3.3	Recovery Time	43
3.7	SCR Mathematical models	44
4	Algorithms	47
4.1	Classic trough to peak method (CTTP)	47
4.1.1	Method	48
4.1.2	Results	48
4.1.3	CTTP method drawbacks	49
4.2	The Lim Method	49
4.2.1	Method	50
4.2.2	Results	51
4.3	The Alexander Method	52
4.3.1	Results	54
4.4	The Ledalab Software	55
4.4.1	The Continuous Decomposition Analysis (CDA)	56
1.	Deconvolution of SC data	57
2.	Estimation of tonic activity	58
3.	Estimation of phasic activity	58
4.4.2	Nonnegative deconvolution (DDA) (Benedek, et al., 2010)	59
4.5	Conclusion	60
4.6	Novel algorithms – BC method	60
4.6.1	Method	61

4.6.2	Appendix	61
5	Surrogate SC signal.....	63
5.1	Method.....	63
5.1.1	Choice of the probability distribution governing spike time occurrences	63
5.1.2	Choice of the proper IR function.....	64
5.1.3	Choice of the probability distribution governing spike amplitudes.....	65
5.1.4	Creation of the phasic part of the signals	65
5.1.5	Tonic signal	67
5.1.6	Adding realistic noise	69
5.1.7	Final SC signal	71
5.1.8	Creation of the datasets	72
6	Comparison of Methods using simulated data	73
6.1	Tuning Barbieri Citi Algorithm	74
6.2	Ledalab	78
6.3	Comparison.....	82
7	Experimental Protocol - Emotions	83
7.1	Method.....	83
7.1.1	Subjects	83
7.1.2	Device	83
7.1.3	Recording Session	83
7.2	Elaboration.....	84
7.2.1	Tests	87
7.3	Result.....	88

8 Conclusions..... 93

References..... 94

List of figures

Figure 2-1: Group of 100 IRF..... 10

Figure 2-2: True Positive (FP), False Negative (FN) and False Positive (FP) 11

Figure 2-3: (Left) ROC curves from BC for S/N ratio level of 10^5 obtained by varying S_w and B_w 11

Figure 2-4: Ledalab and BC comparison..... 13

Figure 3-1: Skin anatomical structure..... 26

Figure 3-2: sweat expulsion mechanism and..... 31

Figure 3-3: Schematic presentation of spiral chains of myoepithelial elements(CME)extending along 32

Figure 3-4: Sweating pattern on the dorsal foot and integrated neurogram of skin sympathetic nerve activity (SSA) in the peroneal nerve obtained in mild thermal condition. (A) spontaneous sweating . (B) sweating evoked by a loud noise. (C) sweating evoked by electrical painful stimulation of the skin. You may notice that sweat expulsions (the onset of which are indicated by numerals 1-10), are always preceded by sympathetic bursts, which are shown by the same numerals. 34

Figure 3-5: Relationship between sudomotor nerve signal and skin conductance 34

Figure 3-6: An ideal impulse (Dirac Delta) causes an Impulse Frequency Response 35

Figure 3-7: Quantitative neuro-effector relationship. Each parameter of (A) the rate of rise of sweat expulsion, (B) the amplitude of sweat expulsion, and (C) the sweat output produced by the expulsive process is plotted to the amplitude of sudomotor burst. 35

Figure 3-8: Plots of frequency of synchronous sweat expulsion (F_{sw}) of spontaneous sweating (solid symbols)..... 36

Figure 3-9: Preferred palmar recording areas for exosomatic EDA recording (Boucsein, 2011)..... 40

Figure 3-10: Skin conductance signal example 40

Figure 3-11: Typical skin conductance response (SCR) curve..... 41

Figure 3-12: Different proposed methods for calculating superimposed SCRs (Boucsein, 2011) 42

Figure 3-13: SCR modeled using 3 exponential functions 44

Figure 3-14: Lim's IRf	45
Figure 3-15: Alexander IR function	46
Figure 4-1: Two superimposed blackman windows	49
Figure 4-2: two overlapping SCRs	51
Figure 4-3: Parameters influence shape.....	52
Figure 4-4: Relationship between sudomotor nerve signal and skin conductance	53
Figure 4-5: Ledalab screenshot.....	56
Figure 4-6: (Top) SC signal with estimated tonic signal, (Middle) Sum of tonic and phasic driver, (Bottom) Phasic driver.....	58
Figure 4-7: Spike sequence from BC algorithm	60
Figure 4-8: Hanning Windows	61
Figure 4-9: Filter frequency responses	62
Figure 4-10: Schematic of the three filter frequency responses.....	62
Figure 5-1: Mean ISI histogram	63
Figure 5-2: Inverse Gaussian. (Wikipedia).....	64
Figure 5-3:Lim's (top) and Alexander's (bottom) impulse response.	64
Figure 5-4: An example of spike sequence: the spikes time instants are governed by an inverse Gaussian distribution whereas the amplitudes are chosen with a Gaussian probability distribution.	65
Figure 5-5: Group of 100 IR curves	66
Figure 5-6:SCR part	66
Figure 5-7: Spike and SCR.....	67
Figure 5-8: IR of tonic signal	67
Figure 5-9: Tonic signal	68
Figure 5-10: Summing of phasic part (red) and tonic one (green). Outcome in blue	68
Figure 5-11: Magnification of a section in Figure 5-12.....	68
Figure 5-13: Pink Noise obtained as the mean spectra of 10 realistic SC signals	69
Figure 5-14 depicts an example of flicker noise with mean 0 and variance 1.	69
Figure 5-15: Example of pink noise with mean = 0 and variance = 1	70
Figure 5-16: Same interval of signal affected with different noise level.	70

Figure 5-17: Surrogate SC signal with SN noise equals to 10^5	71
Figure 5-18: Example of surrogate SC signal with S/N ratio 10^5	71
Figure 5-19: Example of real SC signal	72
Figure 6-1: False Positive, False Negative, True Positive	73
Figure 6-2: ROC curve (left) and Euclidean Distance (right).....	75
Figure 6-3: ROC curve (left) and Euclidean Distance (right).....	76
Figure 6-4: ROC curve (left) and Euclidean Distance (right).....	76
Figure 6-5: ROC curve (left) and Euclidean Distance (right).....	77
Figure 6-6: ROC curve with S/N ratio of 10^6	78
Figure 6-7: ROC curve with S/N ratio of 10^5	79
Figure 6-8: ROC curve with S/N ratio equals to 10^4	79
Figure 6-9: ROC curve with S/N ratio equals to 10^3	80
Figure 6-10: Comparison of ROC curves. Starting from the top:.....	80
Figure 6-11: SE,PP and Amplitude Threshold comparison	81
Figure 6-12: Ledalab and BC Sensibility and Positive Predictive Value	82
Figure 7-1: Example of SC signal with Markers	84
Figure 7-2: An example of BC algorithm output. SC signal with marker signal (top) and spike sequence(bottom)	85
Figure 7-3: Output provided by BC algorithm	85
Figure 7-4: Integrated Activity Curve with WL of 2 seconds	86
Figure 7-5: Zoom of a part of Figure 7-4	87
Figure 7-6: Box Plot of Mean Spike Amplitude for each phase where: B stands for Baseline , (H, F, R, S prefixes) indicate emotions, (L, f1,f2,f3) stand for the 4 phases	88
Figure 7-7: Box Plot of Mean Spike Frequency for each phase where: B stands for Baseline , (H, F, R, S prefixes) indicate emotions, (L, f1,f2,f3) stand for the 4 phases	89
Figure 7-8: Box Plot of AUC for each phase where: B stands for Baseline , (H, F, R, S prefixes).....	89

List of Tables

Table 2-1: ANOVA results.....	14
Table 2-2: T-Test results Baseline versus all remaining phases	14
Table 3-1: EDA complete terminology (Boucsein, 2011).....	39
Table 3-2: Mean parameters (Lim, et al., 1997).....	45
Table 4-1: Lim’s mean values for SCR modeling	51
Table 6-1: BC Results	77
Table 6-2: Ledalab Results	81
Table 6-3: Ledalab and BC performances	82
Table 7-1: ANOVA results.....	90
Table 7-2: T-Test results Baseline versus all remaining phases	90
Table 7-3: T-test results comparing <i>List phases</i> among each other	91
Table 7-4: T-test results comparing <i>Foc1 phases</i> with each other	91
Table 7-5: T-test results comparing <i>Foc2 phases</i> with each other	91
Table 7-6: ANOVA and t-test results comparing <i>Foc3 phases</i> among each other	92

List of equations

Equation 1: IRF proposed by Lim	10
Equation 3-1: Lim’s equation	44
Equation 2: Alexander function.....	46
Equation 4-1: g_1 =gain, T_{os} =response onset time, T_r =rise time constant and T_d =decay time constant.	50
Equation 4-2: Alexander’s equation	53
Equation 4-3: Alexander impulse response	54
Equation 4: Decomposition of SC in parts	57
Equation 5: SC expression.....	57

Equation 6: SE and PP formulas..... 74

Equation 7: Bonferroni Correction..... 87

3 The Galvanic Skin Conductance

Since the 1880s, when psychological factors related to electrodermal phenomena were first observed, electrodermal recording has become one of the most frequently used biosignals in psychophysiology. The main reason for its popularity is the ease of obtaining a clear and distinct electrodermal response (EDR), the intensity of which seems apparently related to stimulus intensity and/or its psychological significance. Moreover, electrodermal recording is possible with rather inexpensive equipment, not only in the laboratory but also under less controlled conditions. Originating in neurology and physiology, it progressively became a tool able to explore psychophysiological human domain (Boucsein, 2011).

Electrodermal phenomena offers a wide window for the evaluation of a number of psychiatric disorders such as schizophrenia (Williams, et al., 2004) hyperactivity and attention deficit (Hermens, et al.), post traumatic stress disorder (Bryant, et al.) and sensory-autonomic neuropathy (Polo, et al., 2000) and allows also the comprehension of brain mechanisms about sleeping (Akane, et al.) decision making (Nasir, et al.), emotional arousal (Fahrenberg, 1988), autism (Schoen, et al., July–September 2008) and so on. Moreover it has been used to evaluate the reaction to pain, central nervous system injuries and peripheral neuropathies (Gladman, et al., 1990), (Gutrech, 1994). Despite the widespread use of it in research and application, electrodermal recording mechanism is not still fully understood but the research has intensified in the last four or five decades and scientific papers and reviews concerning EDA are spread over a wide variety of journals and books. However, a tradition of joint research is lacking in the related disciplines of anatomy, physiology, physics, and psychology, that surely will be developed in future (Boucsein, 2011).

Since GSR is strongly related to the emotions (as we will see), one of the first applications of this technique was done in 1936 by Walter Summer, in the development of methods for “deception detection”, also called “Lie Detection”. However, though the use of electrodermal activity (EDA) as a major variable in the detection of deception is well established, the possible influence of mental, physical, physiological and pharmacological factors, impairs the generalized acceptance of this test in the forensic context.

The use of EDA recording in psycho-physiological research has been mainly considered as a tool to find differences among specific groups of subjects (e.g. control and pathological). To this aim a widely used stimulation protocol is usually a train of punctual acoustic stimuli of various intensity and frequency. Some studies also use visual stimuli (affective picture), yet presented for a short time (few seconds). Nowadays the precise cerebral mechanisms involved in skin conductance events are still not well-known and understood, but more and more is being discovered by means of fMRI (Nagai, et al., 2004) and brain injured patients. Conversely the knowledge about anatomical, physiological and functional phenomena of peripheral body is deeper and more accurate.

3.1 Historical frame

The first experiment that showed a connection between sweat gland activity and current flow in skin was performed in Switzerland by (Hermann, et al., 1878), who observed that an electrical stimulation of the sciatic nerve in the curarized cat resulted in sweat secretion as well as an electric current in the footpad on the same body side. Three years later, Hermann repeated the voluntary movement experiment performed more than 30 years earlier by DuBois-Reymond in 1849 and he found that areas with stronger sweating such as palms and fingers showed greater skin current than other body sites such as the wrist and elbow regions, and this pointed to the importance of human sweat glands in electrodermal phenomena (Neumann, et al., 1970). The observation that first related psychological factors to EDA is traditionally attributed to Vigouroux (1879), an electrotherapist working in France. He observed an electrodermal activity that paralleled changes in the amount of anesthesia in hysterical patients and supposed that both phenomena were dependent upon central processes. However, he did not believe that the sudden changes in EDA he observed could be produced by local processes in the skin itself. Instead, he presumed a change in vascular conductivity, which was in line with the developing research on autonomic nervous control of blood flow at that time. We can state that the fundamental discovery of electrodermal phenomena is, however, attributed to two researchers who might not have been aware of each other, the French neurologist (Féré, 1888) and the Russian physiologist (Tarchanoff, 1889).

Féré observed that hysterical subjects showed a greater current flow (measured with galvanometer) between two electrodes placed on skin surface when patients were presented emotional or sensory stimuli. Moreover he noted that normal subjects in condition of reduced stimulation, for example by closing the eyes, showed a decrease in current flow corresponding to an increase in skin resistance. Later soon those phenomena were labeled as “psychogalvanic reflex” and later “galvanic skin response”. It must be noted that Féré measured, with his method, the skin resistance (SR) signal, that is imposing a fixed small current flowing between the two electrodes on the skin surface and measuring the electrical resistance.

One year later, Tarchanoff's (1890) obtained similar galvanometer deflections observing considerable electrical potential (SP) changes between two electrodes on skin surface following sensory stimulation, imagination, mental arithmetic, expectation, and voluntary muscle contractions. Tarchanoff published his observations in 1889 (just one year after Féré).

3.2 Physiology

3.2.1 Skin

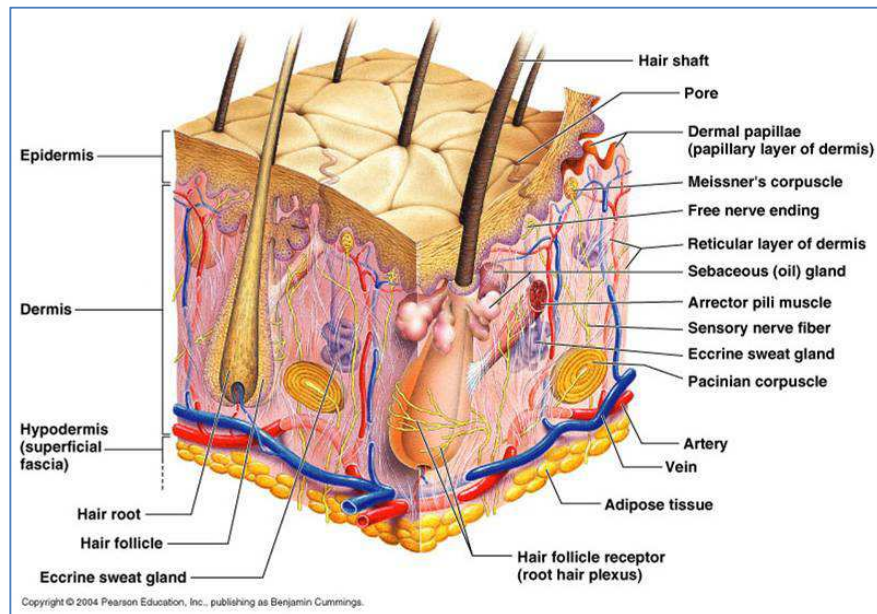


Figure 3-1: Skin anatomical structure.

(http://courses.washington.edu/bioen327/Labs/Lit_SkinStruct_Bensouillah_Ch01.pdf)

We can briefly summarize the skin functions as follow:

1. Helps thermo-regulation: it maintains a constant body temperature through changing blood flow in the cutaneous vascular system and evaporation of sweat from skin surface.
2. It protects against mechanical, chemical stress, certain types of radiation (UV) and infections.
3. Act as a sensory organ sensing touch by mechanoreceptors, heat by thermoreceptors, pressure by baroreceptors, and pain by nociceptors.
4. Prevents loss of moisture.
5. Plays a role in immunological surveillance: it normally contains all the elements of cellular immunity with the exception of B cells
6. Regulates perspiration (by controlling emission of body fluid by sweating, preventing the body from drying out).
7. Regulates blood pressure (by modifying blood vessels volume);

8. Wound healing (skin tissue is auto-repairing);

As abovementioned, skin's function is mainly protective, forming a physical barrier to the environment, allowing and limiting the inward and outward passage of water, electrolytes and various substances while providing protection against micro-organisms, ultraviolet radiation, toxic agents and mechanical insults.

Skin is a dynamic organ in a constant state of change, as cells of the outer layers are continuously shed and replaced by inner cells moving up to the surface. Although structurally consistent throughout the body, skin varies in thickness according to anatomical site and age of the individual.

As we will discuss later, the EDA signal is caused by sweat gland activity from specific glands located in some areas of the skin. The secretory part of the sweat glands (see Chapter 3.3) is between dermis and subcutis and their ducts cross both dermis and epidermis. Nerves and blood vessels are in the subcutis and the bigger vessels that supply the skin start the ramification of small vessels that supply the sweat glands, the hair follicles, and the subpapillary capillary nets. The lymphatic vessels form nets in the dermis and in the subcutis and the main portion of the lymph flows away via subcutaneous lymph vessels. Blood as well as interstitial fluids and the lymph, with their ionic contents, contribute to the relatively high electrical conductivity of the inner strata of the skin.

3.3 Sweat glands

An average person has 2.6 million sweat glands in her skin. Sweat glands are distributed over the entire body, excepts for the lips, inner ear channels, nipples and external genital organs. The mean numbers of sweat glands per cm² of the adult skin are: 233 on the palms, 620 on the soles, 360 on the forehead and 120 on the thighs (Boucsein, 2011). It is interesting to note that the total number of sweat glands in the body is always the same, from birth to death, thus only the surface density lowers with body development. The palmar sweat glands develop in the fetus between the third and fourth month, whereas those on other body sites do not become visible until the fifth month. It is important to highlight the two categories of sweat glands: "eccrine" glands and "apocrine" sweat glands. The classification of apocrine and eccrine was made for the first time by (Schiefferdecker, 1917) describing different mode of secretion.

3.3.1 Apocrine sweat glands

In the apocrine sweat glands, part of the secretion process involves breakdown of secretory cells and the liberation of their contents into the lumen of the gland by means of a necrobiotic process. They are larger, the ducts of which empty out into the hair follicles. They are mainly present in the axillae, ano-genital region, areolae and are basically under thermal control. They become

active at puberty, producing an odourless protein-rich secretion which, when acted upon by skin bacteria, gives out a characteristic odour. The apocrine glands are of little relevance for the electrodermal activity because they only partially react to emotions and stress stimuli, being overall controlled by environment temperature. Only few of them possess an ANS innervation (those in the axilla) and may be partly or even mainly under the control of circulating adrenaline in blood stream (Weiner, et al., 1960). In this thesis work, we will basically deal with eccrine glands because they are more interesting under psychoneurological aspect, showing fiber innervations from ANS.

3.3.2 Eccrine sweat glands

Contrarily to the apocrine sweat glands, eccrine glands are mainly under psychological and only partially under thermal control (only in condition of higher than normal temperature). The watery fluid they secrete contains chloride, lactic acid, fatty acids, urea, glycoproteins and mucopolysaccharides and this fluid passes across an intact membrane from secretory cells into the lumen (Venables, et al., 1973). Being the secretory outcome conductive, the EDA can be recorded.

Eccrine glands are supplied by widely ramified sympathetic sudomotor nerves fibers (Fowles, 1986) with the greatest density being found on the palms, soles, forehead and the least density on the arms, legs and trunk (Kuno, 1956). The eccrine cells on the palmar, plantar and forehead surfaces are mostly involved in emotional sweating, meaning an augment of sweating activity correlated with psychological as well as emotional states which appear for instance in stressing situation or high arousal. Generally eccrine sweat glands respond to orienting responses (OR¹), described by (Sokolov, 1960) as a generalized arousal state following unexpected and novel stimuli. Aversive situations causing alert states causes sweat glands activation bringing about an improved grasping ability (associated with the “flight or fight” reflex (Edelberg, 1972), making skin flexible for better sensory discrimination. Sweating reaction on OR is probably the outcome of a survival evolution mechanism.

¹ The OR is either elicited by external stimuli (called specific OR) or internal mental events (unspecific OR). Specific stimuli include stimuli that can be perceived by body sensors (sounds, images, strong tastes, pain, temperature and so forth) whereas internal stimuli include the outcomes from high level cortex elaborations such as emotions.

3.4 Neurology

3.4.1 Brain areas

All findings concerning the central innervation of sweat glands activity point to several centers, located at different levels of the CNS, and partly independent of one another (Boucsein, 2011).

Much of what is known about the origin of electrodermal phenomena stems from studying the effects of lesions and stimuli in animals (mainly monkeys and cats). Yet, in the last years also the human brain structures involved in EDA have been studied, thanks to the new non-invasive techniques used in brain imaging research, like fMRI (Asahina, et al., 2002), (Williams, et al., 2000) or PET. Tranel (Tranel, et al., 1994) established that amygdala, hippocampus, hypothalamus, brain stem reticular substance, premotor cortex and sympathetic preganglions play an active role. The role of hypothalamus is to control all vegetative functions including human thermoregulation and to play a major role in sudomotor activity. The established influences from the limbic system, especially from hippocampus and amygdala (Edelberg, 1973) on sudomotor hypothalamic areas has been considered as the neurophysiological basis for emotional sweating, appearing the limbic system as the primarily responsible for emotional life. Nevertheless not only the limbic-hypothalamic structures can elicit EDA responses: also cortical areas interacting with the limbic system can influence EDA in humans and primates. In fact, it has been proved (Luria, et al., 1970) that skin conductance orienting responses were diminished, or abolished, in subjects with lateral frontal lesions as compared with lesions in other cortical areas. Thus, the “emotional sweating” seems to be completely under the control of the limbic system² and related cortical structures (the amygdala and the hippocampus). Their action controls the hypothalamic area associated to palmar and plantar sweating.

Moreover experimental evidences show that EDA responses are elicited also by movements, deep inspiration and others. Thus, there are at least other two EDA sources, outside the limbic system and related cortical areas, which can elicit electrodermal responses: the premotor-basal ganglia and the reticular system.

The first is made up of premotor cortical areas (Brodmann area 6) whose fibers for the transmission of skeletal muscle impulses are in close connection with sudorisecretory fibers. When these last areas are naturally or electrically stimulated, or removed, massive sweating is observed.

² The Limbic System, considered as the center of emotional phenomena, influences the hypothalamic function producing EDA responses when an emotional stimulus is coming, by means of the excitatory and inhibitory actions of amygdala and hippocampus, respectively.

In particular, the amygdala, which is a brain structure critical for memory associated with emotional conditions, emotional behaviour, social behaviour, neuroendocrine, and autonomic functions, is thought to play a key role in emotional sweating.

Finally, the “reticular formation” (RF) itself, that is a network of nuclei and fibers in the central core of the brain, important in arousing the cortex and maintaining alertness, in processing incoming sensory stimulation, and in adjusting spinal reflexes, can have eliciting as well as modulating influence on EDA.

3.4.2 *Periferal innervations*

The nervous fibers present in the skin, which innervate sweat glands, belong to the Autonomic Nervous System (ANS) which is composed by two branches: sympathetic and parasympathetic. The sweat glands, being in the subcutis, are highly vascularized and diffusely innervated by a dense net of nerve terminals, both cholinergic and adrenergic. In particular, the secretion of the apocrine glands is stimulated by circulating adrenaline, whereas innervation of secretory part of the eccrine sweat glands is solely via the sympathetic branch of the ANS, which also reaches the dermal part. It is well known that for eccrine glands the postganglionic synapse is cholinergic, having acetylcholine as synaptic transmitter (Venables, et al., 1973).

The sympathetic fibers gather in the skin nerve fascicles of the peripheral nerve. Each skin nerve fascicle exists a mixture of sudomotor, cutaneous vasomotor, and pilomotor nerves. The activity of sweat glands is triggered by postganglionic sudomotor fibers. Each sweat gland is innervated by many different sudomotor fibers (Kennedy, et al., 1994), and each sudomotor fiber innervates a skin area of about 1.28 cm². Changes in palmar and plantar skin conductance (SC) are due to outgoing bursts in the postganglionic efferent sympathetic cholinergic fibres, which respond to changes in central arousal state (Storm, et al., 2000).

It has been found that sweat glands receive only excitatory sympathetic nerve impulses and there is no need to assume the existence of a sweat-inhibiting innervation, since in absence of sudorisecretory impulses the sweat vaporize so quickly that additional sweat inhibition would not reduce the amount of sweat significantly (Boucsein, 2011).

A regional specificity in the innervation of sweat glands also exists, since, for example, the mechanism of thermoregulation, emotional sweating (most important in electrodermal research), or other physiological sweating, are quite different from each other. In fact, for example, the thermoregulatory function of the eccrine sweat glands is normally seen on the forehead or axilla, but at palmar and plantar sites the glands are activated only when the ambient temperature exceeds 30°C. On the contrary, these sweat glands show a greater response only to psychic stimuli (emotions, pain and others, which are mediated by cerebral structures involved in emotional processing), or particular physiological stimuli (movements, deep breathing, etc...). Thus, the eccrine glands in all locations do have the capacity to respond to psychic and thermal stimulation, but there are differences in the thresholds of response: glands of palms and soles respond to psychic stimuli, but intense thermal stimulation is needed to elicit the sweating in these areas; glands in the axilla and forehead occupy an intermediate position, in that they respond to moderate levels of both psychic and thermal stimulation, while those of the remaining areas are exclusively thermoregulatory (Venables, et al., 1973).

3.4.3 Sweat Secretion Mechanism

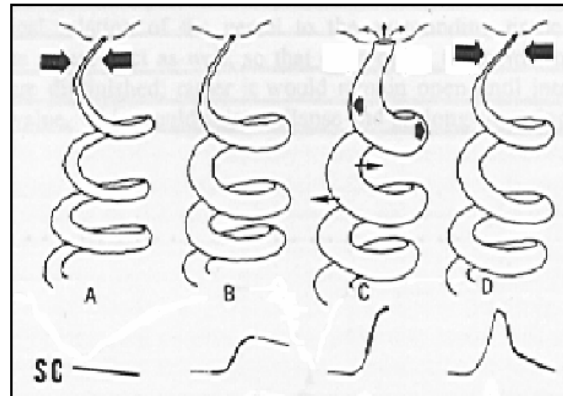


Figure 3-2: sweat expulsion mechanism and its relation with skin conductance (SC) signal

According to Edelberg 1993, Figure 3-2 shows the sequence of events occurring in a sweat gland epidermal duct during an electrodermal response

- 1) At the start of the response, if the superficial layer of the corneum is well hydrated, the sweat pore and the distal portion of the sweat duct are closed under the effect of the pressure exerted by the surrounding corneum (about 20mmHg). Thus, the conductance is not increasing.
- 2) If sweat fills the duct, both laterally and axially, a more conductive path through the relatively resistant corneum (made of dry died cells) is provided, causing a slight increase in conductance.
- 3) If the secretion rate is strong enough, it may generate an intraductal pressure greater than the tissue pressure of 20 mmHg of the corneum. In that case there will be an opening of the duct and sweat pore, which become filled of sweat. As the terminal portion of the duct opens, the conductance increase will be augmented. Sweat will be forced out through the sweat pore but will also continue to move laterally into the corneum as well. The increasing hydration (laterally in the corneum and axially through the duct) is the leading factor that contributes to the fast rise of conductance and is supposed to be responsible of the “phasic components” of electrodermal signal.
- 4) As sweat leaves the ducts, unless secretory rate can keep up with the loss volume, intraductal pressure will fall down. If it falls below the external tissue pressure, the pore and the terminal duct will again collapse, causing a rapid fall of conductance along with sweat evaporation.

(Ogawa, et al., 1993) and (Nicolaidis, et al., 1972) observed in their experiment that sweat flow by eccrine sweat glands is not continuous but pulsatile, that is rhythmically secreted. According to (Ogawa, et al., 1993), pulsatile discharge of sweat can be

interpreted in two ways: sweat may be squeezed out by means of rhythmic contraction of myoepithelial cells (muscular cells around the sweat glands), or secretory cells may produce sweat in a pulsatile manner, or both processes may occur concomitantly. It has been demonstrated (Hurley, et al., 1960) that myoepithelial contraction is involved in discharge of sweat in the apocrine glands. However the function of the myoepithelium in eccrine sweating has not been unanimously understood, though the most classical is pulsatile ejection of sweat by its contraction as in the apocrine glands (Rothman, 1954), (Nicolaidis, et al., 1972), (Ogawa, et al., 1993).

Figure 3-3 shows the hypothetical localization of myoepithelial cells responsible of pulsatile discharge (Nicolaidis, et al., 1972)).

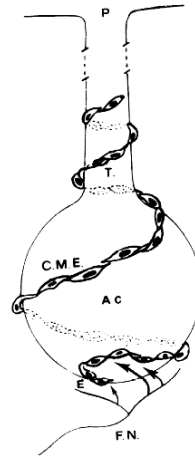


Figure 3-3: Schematic presentation of spiral chains of myoepithelial elements(CME)extending along gland (Ac) from nerve endings (FN) to the tube (T) and its pore (P). Arrows indicate hypothesized direction of propagation of released transmitter before salutatory transmission (Nicolaidis, et al., 1972).

(Nicolaidis, et al., 1972), with hygrophotographic recordings obtained the demonstration of a high-frequency (12-21 cycles/s) pulsatile expulsion of sweat to the cutaneous surface by each eccrine unit. Parallel to this individual expulsion mechanism there is evidence of synchronous fluctuations or waves of increasing-decreasing overall sweat excretion with a period approximating 11-13 seconds in most of the glands observed. In order to explain the pulsatory individual discharge, they suggested the following model: the transmitter is released by the free endings of the sudomotor nerve into the periglandular space and it triggers in a “saltatory” manner the contraction of the myoepithelial cells arranged regularly along the length of the chain. The time of propagation between two consecutive elements of the spiral is between 0.1 sec and 0.05 sec, as the hygrophotographic recordings showed in the form of excretory pulsations. Rhythmic contractions of the myoepithelia, surrounding not only the secretory but also the ductal part of the sweat gland like a helix, finally are regarded as the source of the pulse (Nicolaidis, et al., 1972).

Contrarily, according to (Sato, 1977) sweat can be observed rising and falling in a micropipette brought into the lumen at a frequency of 0.5–2 Hz during low sweating rates. He followed (Kuno, 1956) in arguing that this phenomenon should be due to neural stimulation rather than to myoepithelial contraction. However, the nature of an appropriate innervation remains unclear (Boucsein, 2011) and nowadays the real mechanism is not completely understood yet.

3.4.4 Sudomotor nerve bursts

Probably the most common reason for assessing SC is to obtain an indicator of phasic sympathetic activity (i.e. sudomotor nerve activity SMNA). Changes in palmar and plantar skin conductance (SC) are due to outgoing bursts in the postganglion efferent sympathetic cholinergic fibres, which respond to changes according to central arousal state (Storm, et al., 2000). Human eccrine glands are innervated by postganglionic cholinergic fibers and the sympathetic fibers gather in the skin nerve fascicles of the peripheral nerve. (Ogawa, et al., 1993) inserted a microelectrode³ into the fascicle so recording directly the neural activity of these fibers. Since a mixture of sudomotor, cutaneous vasomotor and pilomotor nerve activities is usually obtained from a specified intrafascicular site where a microelectrode is held, sudomotor, vasomotor, and pilomotor fibers are considered to be intermingled in the fascicle. The authors found that in general skin sympathetic nerve activity consists of multi-unit bursts containing sudomotor, vasomotor (vasoconstrictor) and pilomotor impulses. These bursts occur spontaneously or in response to arousal or mental stimulation with various amplitude and duration.

In literature a number of physiological studies have shown that SCR responses are preceded by discrete bursts of the sudomotor nerves that control the sweat glands (Macefield, et al., 1996) , (Nishiyama, et al., 2001).. (Benedek, et al., 2010) identify a nerve burst as the outcome of the temporal concurrence in the firing of multiple fibers in the integrated nerve record and it corresponds to an observable SCR. Thereby, the nerve bursts are the causes of the sweat responses and are the result of the spatial and temporal integration of the spikes triggered by many different fibers that constitutes the sudomotor nerve. The spike density (as reflected by the amplitude of the nerve burst in the integrated nerve record) is linearly related to the number of recruited sweat glands and to the amplitude of the corresponding SCR. These bursts have a mean duration of 638 ms, much shorter than the duration of the SCR. In addition, the large bursts that produce an SCR are temporally discrete episodes, that is, they are separated by large intervals relative to the duration of the bursts themselves (Nishiyama, et al., 2001). The SCR amplitude can therefore be considered as an index of sympathetic activity. The integrated SMNA (Sudomotor Nerve Activity) thus is conceived as a continuous measure reflecting the spike density of relevant sudomotor neurons and was found to show a stable baseline activity with quite compact peaks of increased activity (see Figure 3-4) .

³ This technique is called “Microneurography”

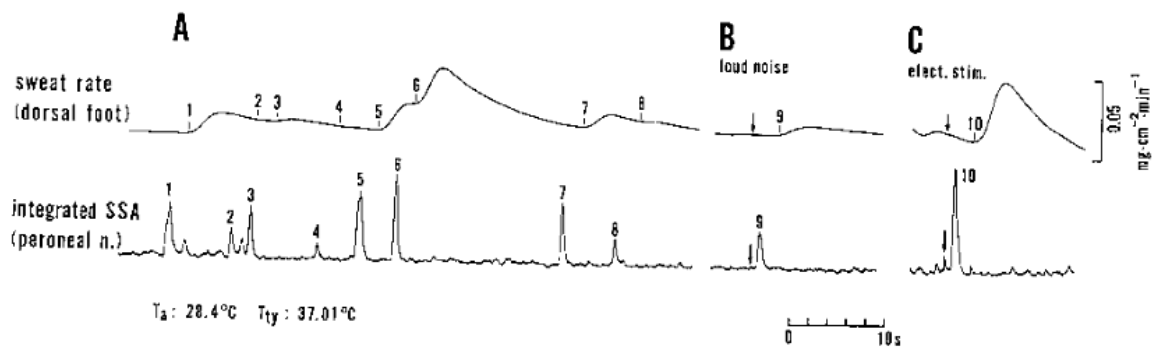


Figure 3-4: Sweating pattern on the dorsal foot and integrated neurogram of skin sympathetic nerve activity (SSA) in the peroneal nerve obtained in mild thermal condition. (A) spontaneous sweating . (B) sweating evoked by a loud noise. (C) sweating evoked by electrical painful stimulation of the skin. You may notice that sweat expulsions (the onset of which are indicated by numerals 1-10), are always preceded by sympathetic bursts, which are shown by the same numerals.

SC is thought to basically reflect SMNA to some extent, but the original signal properties of SMNA are blurred, presumably amongst other things by the influence of slow sweat diffusion processes. Therefore SC no longer shows distinct peaks of phasic activity, but rather is characterized by the superimposition of extended responses, which eventually complicates the assessment of responses (Boucsein, 1992).

The opening of sweat-gland follows in lockstep to these bursts of sudomotor activity (Nishiyama, et al., 2001). The SCR response is delayed in respect the sudomotor burst and this depends on a number of factors, including the slow conduction of unmyelinated axons, neuroeffector transmission, activation of sweat glands, production of sweat and duct filling (Kunimoto, et al., 1991) (Macefield, et al., 1996). The average time for electrical neuroeffector transfer in sweat glands is estimated to be 348 ms (Kunimoto, et al., 1991). This latency is comprised of delays in sweat gland activation and sweat production. Individual sweat glands responding to a sudomotor burst do not operate simultaneously, but vary in activation times within a range of about a second (Nishiyama, et al., 2001).

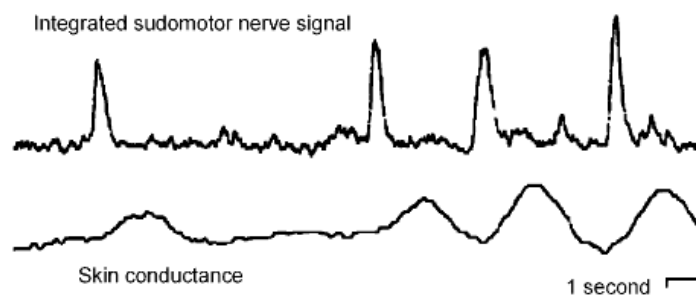


Figure 3-5: Relationship between sudomotor nerve signal and skin conductance signal. Discrete spikes in nerve activity are followed by slower time-constant changes in the skin conductance signal (Macefield, et al., 1996).

Sudomotor nerve activity brings about sweat secretion and consequently changes in skin conductivity. In mathematical terms, sudomotor nerve activity can be considered as a driver composed by a sequence of mostly distinct impulses (i.e. sudomotor nerve burst) which trigger a specific impulse response (Impulse Response Function [IRF]). The process can be represented as:

$$SC_{\text{phasic}} = \text{Driver}_{\text{phasic}} * \text{IRF}$$

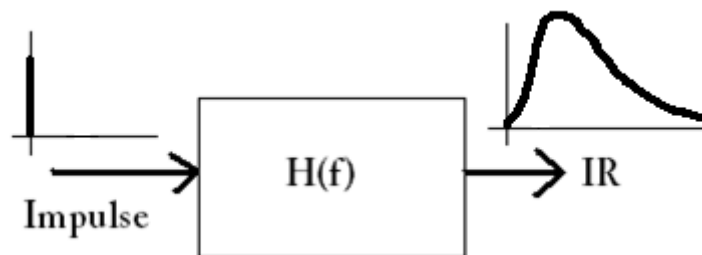


Figure 3-6: An ideal impulse (Dirac Delta) causes an Impulse Response Function (IRF)

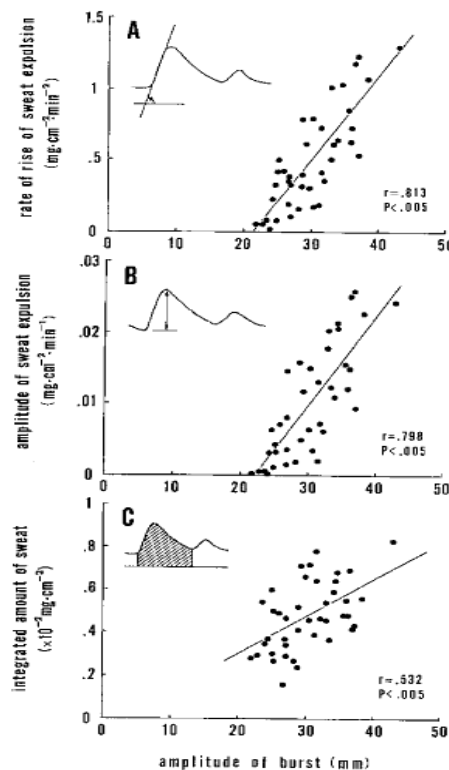


Figure 3-7: Quantitative neuro-effector relationship. Each parameter of (A) the rate of rise of sweat expulsion, (B) the amplitude of sweat expulsion, and (C) the sweat output produced by the expulsive process is plotted to the amplitude of sudomotor burst.

A quantitative relation between sweat expulsions and the corresponding sudomotor bursts has also been analyzed by (Ogawa, et al., 1993). They found that the mean voltage amplitude of a sudomotor burst (an indicator of intensity of the burst) is linearly related

to the rate of rise (Rise time) of the corresponding sweat expulsion, to its amplitude (Response amplitude) or to the sweat output (area under the curve) produced by the expulsive process, when sweat rate is moderate or mild and the fusion of sweat expulsions is minimum. The exact origin of burst discharge of sudomotor drive has not been identified yet. (Wang, 1964) suggested that the central mechanism of synchronizing sweat expulsions on cat's footpads is situated in the striopallidum.

3.5 EDA elicitation

Although the major function of sweating is the regulation of the body temperature, it is well known that sweating on the palms of hands and feet is independent of the ambient temperature (under neutral condition), and is elicited by emotional (fear, pleasure, agitation), physiological (inspiration, tactile stimulations, movements) and stressful (mental exercises) stimuli.

(Ogawa, et al., 1993) claims that the frequency of sweat expulsion (F_{sw}) in thermal equilibrium is a linear function of ambient temperature (T_a) Figure 3-8. F_{sw} is also highly correlated with mean body temperature, when the latter is appropriately estimated as combination of core temperature and mean skin temperature. It is therefore considered that F_{sw} reflects sudomotor neural activity derived from the central thermoregulatory mechanism.

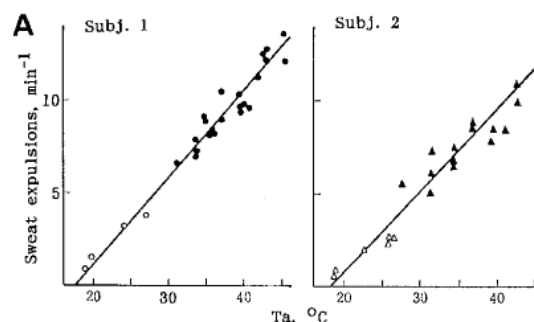


Figure 3-8: Plots of frequency of synchronous sweat expulsion (F_{sw}) of spontaneous sweating (solid symbols) and of pilocarpine-induced local sweating (open symbols) against ambient temperature T_a .

For a deeper knowledge about the relation between thermal sweating and temperature may read the whole article (Ogawa, et al., 1993) where the authors claims more quantitative and analytic relations about variables. Finally, it is clear the thermoregulation function of sweating because the more the temperature rises, the more the frequency and thus the amount of sweat augment, attempting to cool the body by evaporation mechanism. Besides the thermal sweating described in the previous section, (Schliack, et al., 1979) gave evidence for an additional five kinds of sweating which are classified according to the stimuli eliciting them. Every type uses the postganglionic sympathetic neuron, which has its origin in the sympathetic trunk and travels via the peripheral cutaneous nerve to the sweat gland as a final common terminal path. However, their mechanisms of CNS elicitation differ in part.

“Emotional sweating” means increased sweat gland activity as a concomitant of psychological and, especially, emotional states which appear, for example, in high arousal or under stress. It is likely to be elicited via hypothalamic-limbic connections. Emotional sweating is observed mainly on palmar and plantar sites but also in the axillary and genital regions (Millington, et al., 1983), as well as on the forehead (Schliack, et al., 1979). However, (Allen, et al., 1973) reported increased sweating at other body sites during emotional strain induced by arithmetic exercises. They observed the amount of sweating as being directly proportional to the number of sweat glands per region, thus indicating no regional differences in emotional sweating. (Shields, et al., 1987) also considered the possibility of the specific reactivity of palmar and plantar sweating to psychological stimulation as being dependent on the greater sweat gland density on these sites. Thus, the specific role of palms and soles in emotional sweating remains to be considered further (Boucsein, 2011).

“Gustatory sweating” appears when food is consumed which is especially sour, highly salted, or spicy. There are marked interindividual differences with respect to the sites included. Gustatory sweating mainly appears on the face (e.g., on the forehead and the upper lip (Schliack, et al., 1979)) and on the wings or the top of the nose. Its intensity can be irritating without being pathological. However, pathological gustatory sweating may appear after sympathetic nerve lesions. The sweating response can also be elicited in the absence of gustatory stimuli – it does not even require intact gustatory sensation – via chewing and olfactory as well as psychological stimulation (Boucsein, 2011).

During resting conditions (relax), “ubiquitous spontaneous sweating” can be observed on plantar and palmar sites maybe as an expression of a resting tonus (Schliack, et al., 1979) comparable to the resting muscle tonus of motor units whereas (Jänig, et al., 1983) could not find spontaneous sweat gland activity, at least at temperatures below the thermoregulatory neutral zone. (Nicolaidis, et al., 1972) reported an empirical observation demonstrating fast sweat discharge on forehead with frequencies up to 21 Hz. However the existence of such a resting tonus discharge remains debatable and the problem still remains unsolved (Boucsein, 2011). Ubiquitous spontaneous sweating can be observed on palmar and plantar sites, even by a simple magnifying glass. Even in mild thermal environment, where thermal sweating is absent in a resting man, sweat expulsion are recognized on a record of drug induced localized sweating, though low in frequency and amplitude, and are synchronous among different skin areas (Ogawa, et al., 1993).

“Reflex sweating” is an expression that describes sweat gland activity at sites which are innervated from spinal cord segments distal to the locus of certain damage (e.g., paraplegia). The expression is also used for a confined, local sweating following stimulation of an area with radiation, heat, needle punctures, or electricity. It is assumed to be mediated through the so-called axon reflexes.

Pharmacologically produced sweating is a local sweat secretion elicited through either subcutaneous or intracutaneous injection, as well as through iontophoresis with cholinergic substances (e.g., nicotine or pilocarpine).

There is also a special mechanism of sweating which underlies the so-called cold sweat. Startle responses and other strong emotionally tinted responses, as well as deep breathing and coughs – all situations associated with a sudden elicitation of adrenaline – also lead to sweat secretion. Free circulating adrenaline, however, acts in a vasoconstrictory manner similar to a cold stimulus. At the same time, sweat secretion may be activated via hypothalamic centers. Both responses result in cold sweat, which seems to be paradoxical with respect to thermoregulation.

3.6 GSR signal

The terms Galvanic Skin Response (GSR) or Electrodermal Activity (EDA) refer to the time changes of the electrical properties of the skin, occurring under various stimulating conditions or not. With this we mean changes in various electrical properties like conductance (SC), resistance (SR), potentials (SP), impedance (SZ), admittance (SY). These changes can be observed in different parts of the body, although, the most interesting ones occur in the volar part of the hands and palms, and are due almost exclusively to variations in the ionic content of the various skin layers, depending upon the amount of sweat, and hence upon the sweat glands activity. From the analysis of the time changes of the skin's electrical properties, direct information may be obtained on the activity of the autonomic nervous systems (ANS). In fact, the whole secretory part of the exocrine sweat glands, including the myoepithelial layer that surrounds the sweat duct in the dermis, is completely innervated by the sympathetic branch of the ANS (with acetylcholine as a synaptic transmitter).

The terms used to describe EDA have changed over the years; as a matter of fact the term used at the turn of the nineteenth century was "psychogalvanic reflex" but later the term "galvanic skin response" was used. Nowadays most psychophysiologicals favor the term electrodermal activity (Boucsein, 2011). In 1967 a proposal for EDA terminology standardization made by a commission of the Society of Psychophysiological Research had been published (Brown, 1967) which is now generally accepted. (Table 3-1) (Boucsein, 2011).

Methods of recording	Endosomatic	Exosomatic			
		Direct current		Alternating current	
Applied current	Skin potential	Skin resistance	Skin conductance	Skin impedance	Skin admittance
Units					
<i>Abbreviations</i>					
In general	SP	SR	SC	SZ	SY
Tonic (level)	SPL	SRL	SCL	SZL	SYL
Phasic (response)	SPR	SRR	SCR	SZR	SYR
<i>Supplementary abbreviations</i>					
nonspecific response	NS.SPR	NS.SRR	NS.SCR	NS.SZR	NS.SYR
frequency	SPR freq.	SRR freq.	SCR freq.	SZR freq.	SYR freq.
amplitude	SPR amp.	SRR amp.	SCR amp.	SZR amp.	SYR amp.
latency	SPR lat.	SRR lat.	SCR lat.	SZR lat.	SYR lat.
rise time	SPR ris.t.	SRR ris.t.	SCR ris.t.	SZR ris.t.	SYR ris.t.
Recovery time					
63% recovery	SPR rec.tc	SRR rec.tc	SCR rec.tc	SZR rec.tc	SYR rec.tc
50% recovery	SPR rec.t/2	SRR rec.t/2	SCR rec.t/2	SZR rec.t/2	SYR rec.t/2

Table 3-1: EDA complete terminology (Boucsein, 2011)

The electrical activity of the skin can be measured in two ways. First, a small current can be passed through the skin from an external source between two electrodes and the resistance to the passage of current is then measured. This is called exosomatic recording. Methods of exosomatic recording apply either direct current (DC) or alternating current (AC) to the skin. In DC measurement, if voltage is kept constant, EDA is recorded directly in skin conductance (SC) units, while skin resistance (SR) units are obtained when current is kept constant. The exosomatic method has been modified today into the measurement of skin conductance (SC), the reciprocal of skin resistance. On the other hand, endosomatic method is still used to measure skin potential (SP), but skin conductance recording is mainly used today by most researchers.

The study of “skin conductance” has some advantages as compared with other parameters, like skin resistance or potential. For example, Thomas and Korr, in 1957, obtained an essentially linear relationship between the number of active sweat glands per unit area and the measures of skin conductance (Thomas, et al., 1957). Moreover, skin conductance is simpler to measure, and shows a simpler time course, as compared with skin potential. In fact, the SC can be recorded with just two active electrodes on the surface of two fingers, whereas SP measurements need two electrodes inserted into the skin, and may show multiphasic time courses, often difficult to interpret (Boucsein, 2011).

In this thesis work we will focus only on skin conductance.

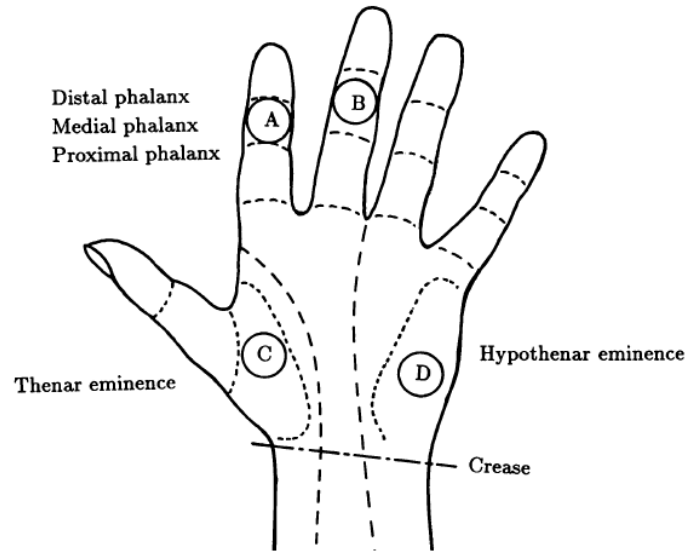


Figure 3-9: Preferred palmar recording areas for exosomatic EDA recording (Boucsein, 2011)

3.6.1 Tonic and Phasic

As a general feature, GSR signal (both SR and SC) is constituted by two different (and quasi-independent) superimposing components: a slowly habituating measure of arousal activity (SCL or skin conductance level) called “tonic component”, and a fast varying component (skin conductance response SCR) called “phasic component”. The two components originate at the peripheral level, but are directly mediated by the central nervous system (CNS) and hence drive different information. In fact, the tonic component is supposed to be related to the broad level of brain activation, (“arousal”) and the properties of the skin(e.g. factors such as degree of moisture in the stratum corneum, membrane permeability etc) (Storm, et al., 2000), whereas the phasic component, small waves superimposed to the tonic part showing a steep incline to the peak and a slow decline to the baseline, may reflect stimulus-specific responses or non-specific responses. SCL and SCR are also assumed to be linked together by some non-linear interactions at the peripheral level.

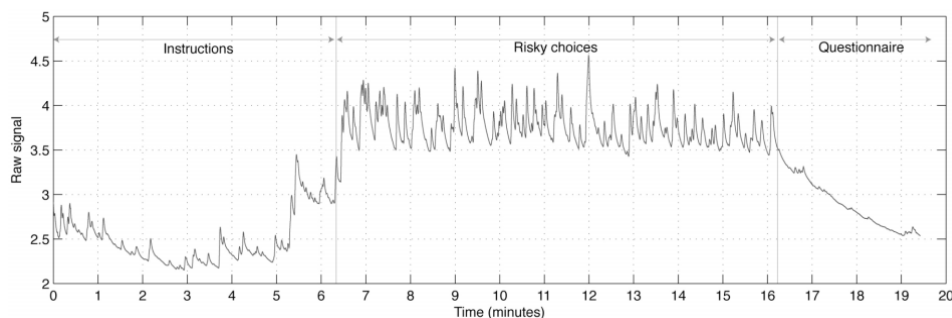


Figure 3-10: Skin conductance signal example

In literature (Ishchenko, et al., 1989) affirmed that “the signal of the tonic and phasic components are not periodic, their spectra are continuous and overlap[...]. The bulk of the energy of the tonic component of the signal is in the frequency band from 0 Hz to 0.05 Hz, and the energy of the phasic component is in the band from 0.05 Hz to 1-2 Hz (Butkevich, et al., 1978)”. According to (Boucsein, 1992), the signal consists of two components: a tonic one that represents a low frequency baseline (0-0.05 Hz), and a fast changing phasic component (0.05 Hz-1.5 Hz) superposed on the tonic part. It is common in literature to find that beyond 3 Hz maximum there is no useful SC signal.

3.6.2 SCR – Specific and non-specific responses

The term SCR (EDR or electrodermal response in general) is usually associated with an evident change in EDA signal as a result of a stimulation (called specific or elicited responses) but there are often phasic parts of EDA which cannot be traced to any specific stimulation. The SCRs are the most commonly used measure of orienting responses (OR) (Graham, 1973), defined by (Sokolov, 1960) as a generalized arousal state following an unexpected stimulus. The OR emitted by stimuli are called specific SCRs, whereas the OR induced as a consequence of internal or mental events are called non-specific SCRs and the typical activity is 1-3 events/min when the subject is at rest (Dawson, et al., 2001). Hence, they are called “spontaneous” or “nonspecific” EDRs which are characterized by the prefix “NS” (e.g., NS.SCR is used as an abbreviation for nonspecific skin conductance response).

3.6.3 Phasic SC parameters

Skin conductance parameters which can be found in literature are more or less standardized (Lykken, 1971). SCR responses can be broken down in to a number of component measures: Onset Time, Rise Time, Amplitude, Recovery Time, Recovery Half Time.

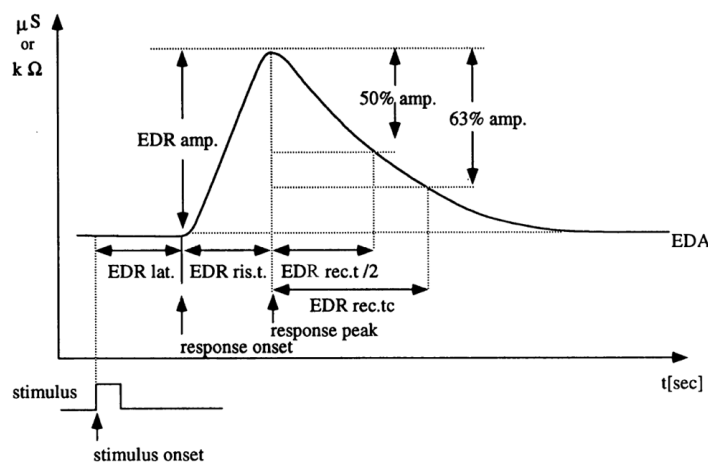


Figure 3-11: Typical skin conductance response (SCR) curve

3.6.3.1 Amplitude

The amplitude parameter (EDR.amp) it is the most common parameter to describe an electrodermal response. The amplitude assessment should be done fixing a minimum amplitude threshold (such as to discard unnecessary information i.e.noise) as well as deciding a criterion to manage superimposed close EDRs (Boucsein, 1992). A common minimum response amplitude used in SCR research is $0.05 \mu\text{S}$ (Dawson, et al., 2001).

As it is possible to notice from Figure 3-11, the amplitude is defined as difference between the conductance values during latency time and the maximum peak. Nevertheless this evaluation might not be easy in case of superimposing EDRs. This situation is often encountered in subjects showing high level of arousal (stressed, anxious...). It is possible to observe that the distortion grade of the second response in case of superimposition depends on the grade of proximity with the previous response (Grings, et al., 1969). (Boucsein, 2011).

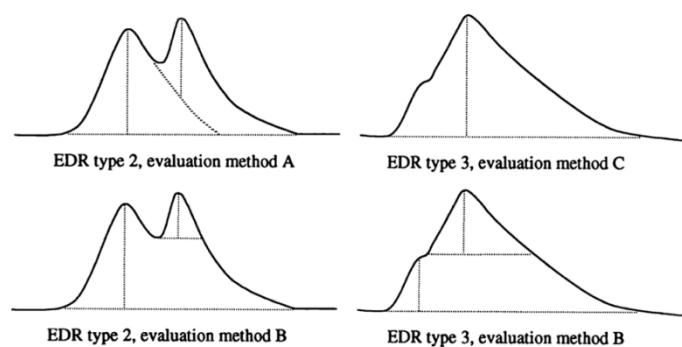


Figure 3-12: Different proposed methods for calculating superimposed SCRs (Boucsein, 2011)

In case of superimposition, literature propose some criteria (Figure 3-12): with “EDR type 2, evaluation method A” the amplitude of the second response is obtained measuring the vertical distance from the peak of the second response to the extrapolated line drawn starting from the decay of the previous response. “EDR type 2, evaluation method B” is easier to calculate and it is the most common in literature (the amplitude of the second peak is obtained as vertical distance from second peak value to the previous trough). (Edelberg, 1967) was able to demonstrate that this leads to correct results in most of the situations. However the amplitude assessment is more problematic in those cases on the right side. In “EDR type 3, evaluation method C” the first response is ignored whereas in “EDR type 3, evaluation method B” no (the latter recommended in (Edelberg, 1967)). Lately they have been developed more sophisticated computer based methods to separate superimposed responses whom we will discuss later.

3.6.3.2 Latency time

The latency time is the time necessary for the signal to start the deflection. EDRs show long latency times if compared with the ones of other biosignals, for example evoked potentials (ERP) or HR variations. The latencies in a exosomatic recording range normally from 1 to 2 seconds (Boucsein, 2011). The temperature alter the latency time, in fact (Edelberg, 1967) reported a latency time of 5 seconds recorded in environment below room temperature: the temperature should always be recorded if different experiments should have been compared, because the latency time depends on the acetylcholine transportation speed, depending on the temperature. After a stimulus delivered to a subject, the most common value of the expected latency time found in literature is 1 to 4-5 seconds, with an average time of 2.3 seconds between the instant of the stimulus presentation till the peak of the phasic response.

A further problem in calculating latency time is due to the impossibility to obtain an accurate and not ambiguous onset time (time instant of the response beginning). In this case it is common calculating the derivative in order to identify it (Boucsein, 2011).

3.6.3.3 Recovery Time

Often it is difficult to determine the exact instant of time where the electrodermal response ends its asymptotic descend, and also usually there's a tonic activity varying during the response not permitting the response to reach the prestimulus value. Thereby, such as to determine the recovery time, (Darrow, 1937) used the half-life time used with radioactive materials: it is defined as the time taken by these materials to half their mass. In a similar way, Darrow expressed the "Half-life time" (HLT) as the time necessary for the electrodermal response to reach 50% of the response amplitude (EDR.amp). Similarly, it is defined EDR Rec.tc the time to reach 63% of EDR.amp.

It is not always possible to measure HLT or Rec.tc because a second EDR may occur before the first decays enough (superimposition). In this cases, (Fletcher, et al., 1982) proposed to use $HLT/2$, because they reported a correlation of about 90% between $\log(Rec.tc)$ and $\log(Rec.tc/2)$. This way they managed to rise the percentage of skin conductance responses of 23%. However, nowadays it must still be demonstrated that these recovery time evaluation techniques of rapid and superimposed responses provide valid, reliable and homogeneous information. At least it is advisable to make sure that the individual response shapes, superimposed, correspond to individual response shapes not superimposed; this could be obtained with a recording period without superimpositions. (Boucsein, 2011). Mathematical solutions with the aim to solve superimposition cases have been proposed recently, mainly based on deconvolution techniques.

3.7 SCR Mathematical models

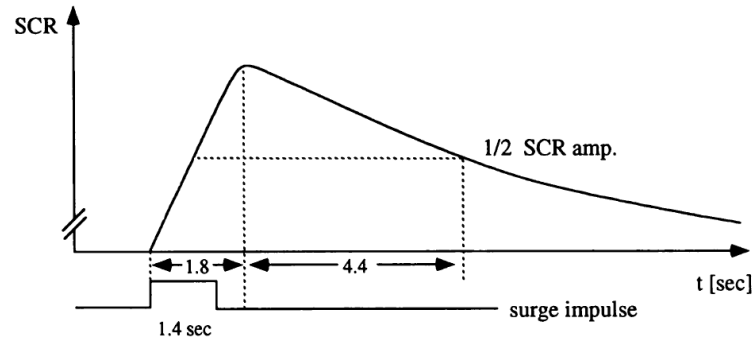


Figure 3-13: SCR modeled using 3 exponential functions

Figure 3-13 depicts a SCR reconstructed using 3 exponential functions, one for the rising part ($\tau = 0.1$ sec) and two for the descending part ($\tau_1 = 0.2$ sec and $\tau_2 = 6$ sec); the simulated curve shows Rec.t/2 of 4.4 sec and Rec.t.c. of 1.8 seconds, values representing a good approximation of a real curve. (Edelberg, 1971) reported a range of values of 1 to 15 seconds, with mean values between 4 sec and 6 sec for the time constants of the descending traits.

More sophisticated models were proposed by (Hunt, 1977), who developed a curve equation based on superimposed gaussian distributions fitting the typical curve, and by (Schneider, 1987), who fitted the real skin conductance response curve with a three compartments model capable to describe the physical properties of sweat ducts, the behavior of the active membrane on sweat duct walls and corneal hydration. He also showed how a typical EDR could be described considering a triangular impulse and as impulse response the sum of two exponentials with time constants of 2 and 20 seconds.

(Ahlberg, et al., 1967), instead, proposed the idea that an alternative way to describe an EDR was using a cubic spline passing through the onset instant time, the peak value and the rest of descending available points.

Although many mathematical models have been proposed, for the practical goal of this thesis, we focus our attention only on certain models we are going to describe below.

(Lim, et al., 1997) proposed in their paper a model of SCR based on 4 parameters controlling every aspect of the curve. The equation is

$$f_{s1} = \frac{g_1^{-((t-T_{os1})/t_d)}}{\{1 + [(t - T_{os1})/t_r]^{-2}\}^2}$$

Equation 3-1: Lim's equation

Where where g_1 =gain, T_{os} =response onset time, T_r =rise time constant and T_d =decay time constant.

The equation is composed combining two functions that is a sigmoid function (describing the rising part) and an exponential decay function for the decay part: the result is a sigmoid-exponential function modeled with 4 parameters. They reports in (Lim, et al., 1997) the mean values of parameters (Table 3-2).

Skin conductance parameters and comparison of peak measurements ($n = 60$)

Variables	Mean	SD
Parameters		
a_0 (μ S)	0.32	0.37
g_1	3.69	3.91
t_d (s)	2.98	2.13
t_r (s)	1.59	0.68
T_{os1} (s)	1.51	0.37
c (μ S)	8.87	2.19
SCR peak latency (s)		
fitted	4.13 ^a	1.13
standard	3.99 ^a	0.10
SCR peak amplitude (μS)		
fitted	0.46 ^b	0.38
standard	0.39 ^b	0.32

^aPaired t -test, $P < 0.0001$

^bPaired t -test, $P < 0.00001$

Table 3-2: Mean parameters (Lim, et al., 1997)

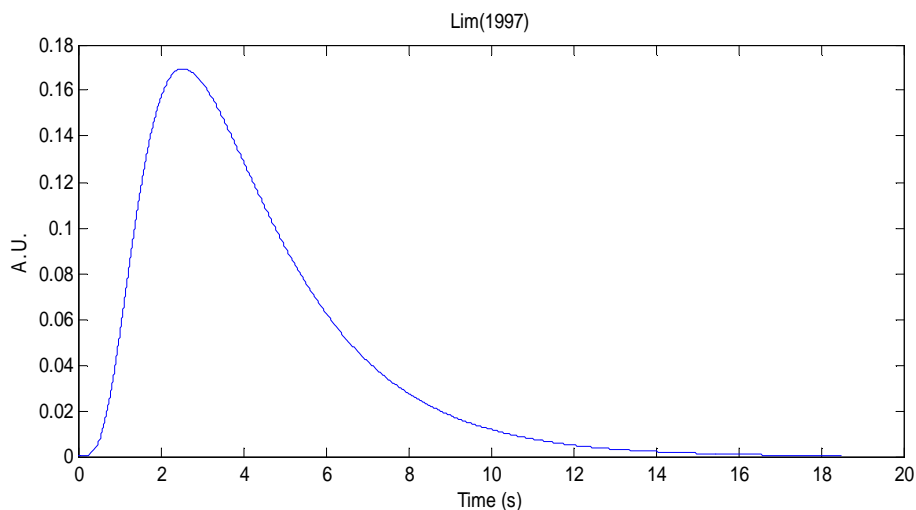


Figure 3-14: Lim's IRf

The model proposed by (Alexander, et al., 2005) is based on a bi-exponential function. This equation has been previously used to model the effects of individual nerve impulses on synaptic activation of the neuronal membrane

The larger time-constant (taken to be τ_0) describes the decaying tails of the SCRs, whilst the shorter time-constant (τ_1) governs the rise time in response to a peak in the driver.

$$y(t) = e^{-(t/\tau_0)} - e^{-(t/\tau_1)}$$

Equation 2: Alexander function

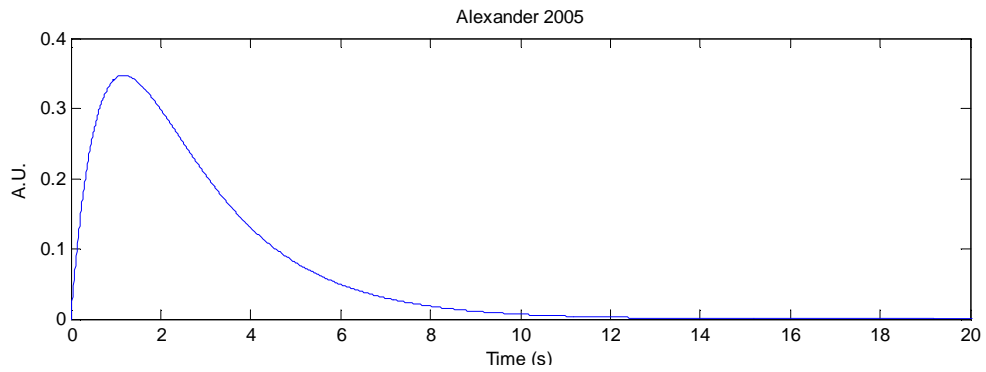


Figure 3-15: Alexander IR function

4 Algorithms

Spontaneous and elicited changes in skin conductance signals have been proposed as a measure of neurophysiologic arousal followed by activity in the sympathetic nervous system (Wallin, 1981) so as an indicator of sympathetic activity. These physiological changes in SC can provide an objective method for evaluating a person's state of arousal and will help detect covert changes that may escape subjective evaluation or direct observation (Storm, et al., 2000). When an outgoing sympathetic nervous burst occurs, a wave of skin conductance will follow so during spontaneous skin conductance changes, increased number per second (and amplitude) of the waves is interpreted as increased activity in the sympathetic nervous system (Lidberg, et al., 1981). Measuring parameters relative to SCRs with CTPP method creates problem when SCRs overlap, a problem that becomes endemic in experimental paradigms that use short inter stimulus intervals. Short ISI paradigms, such as those usually employed in cognitive research, confound measurement of each discrete phasic SCR. The overlapping SCRs introduces distortions into all SCRs measured distorting amplitude and locations. The least affected is response frequency (Dawson, et al., 2001), but even this can be distorted if temporally near-contiguous SCRs are scored as a single event. We describe the methods in literature and a novel algorithm to assess the sudomotor bursts triggered by ANS causing SC responses that permit to solve overlapping problems.

As we will see with (Alexander, et al., 2005), (Benedek, et al., 2010a), (Benedek, et al., 2010) the deconvolution technique is a common tool. Deconvolution relies on the precondition that there exists a stable impulse response function (IRF): if the IRF shows a too slow recovery process the driver (burst activity signal) may become negative for some SCRs and a negative driver cannot be interpreted in terms of sudomotor activity. On the other hand, if the recovery process of IRF is chosen too fast, the deconvolution analysis results in less compact impulses in the driver function.

It can be easily be shown that deviations of the SC data from a model IRF result in implausible driver responses (Benedek, et al., 2010).

4.1 Classic trough to peak method (CTTP)

The algorithm was designed for analyzing spontaneous and external elicited SC changes for infants and adults (Storm, et al., 2000). It calculates the number and mean amplitude of the waves as well as the mean basal level in the SC signal analyzed by means of detecting the characteristics of SC fluctuations (waves). The program analysis was carried out using a number of different values for the minimum amplitude, maximum slope and minimum width of the spontaneous waves for infants and adults, and the results

were compared with those obtained with manual counting of the waves. The program was used also to perform coherent averaging of repeated elicited SC changes, assessing the latency time, response amplitude and recovery time of the mean elicited skin conductance response.

4.1.1 Method

The program records and counts the number of waves per second by defining the valleys and peaks and calculates the mean waves amplitudes as well as the mean basal level in the studied period of the spontaneous skin conductance activity. The valley and peaks were established when the derivative of the wave was zero (Storm, et al., 2000). This is the most intuitive and simple way to assess amplitude, as we can find for example in (Boucsein, 1992) and (Edelberg, 1967).

The amplitude of waves is here calculated from the bottom of the valley prior to the peak to the height of the peak (Storm, et al., 2000). The slope of an SCR is defined as the mean distance valley to the peak / time to reach peak. The width of the wave defines the number of measured data points following directly after a valley. Broad widths can reduce the apparent amplitude of peaks and alter the apparent location. The program is based on an algorithm that fits a quadratic polynomial to sequential groups of data points. The number of data points used in the width is specified by width. For each peak or valley, the quadratic fit was tested against the threshold level: peaks with heights below threshold or valleys with troughs above threshold are ignored (Storm, et al., 2000). The amplitude and width threshold are set in order to eliminate eventual noise influences, the slope threshold to eliminate noise from electrode slipping. For external elicited skin conductance changes, the program can perform a coherent averaging in order to calculate the reaction in time (for example to a medicine) providing mean amplitude, mean latency time and mean recovery time.

The present program does not mention at all a preprocessing method as additional smoothing or filtering, thus they probably perform their algorithm on SC raw signal directly.

4.1.2 Results

The authors proposed a 0.02 μS as the optimum threshold to discriminate genuine waves (physiological) from waves due to noise. The authors set a maximum limit value for the calculated slope as 2 $\mu\text{S/s}$ for infants and adults, value able to separate physiological waves from motion artifact waves and electrode slipperying. The width of the waves should be at least 1 s for adults, and unlimited for infants. The coherent average method was found to be a satisfactory method for revealing whether a subject responded to stimuli, and is recommended, especially for infants (Storm, et al., 2000).

4.1.3 CTPP method drawbacks

The CTPP method is affected by drawbacks and it should be used only to roughly estimate the number of fluctuations. However can fail in presence of overlapping SCRs, when also manual counting can fail due to the superimposition phenomenon.

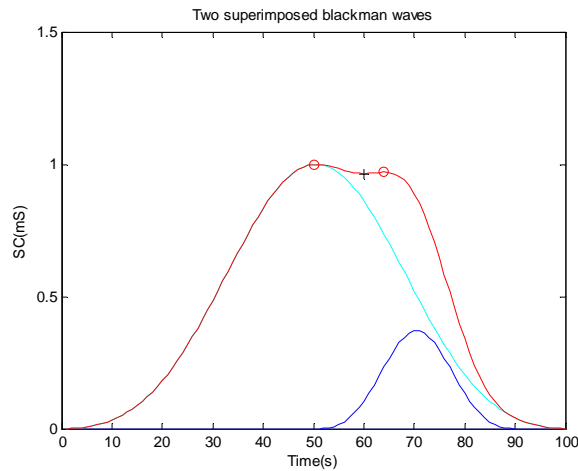


Figure 4-1: Two superimposed blackman windows

In Figure 4-1 there are two blackman windows (cyan and blu) and their sum (red curve). The detection as performed in (Storm, et al., 2000) is not reliable because the right trough-to-peak amplitude detected is only $0.0045 \mu\text{S}$ but the window is of $0.4 \mu\text{S}$ so this algorithm distorts SCRs amplitudes.

4.2 The Lim Method

A possible solution for a computer-based treatment of overlapping SCRs has been suggested by (Lim, et al., 1997). Their modeling was based on the assumption of the stereotypical nature of the SCR waveform within each subject, so a unique SCR shape within each subject. This hypothesis has been objected by many authors, being a radical assumption and a simplification.

The model proposed by (Lim, et al., 1997) performs a curve fitting adopting a four to eight parameter sigmoid-exponential SCR model describing the entire response (SCR) accounting for the SCL, the slope of preceding SCR and the shape of one or two overlapping SCRs. This method aims to split the SC signal into a phasic and a tonic component actually obtaining the “true” SCR shape getting rid of SCL (tonic component) and any other distortion due to SCRs in proximity of it.

4.2.1 Method

Individual SCRs are fitted with a function based on an asymmetrical sigmoid and an exponential function, and the method iteratively optimizes the model parameters to minimize the mean-squared difference between the fitted and actual curve. Equation 4-1 reports the four parameter model of ‘pure’ SCR (excluding SCL) based on a combination of an asymmetrical sigmoid and an exponential function. The pure SCR (excluding SCL) is comprised in the so called “Case1”, the most simple case.

$$f_{s1} = \frac{g_1 e^{-((t-T_{os1})/t_d)}}{\{1 + [(t - T_{os1})/t_r]^{-2}\}^2}$$

Equation 4-1: g_1 =gain, T_{os} =response onset time, T_r =rise time constant and T_d =decay time constant.

This model and its extensions can characterize a wide variety of response waveforms, size and combinations. The algorithm can decompose the SC activity into its components, namely, the residual from the previous SCR tail, the pure SCR and SCL. Different terms have to be added to Equation 4-1 if a single SCR is superimposed on a fixed SCL, if a SCR occurs on a decaying limb of a previous response or if two overlapping SCRs occur on a decaying slope (Lim, et al., 1997).

The authors visually inspected and categorized SC segments into 3 cases deriving from “Case 1” in Equation 4-1 and modeled incrementally the SC signals in 3 cases of increasing complexity. The reader may notice that Case1 requires 4 parameters.

- Case 2: “Pure” SCR on a flat baseline, described with a 5 parameters model (Case 1 + flat baseline)
- Case 3: as Case 2 but with a sloping baseline (mainly the tail of the previous response), described with 6 parameters model (Case 2 + sloping baseline)
- Case 4: the most complex, containing two overlapped SCRs on a sloping baseline, described with an 8 parameters model (Two time Case 3).

Specifically, a computer program is used to automatically scan the entire data file and to detect SC trough- and peak-latencies and their amplitudes for a rough estimate of the initial model parameters. Thereafter, the waveforms are visually inspected, providing the opportunity to accept or modify the automatically generated initial values before curve fitting process (using a standard non-linear least squares method) is committed. After 10–30 iterations, success of the fit should be apparent by visual inspection. If not, the initial values may be modified again until a satisfactory fit is achieved. Then, a residual (residual between the fitted curves and the SCR data), reflecting the not-perfect fitting model, is obtained and in most of cases is less than 5%. The fitted curves were demonstrated to

be almost indistinguishable from their respective raw response complexes. Now the SCRs are free from superimpositions and analyzed.

4.2.2 Results

The method was applied by Lim et al. (1997) to more than 60 SC segments, each containing one SCR or two overlapping SCRs on a sloping baseline elicited by 80 dB tones with ISIs as short as to 1.32 s, obtained from 20 normal participants and recorded with standard methodology CTTP (Storm, et al., 2000) as depicted in the next Figure 4-2.

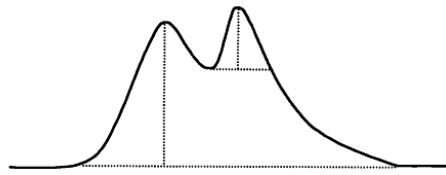


Figure 4-2: two overlapping SCRs

In comparison with CTTP, their decomposition methodology yielded a significant mean amplitude increase of 14% and an increase in peak latencies of 140 ms. The latency increase can be regarded as a consequence of removing the disguising effect of the preceding SCR's tail on the onset of the subsequent SCR.

The four parameter values (adding also a_0 : the initial SC value at stimulus and c :SCL value) emerging from this experiment were used to calculate the across-subject parameters means, Standard deviation (SDs), coefficients of variations and maxima values as well as mean peak latencies and amplitudes obtained with CTTP and Lim's method.

Skin conductance parameters and comparison of peak measurements ($n = 60$)

Variables	Mean	SD
Parameters		
a_0 (μS)	0.32	0.37
g_1	3.69	3.91
t_d (s)	2.98	2.13
t_r (s)	1.59	0.68
T_{os1} (s)	1.51	0.37
c (μS)	8.87	2.19
SCR peak latency (s)		
fitted	4.13 ^a	1.13
standard	3.99 ^a	0.10
SCR peak amplitude (μS)		
fitted	0.46 ^b	0.38
standard	0.39 ^b	0.32

^a Paired t -test, $P < 0.0001$

^b Paired t -test, $P < 0.00001$

Table 4-1: Lim's mean values for SCR modeling

The mean and SDs of the four parameters are used to reconstruct a family of curves which demonstrate the influence of the parameters on SCR shape. Figure 4-3 shows the influence of the 4 parameters on SCR shape.

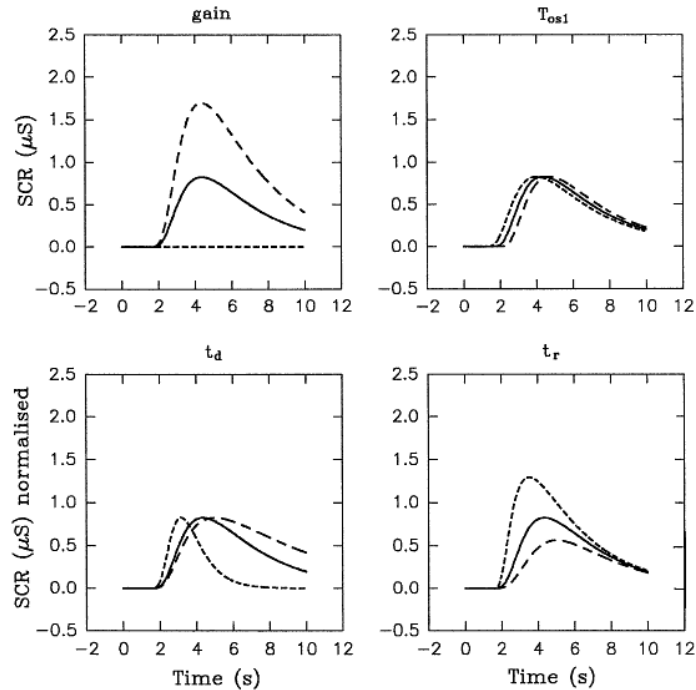


Figure 4-3: Parameters influence shape

The Lim method has been applied later by (Williams, Brown & Das, 2004) studying 22 non pathological subjects viewing four blocks of fearful alternated with four blocks of emotional neutral faces. Despite the quite short ISI (0.75 s), fear and neutral stimuli could have been significantly differentiated by means of SCR amp, leading to some hint about the validity of this evaluation method.

4.3 The Alexander Method

An evolution of (Lim, et al., 1997) method was reported (Alexander, et al., 2005) which overcomes the necessity of a judicious choice of initial parameters and visual inspection of curve fitting. As Lim, they describe a method designed to overcome the problem of overlapping skin conductance responses. They proposed an automated method for scoring individual SCR by converting the SC signal into a time series with a shorter time constant, relying on the assumption that the underlying sudomotor nerve signal has a shorter time constant than skin conductance signal and that the sudomotor bursts arrive as discrete, separated peaks. The algorithm performs a deconvolution of SC data with an appropriate impulse response function (IRF also called transfer function): the IRF represents the basic SCR shape that would result from a unit impulse. They claim to be able to extract the separated peaks and

estimating the underlying driver signal. The separated driver peaks are then used to re-estimate each individual skin conductance response.

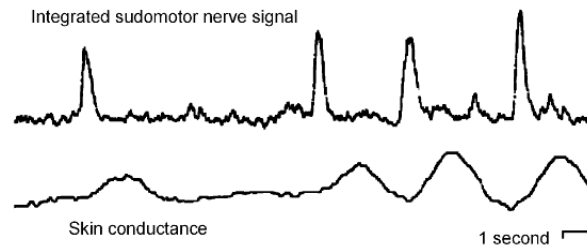


Figure 4-4: Relationship between sudomotor nerve signal and skin conductance signal. Discrete spikes in nerve activity are followed by slower time-constant changes in the skin conductance signal.

The method scoring individual SCRs described in this paper relies on two key assumptions:

1. Sweat activity results from discrete episodes of bursting of the sudomotor nerves
2. The apparent time-constant of the bursting episodes is much shorter than the measured SCR.

Those assumptions allow that, even where individual SCRs are highly overlapping, the estimated underlying burst time-series shows discrete, separate events. We can say that it is a sort of SC signal transformation into an approximation of the original bursting episodes.

The authors makes use of a Bateman function (biexponential function) to model the relationship between the driver and the SCRs. (Schneider, 1987) originally proposed a physiological rationale for the biexponential shape based on a two-compartment diffusion process. The following is considered by the authors the differential equation relation governing the SC time series.

$$(\tau_0 \tau_1) \frac{d^2 y}{dt^2} + (\tau_0 + \tau_1) \frac{dy}{dt} + y = q(t)$$

Equation 4-2: Alexander's equation

In Equation 4-2, τ_0 and τ_1 are time-constants, $y(t)$ the skin conductance and $q(t)$ the driver function, which the authors interpret as being representative of the activity of the sudomotor nerve. The larger time-constant (taken to be τ_0) describes the decaying tails of the SCRs, whilst the shorter time-constant (τ_1) governs the rise time in response to a peak in the driver. In the limit $\tau_0 \rightarrow 0$, the previous equation becomes equivalent to an RC circuit. So an impulse spike in the driver at $t=0$ generates a biexponential function form as below:

$$y(t) = e^{-(t/\tau_0)} - e^{-(t/\tau_1)}$$

Equation 4-3: Alexander impulse response

Equation 4-2 defines the SC signal ($y(t)$) as the convolution of the driver function $q(t)$ with a biexponential function: as a matter of fact by deconvolving the signal with Equation 4-2 it is possible to obtain the driver where now the peaks are well separated and can be easily detected. This evaluation method consists of 3 steps:

1. Performing a deconvolution of the SC signal so as to obtain the driver signal.
2. Isolating single peaks, now well separated (as in Figure 4-4) in the driver signal
3. Convolution of the peaks recognized in the driver function with Equation 4-3 in order to reconstruct the individual SCRs and so being able to assess parameters about SCR shape. For a minority of SCRs, i.e., where the driver does not conform to the standard function or where the driver signal contains overlapping peaks, an iterative procedure is applied to the sequence of potential peak intervals, until no further changes occur.

The mathematical symmetry underlying the deconvolution/convolution means that altering τ_0 and τ_1 values changes the driver time-series, but not the re-estimated SCRs. So long as τ_0 and τ_1 are chosen such as the peaks in the driver signal are fully separated by a relatively long baseline between them, the exact values do not make a major difference to the scoring of the peaks (Lim, et al., 1997).

4.3.1 Results

Using surrogated data, they were able to distinguish SCRs till a distance of 1.3 seconds. At offsets of less than 1.3 seconds, the two SCRs appear as single SCR upon qualitative observation.

In order to verify their method, the authors set up an experiment in which 735 subjects were presented auditory stimuli with ISI of 1 s in an odd-ball paradigm⁴ originally designed for ERP recordings. They found that optimal values for time constants were respectively 2.0 s and 0.75 s for τ_0 and τ_1 , which work well for all time series in the database, moreover verifying that the present method is not excessively sensitive to the values of parameters involved in phasic and tonic separation. This method was also applied

⁴ The oddball paradigm is a technique used in evoked potential research in which trains of stimuli that are usually auditory or visual are used to assess the neural reactions to unpredictable but recognizable events. The subject is asked to react when a target stimulus is detected, the latter being hidden as rare occurrences amongst a series of more common stimuli, that often require no response.

by (Davis, et al., 2009) in a learning task experiment, in which about 40 subjects were asked to classify beetles pictures according to a complicated set of category structures, finally being able to study the relations between stimuli and anticipatory SCR. In conclusion the method was found to be useful and effective in experimental settings where tight sequences of stimuli are presented, extracting individual ‘bursts’ so as to reconstruct the individual SCRs.

CTTP method is unable, they claim, to handle SCRs temporally contiguous in a satisfactory fashion, because CTTP underestimates the true amplitude, onset time, rise-times and number of SCRs. The underlying assumptions are also simpler than the method of (Lim, et al., 1997) and no function fitting is required. Scoring is completely automated, requiring not human supervision once parameters setting have been chosen.

4.4 The Ledalab Software

It is a Matlab-based software for the analysis of skin conductance data (SC; i.e., EDA, GSR). It can import various file formats (including BioPac, Biotrace, CassyLab, PortiLab, PsychLab, VarioPort, VisionAnalyzer, VitaPort) and provides many preprocessing functions. It can perform event-related analysis relative to events/marker and returns various parameters of phasic and tonic activity. It can be used via an interactive GUI or in an efficient batch-mode via the Matlab command window. It currently provides two EDA analysis methods:

1. The Continuous Decomposition Analysis (CDA) performs a decomposition of SC data into continuous signals of phasic and tonic activity. This method takes advantage from retrieving the signal characteristics of the underlying sudomotor nerve activity (SNA). It is beneficial for all analyses aiming at unbiased scores of phasic and tonic activity.
2. The Discrete Decomposition Analysis (DDA) performs a decomposition of SC data into distinct phasic components and a tonic component by means of Nonnegative Deconvolution. This method is especially advantageous for the study of the SCR shape.

Ledalab has been used at more than 60 universities and research facilities and is licensed under the GNU General Public License. (www.ledalab.de).

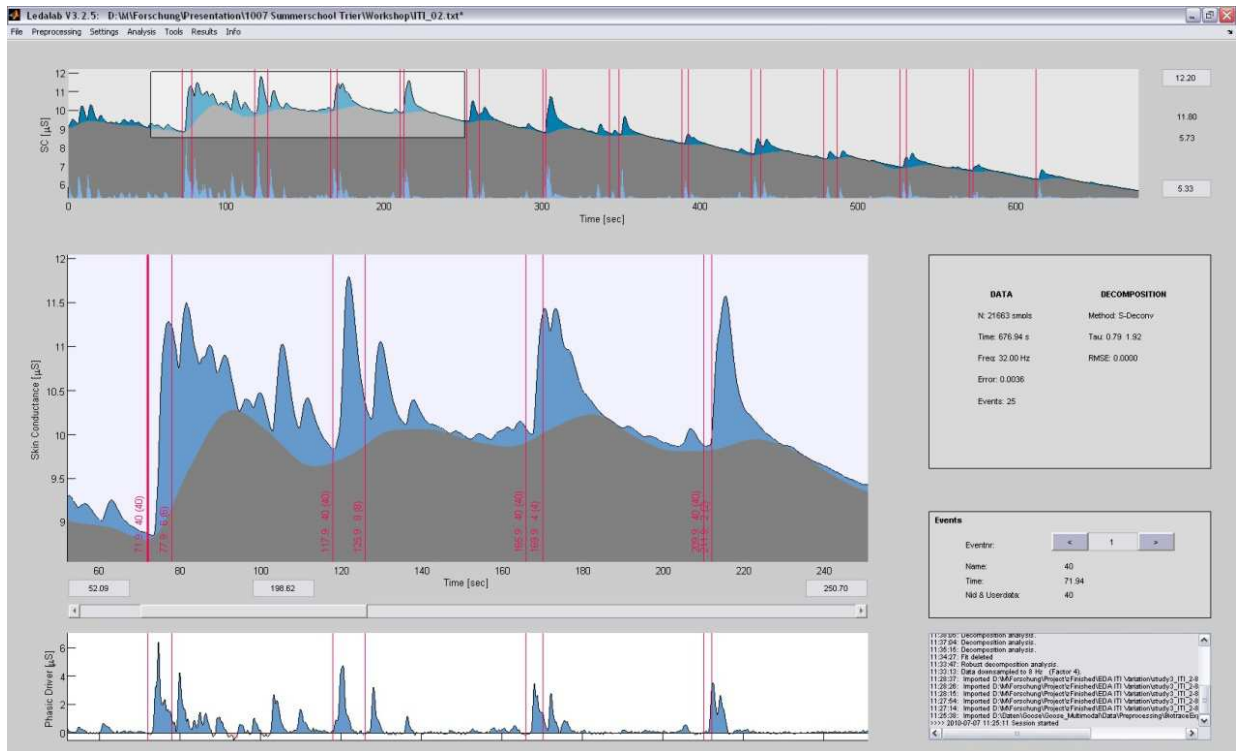


Figure 4-5: Ledalab screenshot

4.4.1 The Continuous Decomposition Analysis (CDA)

The outcome of this algorithm is a continuous tonic and phasic signal constituting SC signal. The resulting driver shows a zero baseline and overlapping SCRs represented by predominantly distinct, positive, compact impulses showing an average duration of less than 2 sec. A time integration of the continuous driver activity is proposed a straightforward indicator of event-related sympathetic activity (Benedek, et al., 2010a).

This is based on a standard deconvolution algorithm. By employing inter-individually adjusted IRFs with short time constants combined with a technique for the estimation and subtraction of tonic activity, one continuous estimate of phasic activity is obtained, which is compatible with a stable IRF. This approach is different because it abandons the concept of single, discrete responses in favor of a continuous measure of phasic activity. The advantage in obtaining a continuous phasic activity is the assessment of a straightforward indicator of event-related activity by means of response window integration. The extraction process is based on 3 steps:

1. Deconvolution of SC data
2. Estimation of Tonic activity
3. Estimation of phasic activity.

1. Deconvolution of SC data

The deconvolution process is performed initially using a predefined parameter set ($\tau_1=0.75$ s , $\tau_2=2$ s), parameters which characterize the shape of the IRF. After the first iteration of deconvolution, a performance parameter describing the goodness of the IRF applied to the signal under analysis is determined. The performance parameter takes into consideration the rate of negativity (*neg*) of the phasic driver (undesired condition) and the indistinctness (*ind*) of the impulses in the phasic driver (situation of distinct, compact (short support) impulses). By rerunning all 3 steps for each new parameter set, the model goodness is brought to its optimum. Hence, it has been obtained the total driver signal.

The rationale under their algorithm is represented by the next formulas (Equation 4 and Equation 5):

$$SC = SC_{\text{tonic}} + SC_{\text{phasic}} = SC_{\text{tonic}} + \text{Driver}_{\text{phasic}} * \text{IRF}$$

Equation 4: Decomposition of SC in parts

$$SC = (\text{Driver}_{\text{tonic}} + \text{Driver}_{\text{phasic}}) * \text{IRF}$$

Equation 5: SC expression

The SC signal is conceived to be composed by the tonic and phasic signals. As phasic signal, the tonic signal activity can equally be represented as the convolution of some sort of tonic driver function convoluted with the same IRF used for estimating the phasic driver. Although mathematically correct, this procedure is not physiologically motivated but this is not relevant because the tonic signal will be re-obtained by means of convolution process when phasic driver will be estimated. The phasic driver and tonic driver are represented in the second plot in Figure 4-6.

2. Estimation of tonic activity

It must be noted that the total driver signal shows time intervals of inactivity between the compact distinct phasic driver bursts. Those time intervals can be used to estimate the tonic activity. After a threshold on amplitude of phasic driver peaks and a specific smoothing operation on the entire driver signal, a cubic spline interpolation procedure is applied in order to extend the estimation of the tonic driver to the total time range. The slow varying parts of the total driver signal corresponding to the time intervals characterized from the absence of phasic peaks is conceived as the tonic driver. Hence, the tonic driver is interrupted by the occurrence of distinct, positive and compact phasic activity peaks. The cubic spline is used to estimate the tonic driver discarding the phasic driver activity. The spline passes by the points of the total driver signal between the phasic peaks on a grid made of 10 seconds spacing points. The obtained tonic driver is then convolved with the IRF and the tonic signal is estimated.

3. Estimation of phasic activity

The phasic driver is then obtained subtracting the tonic driver (estimated by the cubic spline) by the total driver signal. Hence it should be obtained a phasic driver with zero baseline and positive deflections (last plot in Figure 4-6).

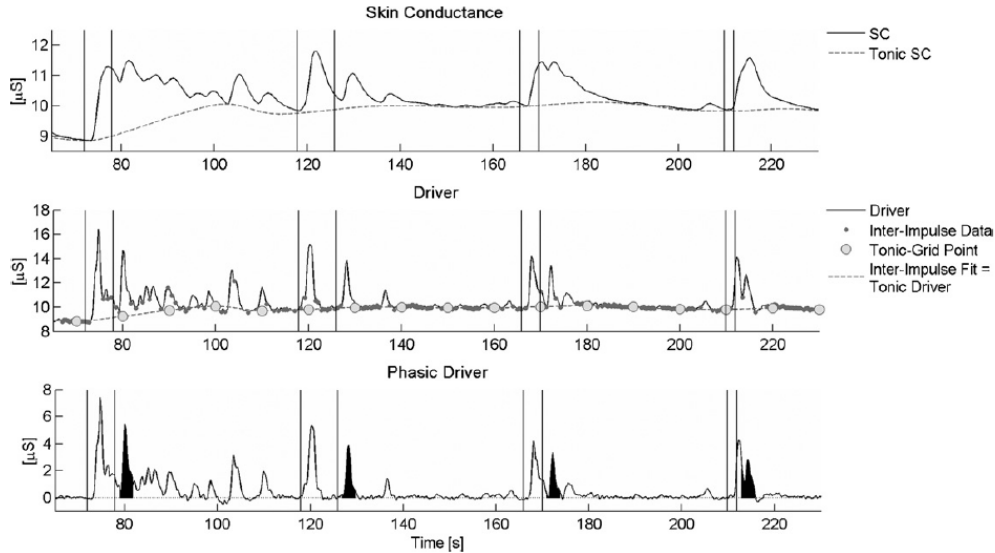


Figure 4-6: (Top) SC signal with estimated tonic signal, (Middle) Sum of tonic and phasic driver, (Bottom) Phasic driver

In contrast to non-negative deconvolution, the phasic drive may assume negative values. These negativities may arise from the selection of a sub-optimal IRF or from artifacts in the recorded SC data. In contrast to non-negative deconvolution (Benedek, et al., 2010), the phasic drive may assume negative values. These negativities may arise from the selection of a sub-optimal IRF or from artifacts in the recorded SC data. Hence this could be an information on the quality of the extraction algorithm and of the original SC

data. Again, phasic SC data could be retrieved by convolution of the phasic driver with IRF. Adding phasic and tonic data perfectly adds up to the original SC data.

4.4.2 Nonnegative deconvolution (DDA) (Benedek, et al., 2010)

A new approach has been recently published by (Benedek, et al., 2010), attempting to decompose superimposed SCRs not only by a mathematical modified deconvolution method (non-negative) but as well taking into account a particular model of the electrodermal system, i.e. the “poral valve model” (Edelberg, 1993).

Actually we can synthesize it as a “two-compartment diffusion model”. The innovation introduced by those authors, consisted in affirming that SCR shape could be described by contribution of two different underlying physiological processes:

1. an unconditional slow diffusion process which would cause a rather flat SCR
2. a pore-opening process, having the property bring about a steep peak to this basic SCR shape.

Thereby now we have two different processes involved in creating the SCR shape. Their quantitative approach to the slow process (1) is based on a diffusional model describing the dynamics of sweat concentration in the corneum, supposed to be ruled by the laws of diffusion (Schneider, 1987), (Edelberg, 1993). To describe the aforementioned model dynamics, they use the “Batemat function”, well known from pharmacokinetics area, where a biexponential function has been used to quantitatively describe the course of the drug concentration observed in a body compartment, being a result of its first-order invasion into this compartment and its first-order evasion out of it (Boucsein, 2011). An equivalent assumption explaining pore-opening component has not been made. By means of SC signal can be decomposed into a tonic component and a number of separate phasic components.

The authors addressed the problem of the possible negative driver signal values and put forward the decomposition of SC data by means of non-negative deconvolution. This method claims non-negativity of the driver and maximal compactness of the impulses. It offers a technique for the estimation of the tonic activity based on a fit of the inter-impulse intervals of the driver resulting from standard deconvolution. Phasic activity can then be extracted by subtracting the SCL from the SC data. Non-negative deconvolution, applied to the phasic SC data, results in two phasic signals, a non-negative phasic driver and a remainder. The phasic driver is found to exhibit a zero baseline intermitted by predominantly distinct peaks whereas the remainder signal captures all deviations from the standard SCR shape. These deviations were found to show a specific pattern contingent to the SCR peak and the authors hypothesized that they reflect a pore opening process. This method accounts for inter-individual differences in the SCR shape and

selects the most adequate τ parameters for the IRF in the course of an optimization procedure. The slow recovery process revealed by this method seems to correspond closely to the sweat diffusion from the skin. This approach is based on the assumption that variations of the shape of the SCR are due to pore opening processes occurring in close temporal vicinity to the SCR peaks.

4.5 Conclusion

To sum up, the various based deconvolution methods offer considerable progress in the evaluation of overlapping SCRs which are very common to stimulus sequences with short ISIs. However, they all have in common that – once the basic evaluation procedure has been determined – EDA data are parameterized fully automatically. This surely saves evaluation time compared with the traditional evaluation of superimposed EDRs, but it also bears the disadvantage of losing the contact to the original EDA signal, thus overlooking critical events such as types of artifacts which cannot be automatically detected. Therefore, for the time being, semiautomatic interactive evaluation procedures should be at least applied in parallel to highly automated evaluation procedures.

4.6 Novel algorithms – BC method

Barbieri-Citi algorithm estimates the spike sequences underlying SC signals providing spike amplitudes and temporal occurrences. This algorithm has been developed by Citi Luca and Barbieri Riccardo, from MIT laboratory in 2010. Till now (June 2013) it is unpublished. In chapter 6.1 the determination of S_w and B_w parameters.

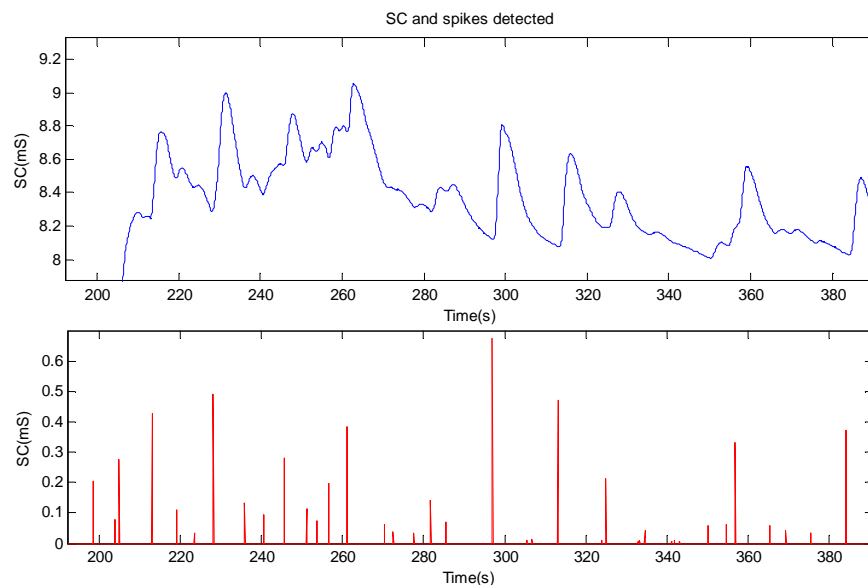


Figure 4-7: Spike sequence from BC algorithm

4.6.1 Method

Hanning window (H_{sw}) with a number of coefficients equal to twice the product between the sample frequency of SC and a chosen S_w parameter is obtained and then normalized dividing it by half the number of coefficients. This is an area normalization which makes unitary the area under H_{sw} . The filtered SC first derivative (FD) by H_{sw} provides FD_{sw} . A second hanning window (H_{bw}) is obtained as for H_{sw} but using B_w instead of S_w . FD_{sw} is then filtered by H_{bw} and the result (FD_{swbw}) is subtracted from FD_{sw} obtaining Q signal.

After the negative Q signal part is suppressed (Q+), the first derivative is calculated (DD2) and its zero crossing with negative first derivative (positive to negative) and positive first derivative (negative to positive) are obtained (Max and Min respectively). The first and last Min values must be respectively lower than the first and last Max values. The spike amplitudes correspond to Q+ signal values calculated at Max indexes whereas they are located according to Min indexes.

4.6.2 Appendix

In Figure 4-8 some normalized hanning windows as described in chapter 4.6.1

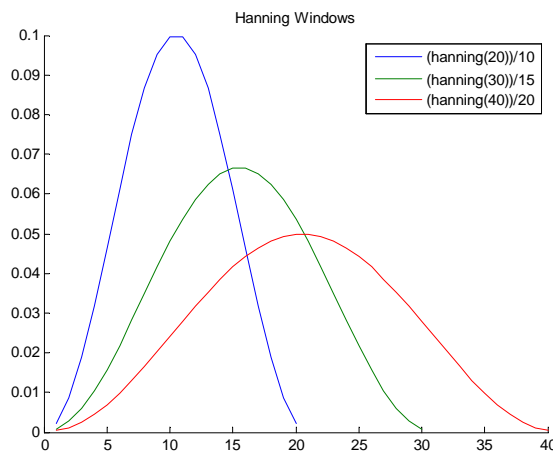


Figure 4-8: Hanning Windows

The SC signal is processed with a cascade of three filters. The Derivative Filter, H_{sw} , H_{bw} and cascade filter frequency responses are depicted in Figure 4-9.

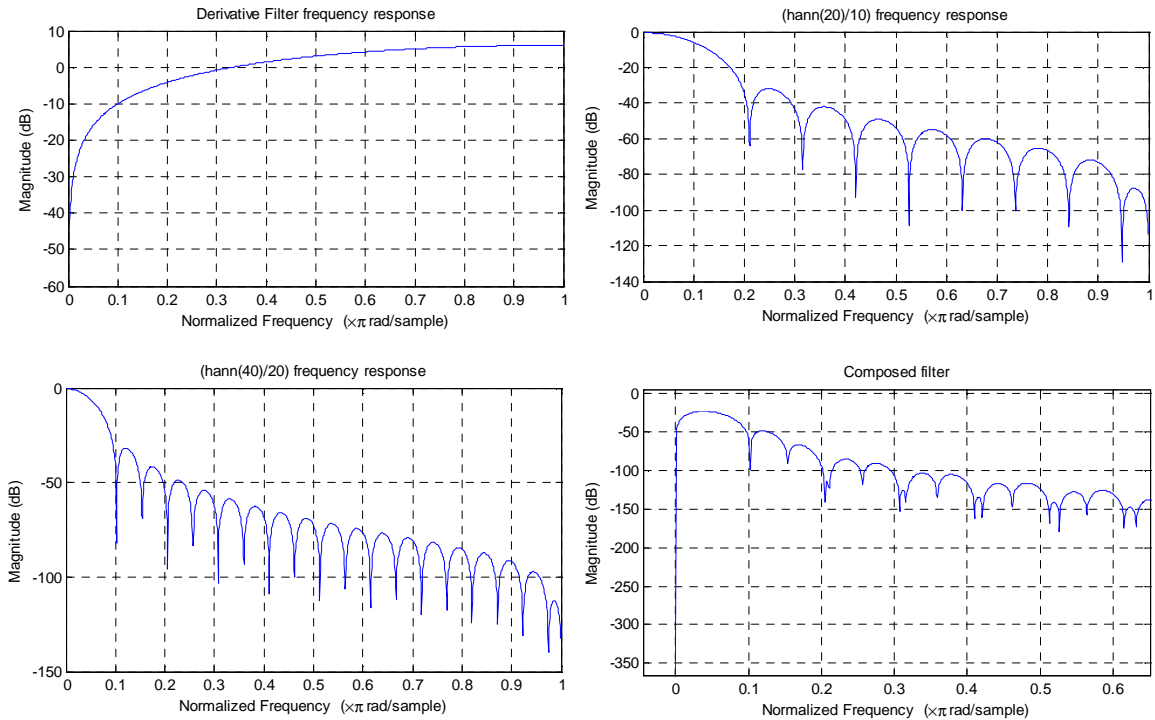


Figure 4-9: Filter frequency responses

It must be noted (Figure 4-9) the dependence of the hanning windows cut-off frequencies on hanning shapes (Figure 4-8) so that the more the number of coefficients the lower the cut-off frequency. The cascade is a band-pass filter. In Figure 4-10 a schematic of the three filter frequency responses. The first derivative excludes continuous frequency (0 Hz) whereas S_w and B_w determine the band pass cut-off frequencies. To obtain *Cutoff* B_w minor than *Cutoff* S_w (Figure 4-10) B_w must necessarily be greater than S_w (Figure 4-10) if not their positions would be switched. Figure 4-10 agrees with this. They must be inevitably different to design a bandpass filter but their relation is not imposed.

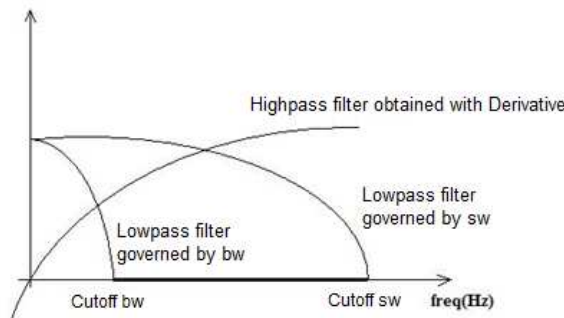


Figure 4-10: Schematic of the three filter frequency responses

The algorithm relies on the proper S_w and B_w values and we will investigate them as described in chapter 6.1.

5 Surrogate SC signal

In this chapter we will describe how we generated the surrogate SC signals. We aimed at obtaining a surrogate SC signal which mimics as close as possible the real one. Therefore, we modeled both phasic and tonic parts, which were generated separately.

To model the phasic part of the SC signal, we started by generating a sequence of spikes (imitating the sequence of the sudomotor nerve bursts underlying the skin conductance responses) and then convolving them with a properly chosen impulse response function (IR_p). In doing this we had to select the spike probability distribution and select the most appropriate IR.

To model the tonic part we used the spike sequence already used for the phasic part and then convolving them with a properly chosen response function called IR_t .

Finally, a realistic noise was added to the surrogate SC signal. The property of the noise was derived from real recordings. Details about the procedures are described above.

5.1 Method

5.1.1 Choice of the probability distribution governing spike time occurrences

This probability distribution depicted in Figure 5-1 rules the occurrence (time instant) of the spikes in the sequences. We chose an inverse Gaussian distribution and the reason of this choice is depicted in Figure 5-1:

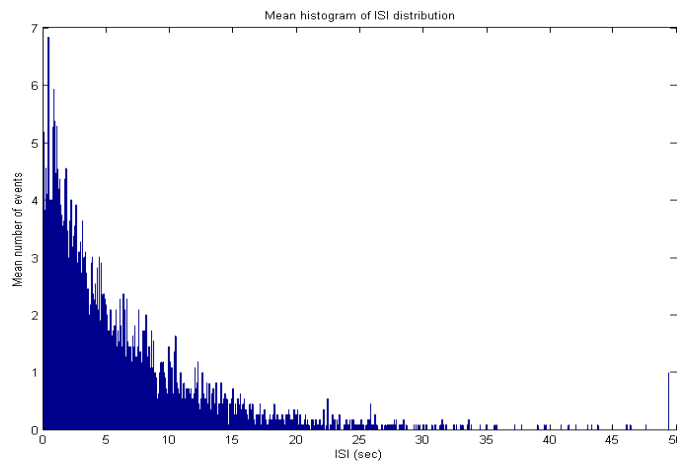


Figure 5-1: Mean ISI histogram

Figure 5-1 depicts the mean histogram obtained from 11 different histograms. Each of them is estimated from real SC data by calculating the time (in seconds) existing between two successive local minima in the signal. We assumed that each local minimum is approximately the time instant where a sudomotor burst starts. In Figure 5-1 we can observe a curve approximating an inverse Gaussian probability distribution function. The theoretical inverse Gaussian distribution is depicted in Figure 5-2.

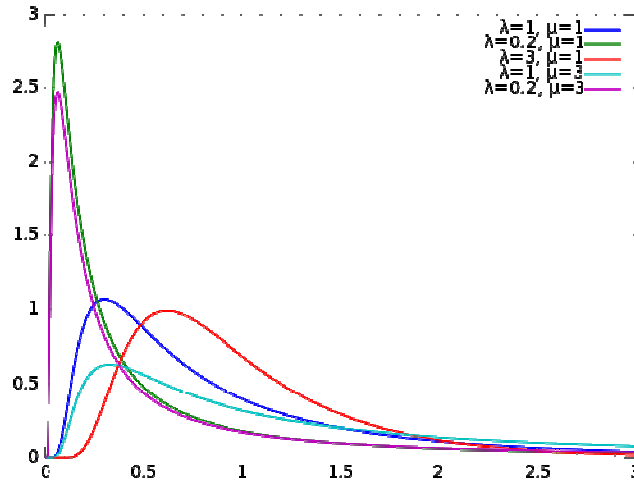


Figure 5-2: Inverse Gaussian. (Wikipedia)

5.1.2 Choice of the proper IR function

We focused our attention on two candidates for IR function: the first one was proposed by (Alexander, et al., 2005), and the second by (Lim, et al., 1997), which were presented in chapters 3.7. Between them we selected the Alexander's one because the underlying model allows a better control on several IR properties including IR magnitude, rising time, decaying time and onset time. In addition the resulting shape is more realistic. In Figure 5-3 the two functions are shown.

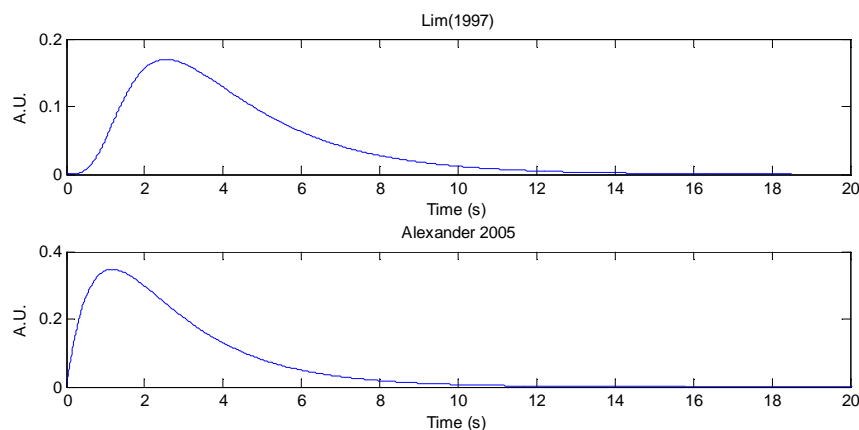


Figure 5-3: Lim's (top) and Alexander's (bottom) impulse response.

We notice the lack of control in onset time in Alexander's curve (bottom).

5.1.3 Choice of the probability distribution governing spike amplitudes

The amplitude of the spikes in the sequences is chosen randomly according to a Gaussian distribution with mean of 20 a.u. and STD 19 a.u. with a suppression of sign is applied to the outcome in order to avoid negative amplitude values. In Figure 5-4 an example of a sequence of 100 spikes is depicted.

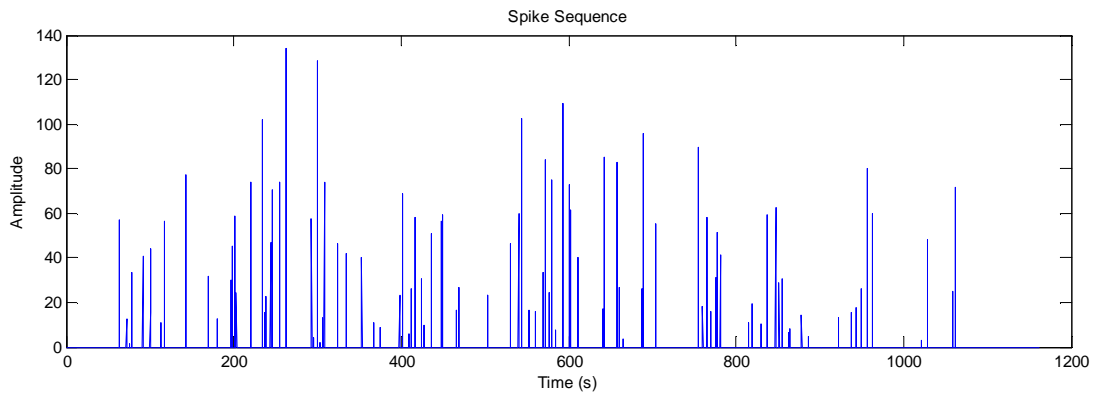


Figure 5-4: An example of spike sequence: the spikes time instants are governed by an inverse Gaussian distribution whereas the amplitudes are chosen with a Gaussian probability distribution.

5.1.4 Creation of the phasic part of the signals

We are now able to obtain the phasic part of the SC signal by convolving the spikes of the sequences with the selected IR function; in the convolution process for each spike is used a slightly different IR shape: this was obtained by varying the Lim's IR function parameters for each spike.

This choice was motivated because of research results on differences in SCR rise-time and recovery-time indicate that SCR shape shows not only a significant inter-individual variability but also a significant intra-individual variability (Breault, et al., 1993), (Edelberg, et al., 1981), (Janes, et al., 1985).

In details, the IR variability was obtained by randomly changing the governing parameters by means of a Gaussian distribution with a selected mean and SD for each parameter. In the following the list of modified parameters and the indication of their range.

- Onset time parameter= mean 0.001 s, STD 0.001 s
- Magnitude= mean 2, STD 0.01 s
- Rising time = mean 1.59 s, STD 0.09 s
- Decaying time=mean 3 s, STD 0.25 s

An example of 100 generated IRs is shown in Figure 5-5

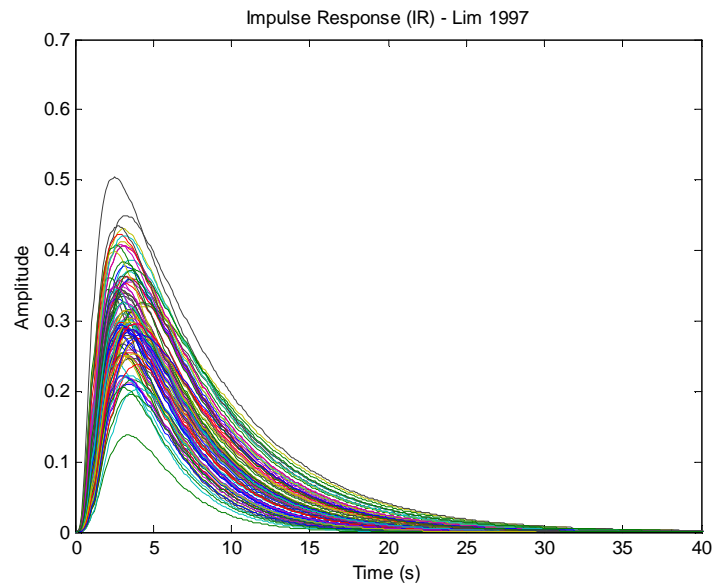


Figure 5-5: Group of 100 IR curves

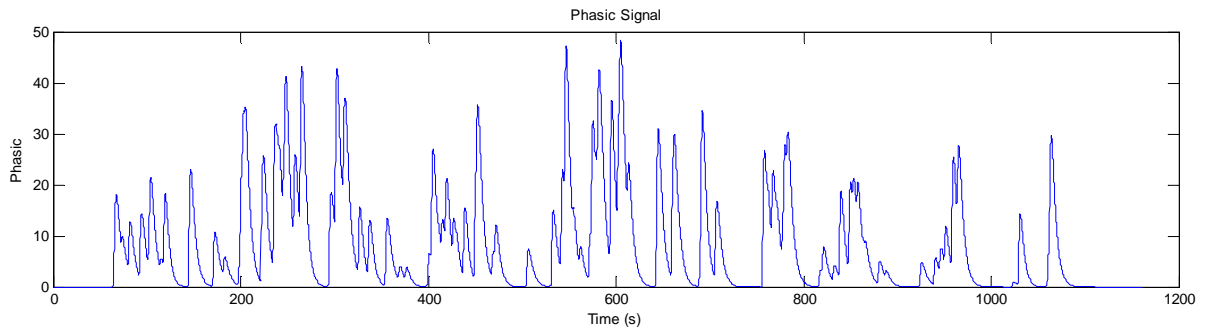


Figure 5-6:SCR part

Figure 5-6 shows an example of signal, obtained convolving the sequence of spikes in Figure 5-4 with the IR curve in Figure 5-5.

Figure 5-7 depicts the relation between a spike and the subsequent skin conductance response: the latency time between a spike and the subsequent SCR in a exosomatic recording range normally from 1 to 2 seconds (Boucsein, 2011), and in the surrogate signal this requirement is accomplished.

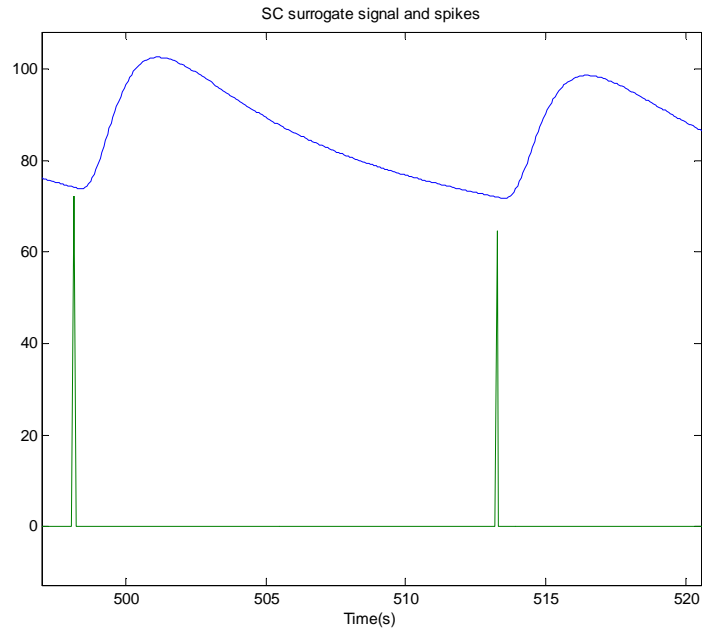


Figure 5-7: Spike and SCR

5.1.5 Tonic signal

In order to obtain the tonic part, we computed the convolution between the same spike sequences used for the phasic part and a fixed IR properly chosen. We used Lim's IR function this time with a low value for T_r parameter (rising time constant) and a high value for T_d (decaying parameter) according to the following proportion $T_r/T_d=1/55$. In this way, the rising part of the curve is steep compared to the decaying part (tail) which is much slower. It can be observed that the rising part is much more steep than the tail (decaying part).

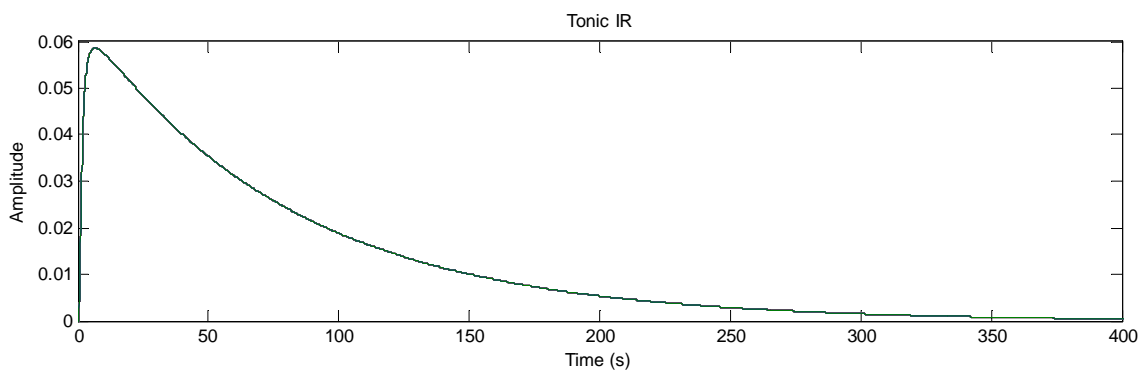


Figure 5-8: IR of tonic signal

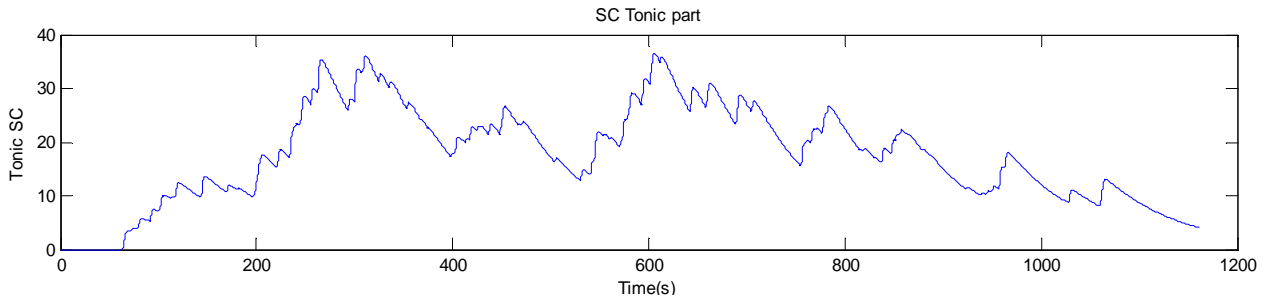


Figure 5-9: Tonic signal

We obtained a slow varying signal, typical of a tonic signal. The reason why we adopted this technique (using a convolution to obtain the tonic part) is because it is well-known that the phasic and tonic activity in a SC signal are not completely independent: when the phasic part increase its activity (more frequency of sudomotor spikes) the tonic part increases as well, so that an higher sudomotor activity (simulated with many spikes packed together in time) generate an higher activity both in phasic and tonic part, as depicted in Figure 5-10 and Figure 5-11 where phasic and tonic parts have been superimposed. The red curve is the phasic part whereas the green one is the tonic part. In blue the final result.

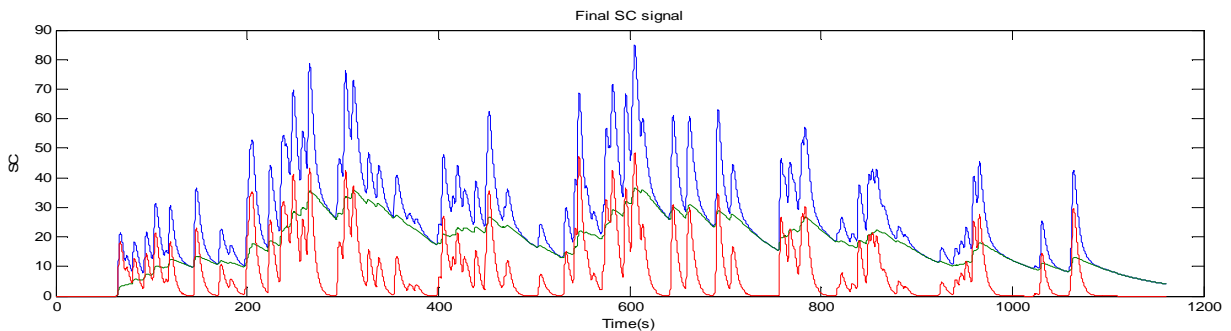


Figure 5-10: Summing of phasic part (red) and tonic one (green). Outcome in blue

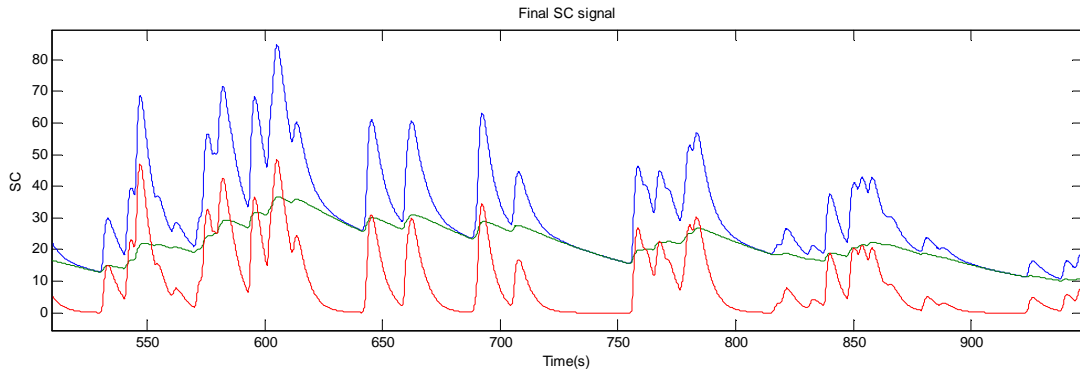


Figure 5-11: Magnification of a section in Figure 5-12

5.1.6 Adding realistic noise

In order to make our surrogate signals as realistic as possible we also added a noise contribute. Choosing the proper noise characteristics is not such straightforward because real SC signals might be influenced by external or internal stimuli acting as noise sources (see Chapter 3.5 EDA elicitation at pag. 36) such as deep breathing, cough or movements due to psychological and physical stress.

We determined the noise features by calculating the mean spectrum obtained from 10 real SC signals chosen from the Emotion DataSet. Figure 5-13 depicts the mean spectrum in a log-log scales. It has to be noticed that at high frequencies the spectrum power falls 10 dB/decade according to the characteristic pattern of a Pink noise (also known as 1/f noise or flicker noise) whose power spectral density is inversely proportional to the frequency. It occurs in many physical, biological and economic systems and some researchers describe it as being ubiquitous [3].

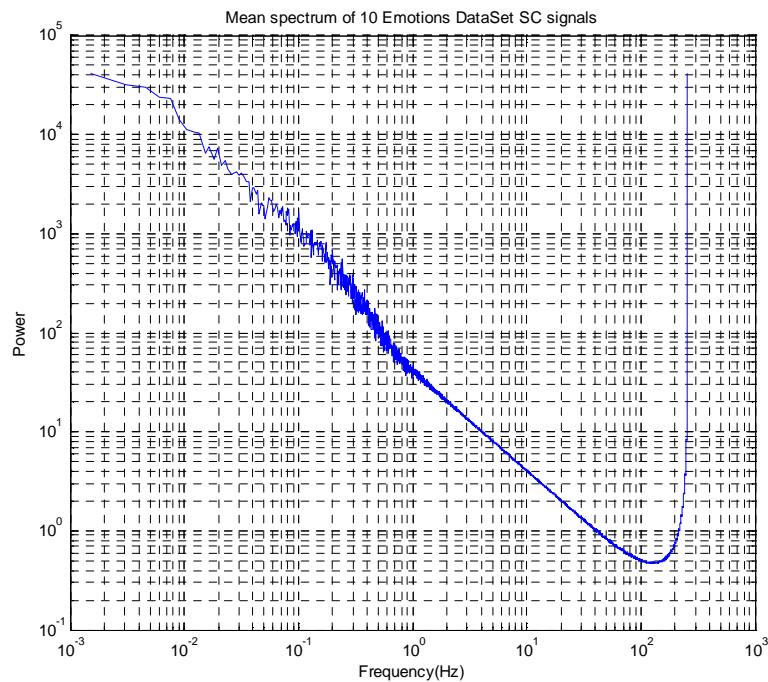


Figure 5-13: Pink Noise obtained as the mean spectra of 10 realistic SC signals from “Emotion Dataset” (see chapter 7)

Figure 5-14 depicts an example of flicker noise with mean 0 and variance 1.

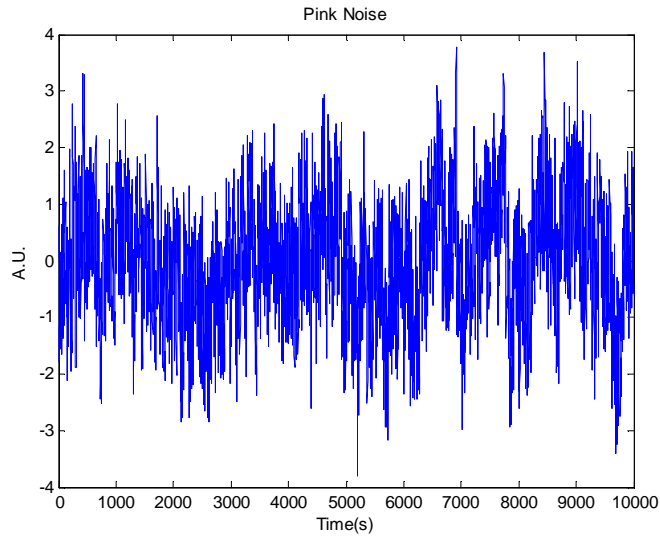


Figure 5-15: Example of pink noise with mean = 0 and variance = 1

To obtain the proper flicker noise to add to the signals, it is necessary to calculate the variance of the final SC signal (from now “SC_clean” to distinguish it from the noisy signals) and then create a flicker noise with a variance calculated according to a specified signal-noise ratio (S/N ratio). To achieve this goal we calculated the variance of the surrogate SC signal after having discarded the beginning 20% and final 10% sections of signal length, to avoid the transients epoch at the beginning and end of surrogate data To demonstrate the effect of the noise, Figure 5-16 depicts the same interval of a chosen surrogate affected from noise but with varying S/N ratio (read titles of the plots).

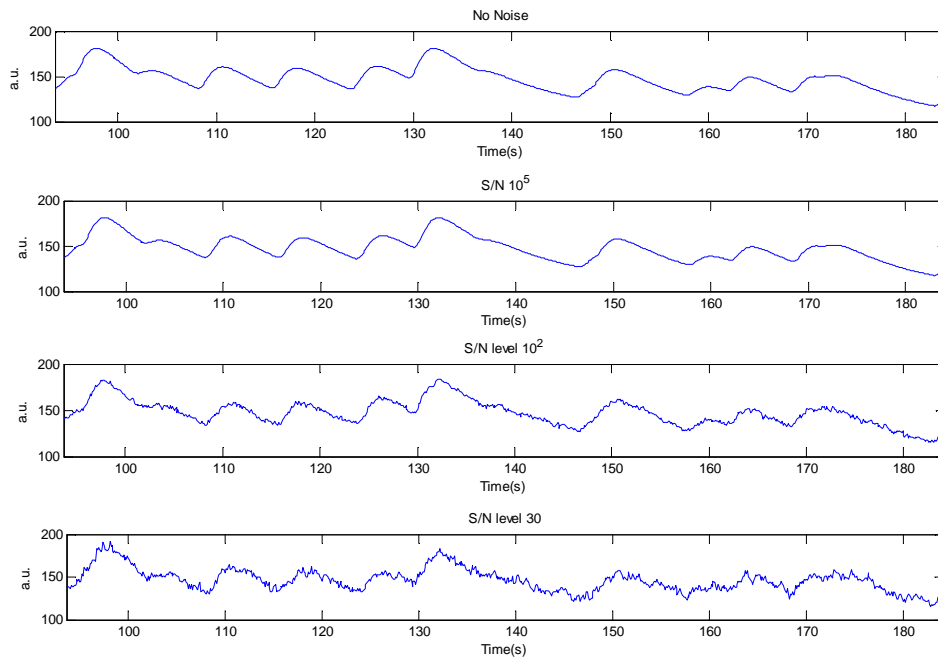


Figure 5-16: Same interval of signal affected with different noise level.

The bottom plot is the most noisy.

5.1.7 Final SC signal

In Figure 5-17 and Figure 5-18 are shown two examples of surrogate signals and in Figure 5-19 a real SC signal from Emotion DataSet (see chapter 7) is depicted.

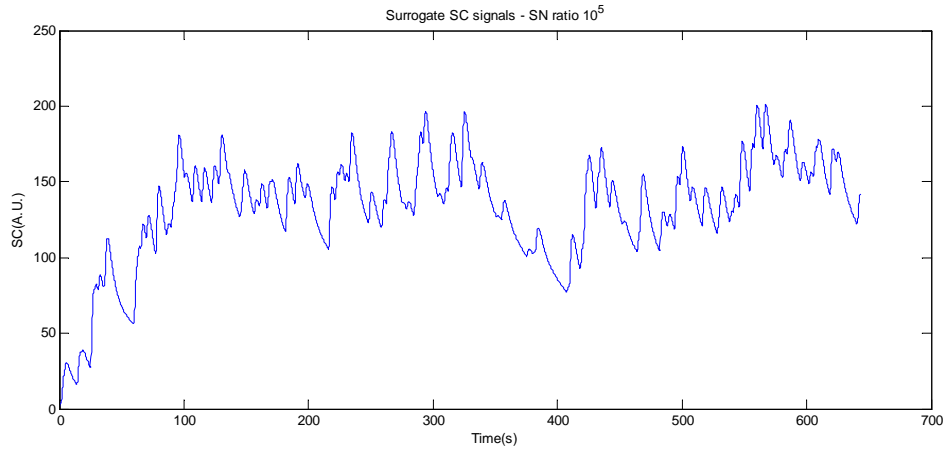


Figure 5-17: Surrogate SC signal with SN noise equals to 10^5

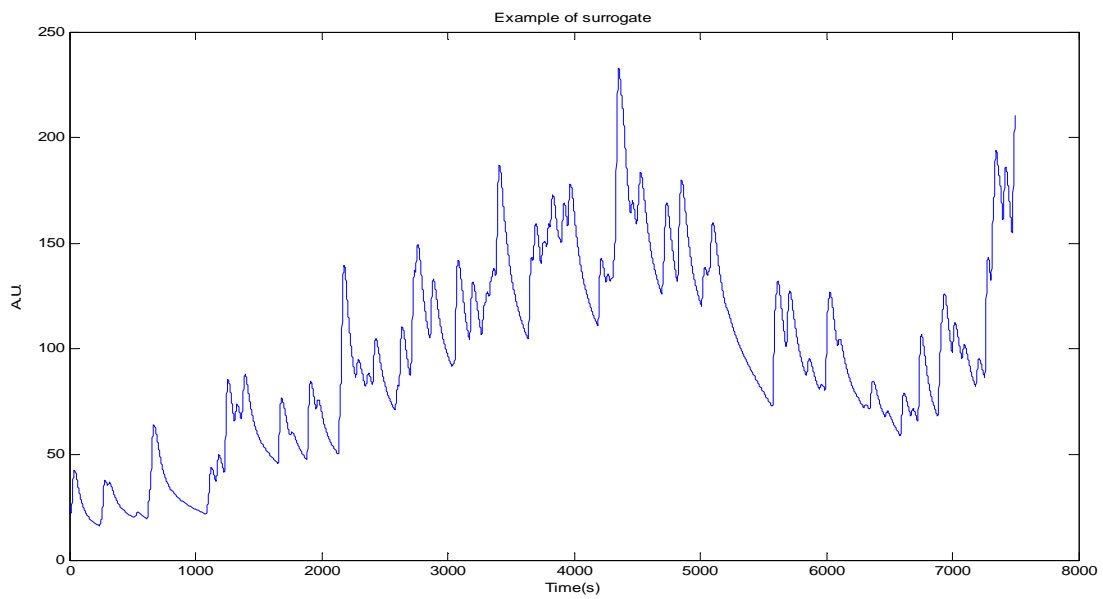


Figure 5-18: Example of surrogate SC signal with S/N ratio 10^5

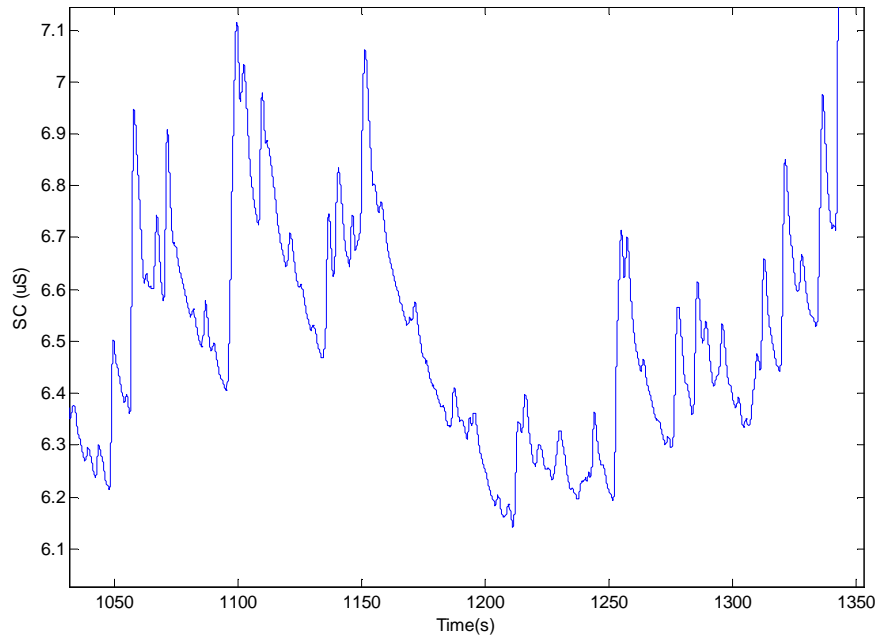


Figure 5-19: Example of real SC signal

5.1.8 Creation of the datasets

We created, starting from a noiseless dataset (SC_clean) 4 datasets containing the same surrogate SC at different S/N levels: $10^3, 10^4, 10^5, 10^6$ respectively. SC_clean was created according to the following specifications:

- The inverse gaussian distribution mean (determining the temporal occurrence of the spikes) is fixed for each generated sequence and ranges between 6 s and 15 s according to a uniform distribution.
- The inverse gaussian distribution variance (determining the temporal occurrence of the spikes) is fixed in each generated sequence and ranges between 7 s^2 and 12 s^2 according to a uniform distribution.
- Number of spikes for each sequence is set to 100.
- Total number of surrogate signals is 78.
- The sample frequency is 10 Hz.

6 Comparison of Methods using simulated data

We estimated the detection performances by comparing the True Spikes (TS) sequences generating the surrogate SC signals with the Spikes (GS) sequences as output by BC and CDA Ledalab algorithms. The software matches the sequences of TSs and GSs distinguishing three cases (Figure 6-1)

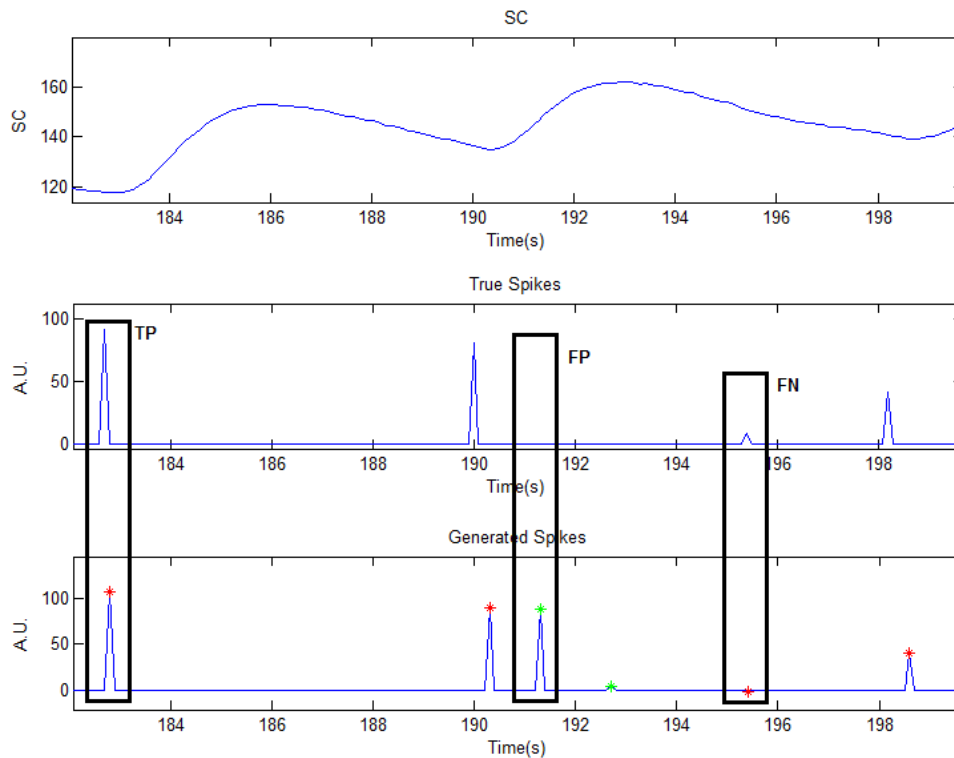


Figure 6-1: False Positive, False Negative, True Positive

A GS is recognized as True Positive (TP) when it is closer than 1.5 seconds backwards or afterwards to a TS and in case of detection of many GSs the closer one is counted as TP ignoring the others. Before proceeding further this GS is deleted from the sequence in order not to interfere with successive detections. When it is not possible to detect a GS in correspondence of a TS (within the temporal window), a False Negative (FN) is counted. The GSs not marked as TP and FN are marked as False Positive (FP).

In case of fixed shift in GSs sequence causing a skew between the spikes of the two sequences, an iterative process of detection is performed each loop shifting GS sequence. It is then chosen the delay that maximizes the number of TP.

After calculating the FPs, FNs and TPs from each surrogate signal in a dataset, we obtained the total number of FP, FN and TP of the dataset. The Sensitivity (SE) and Positive Predictive (PP) Value are obtained as follows.

$$SE = \frac{TP}{TP + FN}$$

$$PP = \frac{TP}{TP + FP}$$

Equation 6: SE and PP formulas

6.1 Tuning Barbieri Citi Algorithm

We tested the performances of BC algorithm on with various S/N ratio on the 78 surrogate signals of DataSet10Hz and at the same time we tuned up the parameters governing the algorithm to make it reach the best performances. We estimated its performances in detecting burst activities by means of ROC curves.

The algorithm is characterized by two parameters S_w and B_w , both determining the cut off frequencies of two low-pass filters. We tested the algorithm in various working conditions by varying $S_w=[0.1:0.1:1.3]$ and $B_w=[0:5:100]$ and examining the output for every possible combinations of those parameters. Here it is important to highlight that when B_w is equal to zero then the filter governed by B_w is not applied in BC algorithm.

As a result, we have a SE and PP value for each S_w and B_w combination, which are used to build the ROC curves. In order to assess the best combination of parameters the closest (in terms of euclidean distance) point of the ROC to the point $(SE,PP)=(100\%,100\%)$ is determined. This procedure is repeated for each S/N level.

The ROC curves are plotted by fixing B_w values while varying S_w values according to the above mentioned ranges. Figure 6-2 shows the results obtained with S/N ratio equals to 10^6 .

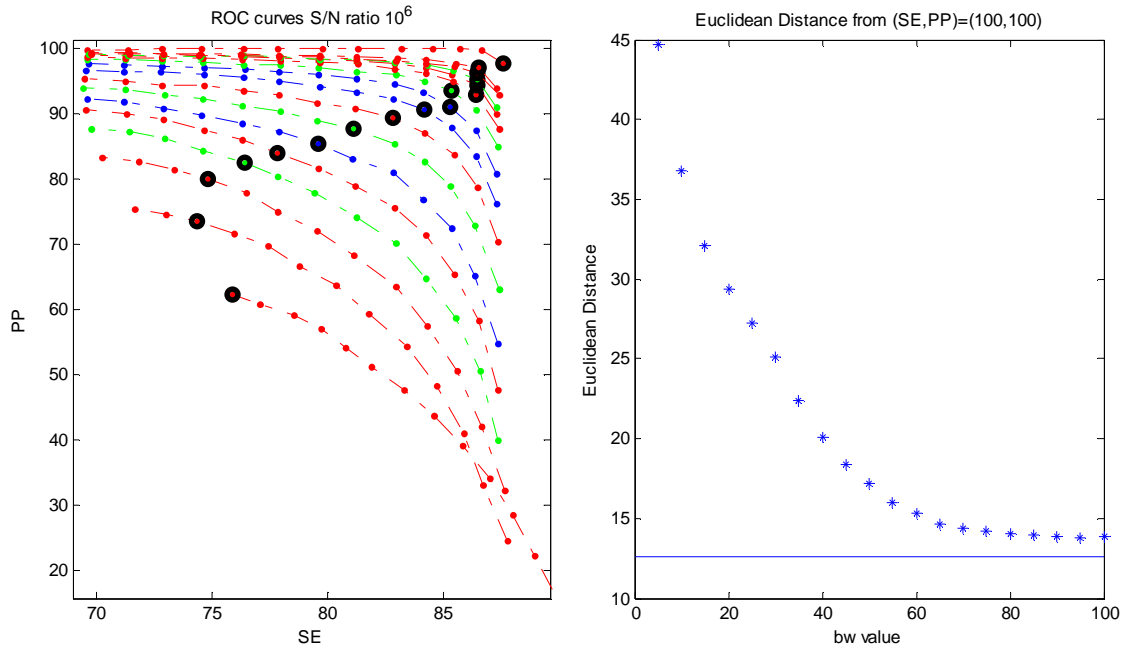


Figure 6-2: ROC curve (left) and Euclidean Distance (right)

The ROC curves of Figure 6-2 (left) move from bottom to top as the B_w value increases. On each ROC curves, the black thick circles indicate the closest points (in terms of Euclidean distance) to $(SE,PP)=(100,100)$. The value of the Euclidean distance is plotted in Figure 6-2 (right). It can be clearly observed that the more B_w value increases, the more the distances diminish asymptotically. This asymptote has been determined and plotted. Before explaining how we assessed it, it is necessary to observe Figure 4-10 in chapter4.6.2.

The consequence of increasing B_w value is a progressive shift of “Cutoff B_w ” towards zero. When $\lim B_w \rightarrow +\infty$ this would be 0^+ Hz and we can reproduce this condition not applying this filter. Thus the asymptote depicted in Figure 6-2 (right) is obtained for not applying the lowpass filter governed by B_w and the corresponding ROC curve is the very top one in Figure 6-2 (left).

In conclusion, for this S/N ratio (equals to 10^6), the best performance are obtainable when the B_w filter is not present and S_w is 0.1. The best performances are $SE = 87.61\%$ and $PP = 97.83\%$. The result for S/N level of 10^5 is depicted in Figure 6-3:

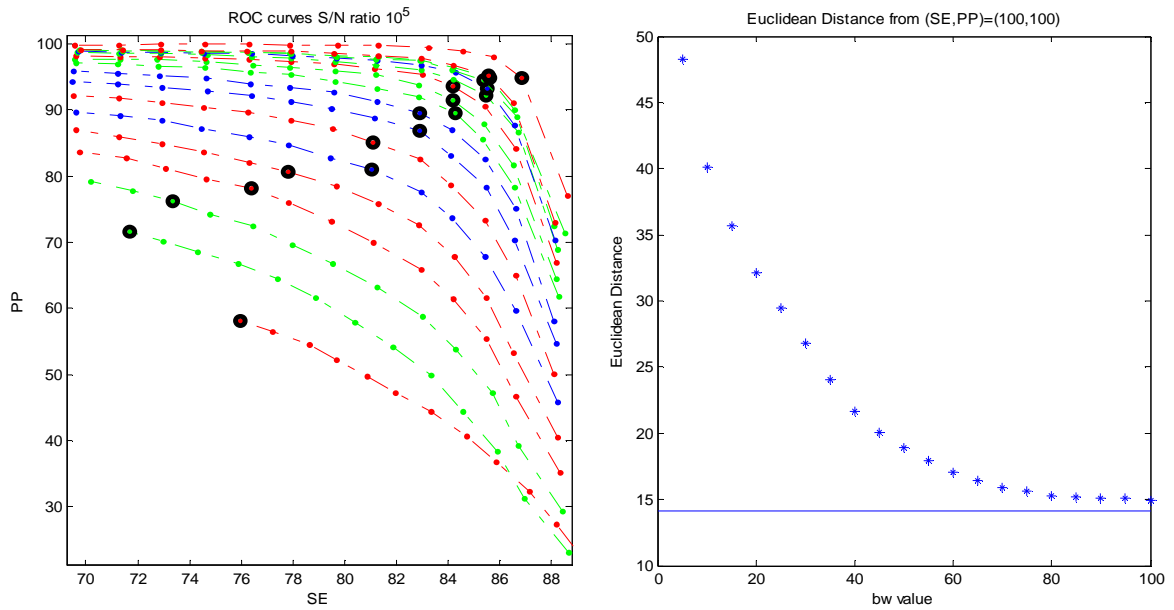


Figure 6-3: ROC curve (left) and Euclidean Distance (right)

It can be observed that ROC curves are shifted downwards in respect to the previous case. Again, the best results are obtained when the lowpass filter governed by B_w is not applied : the minimum Euclidean distance of 14.14 for $S_w=0.2$ and the SE is 86,84% and PP is 94,82%.

When signal-to-noise ratio is further decreased the previous trend is confirmed. Results are plotted in Figure 6-4 and Figure 6-5 respectively.

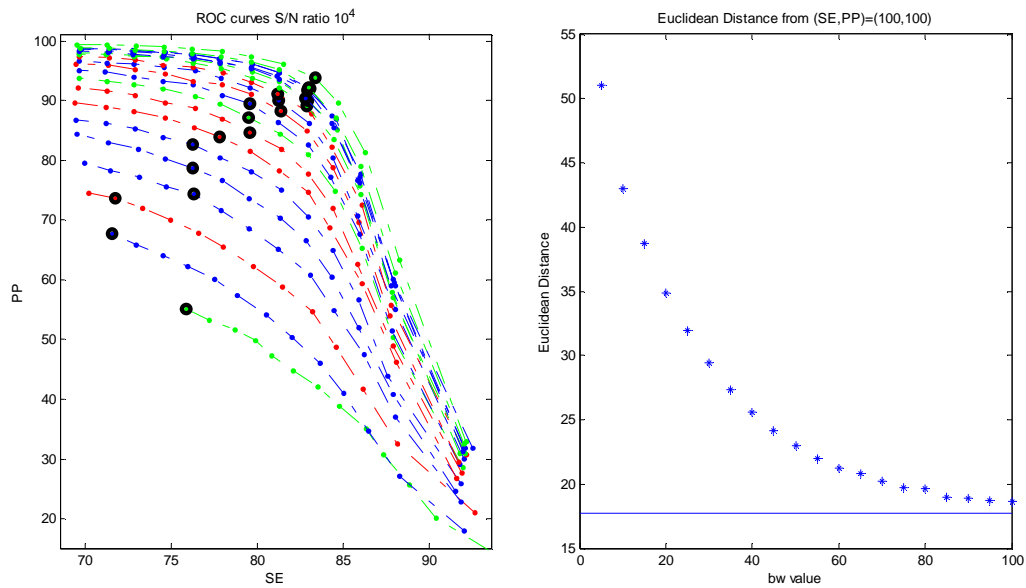


Figure 6-4: ROC curve (left) and Euclidean Distance (right)

Finally, for S/N ratio equals to 10^3 , the result is depicted in Figure 6-5:

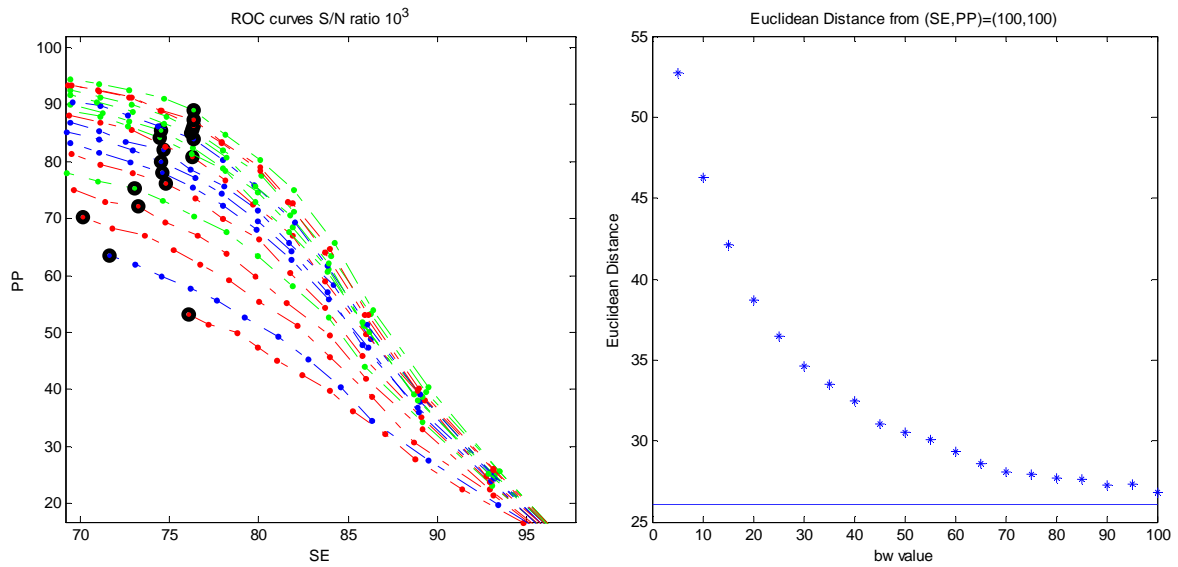


Figure 6-5: ROC curve (left) and Euclidean Distance (right)

For a better focus the best result for each investigated S/N ratios are reported in Table 6-1. We can notice a decay of the investigated parameter (SE and PP) when the S/N ratio decreases. This result was expected because the more the noise level is increases, the more the burst detection ability is compromised.

About the Euclidean distance, we can observe that the more the noise power decreases, the more the distances increases and this result is in agreement with SE and PP trends.

SN ratio	10^6	10^5	10^4	10^3
SE (%)	87,61	86,84	83,37	76,35
PP (%)	97,83	94,82	93,85	89,01
Eucl.Distance	12,58	14,14	17,73	26,08
Sw	0,1	0,2	0,5	0,9
Bw	Not appl.	Not appl.	Not appl.	Not appl.

Table 6-1: BC Results

6.2 Ledalab

We preferred the CDA method offered by Ledalab instead of DDA method (see chapter 4.4.2) because the CDA method tends to retrieve the signal characteristics of the underlying sudomotor nerve activity (SNA). In this way, a direct comparison with BC software is feasible.

Data must be a structure. Among the CDA algorithm setup, Ledalab let us choose to delete the detected spikes with amplitude less than a default value (0.2 uS as default value) but we did not eliminate any of them. Ledalab exports a structure containing the time instants of the spikes and the corresponding spike amplitudes according to “CDA” and “TTP” (Trough-to-peak analysis – see chapter 4.1) analysis. From these data, as described before we obtained the ROC curves varying the spike amplitude threshold from 0 uS to 20 uS with step of 0.2 uS.

On each ROC curves (Figure 6-6, Figure 6-6, Figure 6-7, Figure 6-8) the black thick circle indicates the closest points (in terms of Euclidean distance) to $(SE, PP) = (100\%, 100\%)$. In Figure 6-6 the ROC curve obtained with S/N level of 10^6 are shown. The best performances are SE and PP of 90.18% and 93.93% respectively for an amplitude threshold of 3.6 uS.

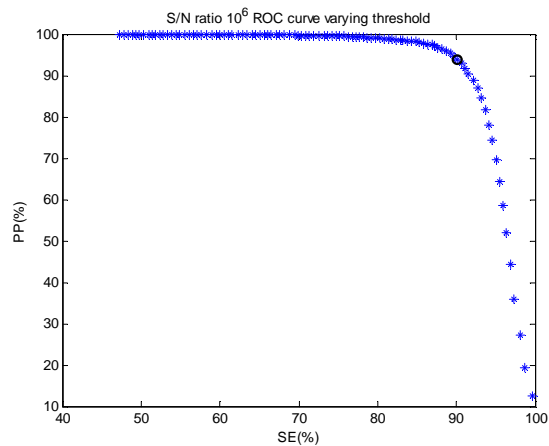


Figure 6-6: ROC curve with S/N ratio of 10^6 .

In Figure 6-7 the ROC curve for S/N level of 10^5 .

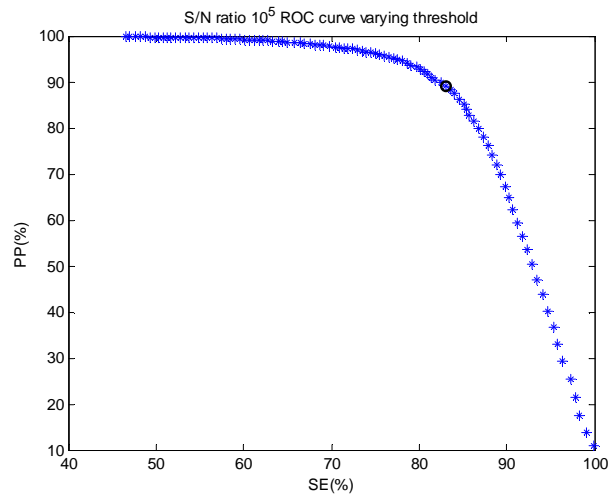


Figure 6-7: ROC curve with S/N ratio of 10^5 .

The best performance is 83.07% and 89.15% respectively for SE and PP with an amplitude threshold of 6.2 uS. In Figure 6-8 the ROC curve for S/N level of 10^4 :

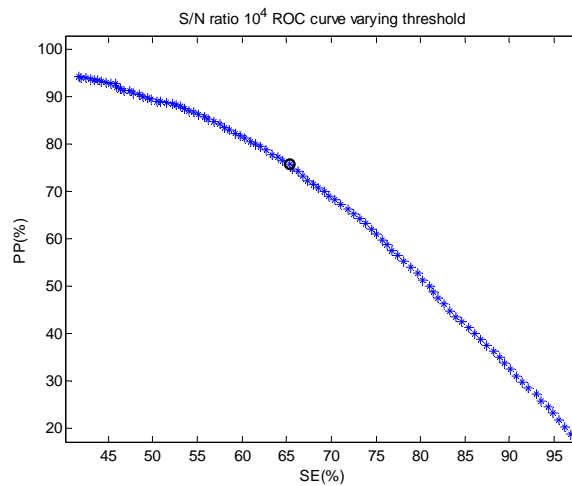


Figure 6-8: ROC curve with S/N ratio equals to 10^4

The best performance is 65.31% for SE and 75.77% for PP with an amplitude threshold of 11 uS.

In Figure 6-9 the ROC curve for S/N level of 10^3 :

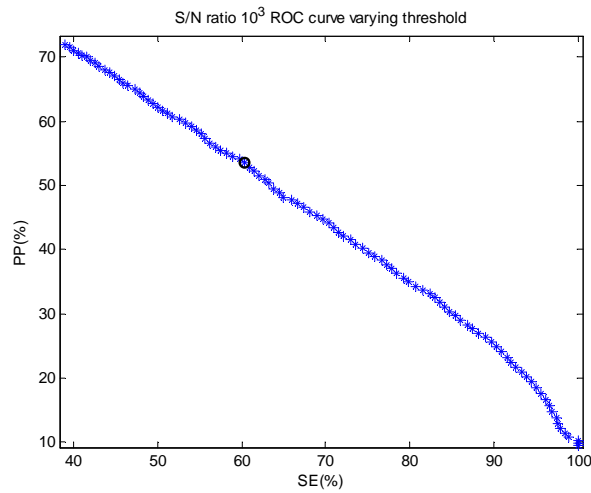


Figure 6-9: ROC curve with S/N ratio equals to 10³.

The best performance is 60.35% and 53.56% for respectively for SE and PP with an amplitude threshold of 12.8 uS. Figure 6-10 compares the previous ROC curves.

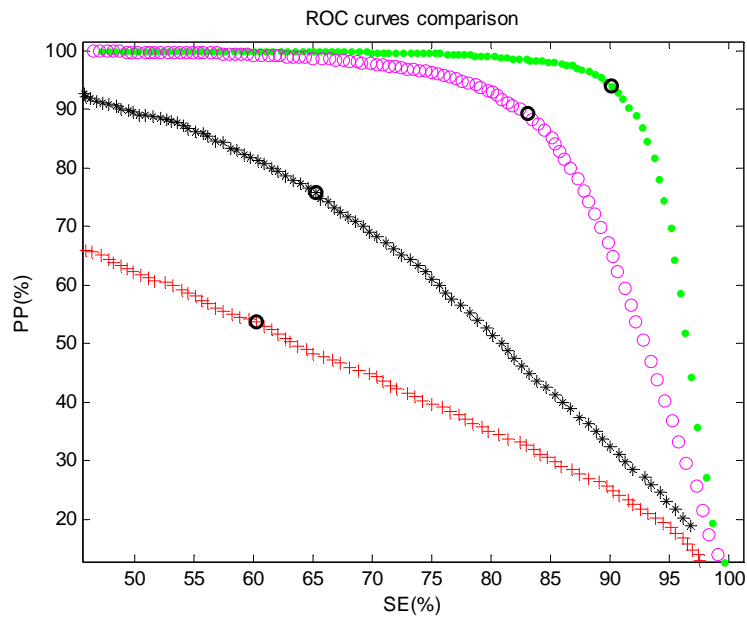


Figure 6-10: Comparison of ROC curves. Starting from the top:

S/N ratio 10⁶ curve (point marks), S/N ratio 10⁵(circles marks), S/N ratio 10⁴(star marks), S/N ratio 10³(plus marks)

Figure 6-10 shows the worsen of performances: the more the S/N level decreases the poorer are the performances drastically passing from 10⁵ to 10⁴. Figure 6-11 reports the best results for each investigated S/N level.

6. Comparison of Methods using simulated data

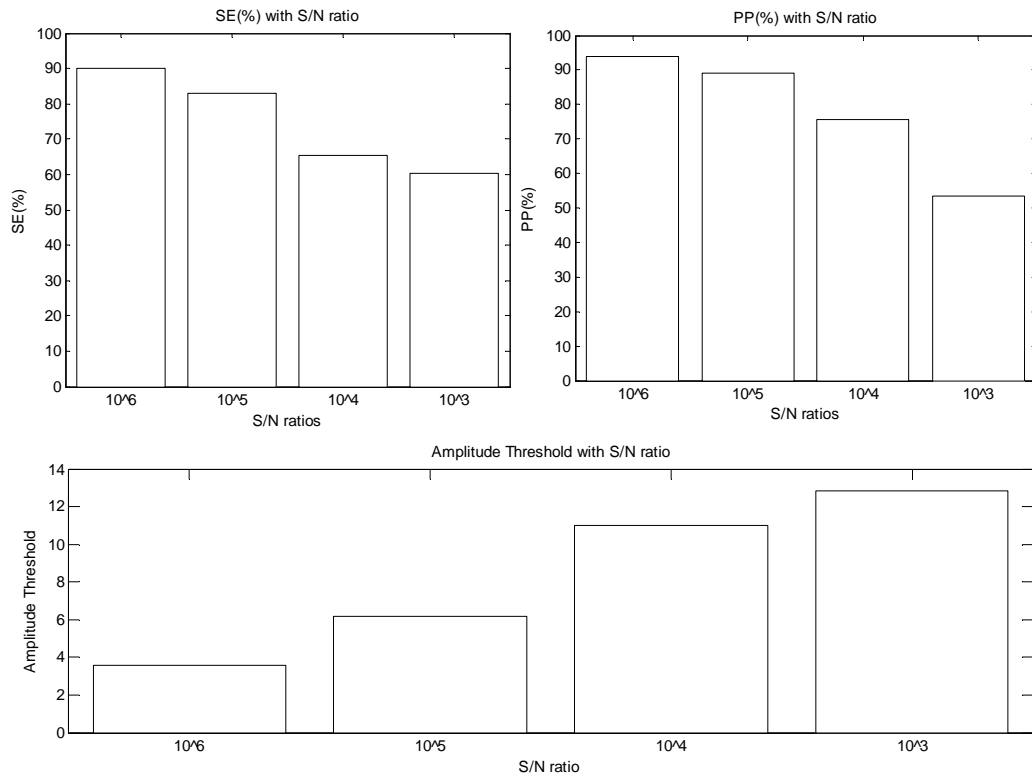


Figure 6-11: SE,PP and Amplitude Threshold comparison

Table 6-2 reports the previous results

SN ratio	10⁶	10⁵	10⁴	10³
SE (%)	90,18	83,07	65,31	60,35
PP (%)	93,93	89,15	75,77	53,56
Thr.(microS)	3,60	6,20	11,00	12,80

Table 6-2: Ledalab Results

6.3 Comparison

In Figure 6-12 the bar plots of the best Ledalab and BC performances based on Table 6-3.

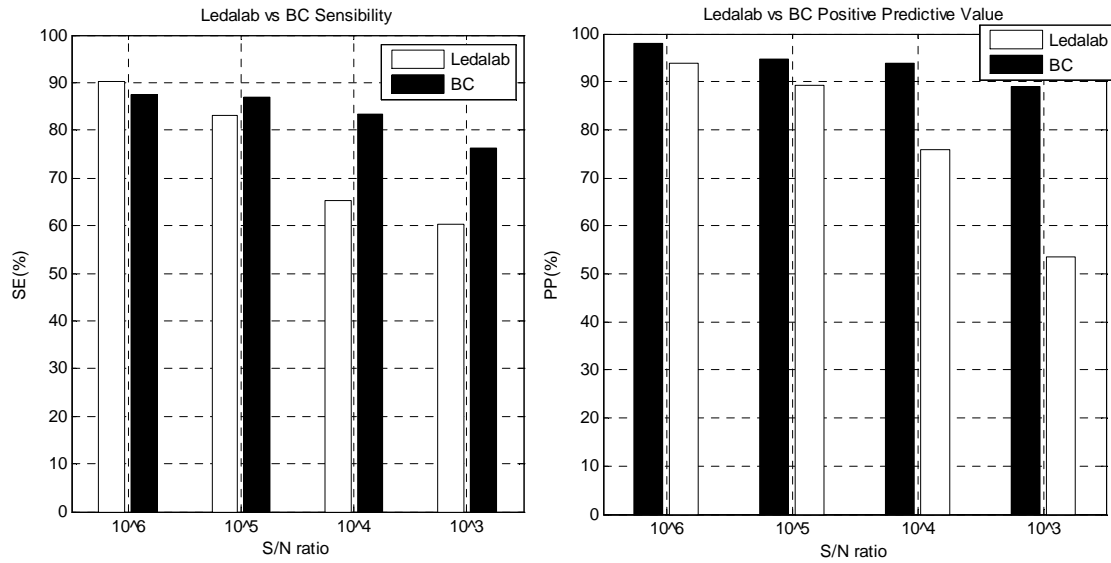


Figure 6-12: Ledalab and BC Sensibility and Positive Predictive Value

SN ratio	LEDALAB				BC algorithm			
	10 ⁶	10 ⁵	10 ⁴	10 ³	10 ⁶	10 ⁵	10 ⁴	10 ³
SE (%)	90,18	83,07	65,31	60,35	87,61	86,84	83,37	76,35
PP (%)	93,93	89,15	75,77	53,56	97,83	94,82	93,85	89,01

Table 6-3: Ledalab and BC performances

The BC algorithm shows better performances (only exception SE for S/N level 10⁶).

7 Experimental Protocol - Emotions

The experimental protocol is inspired by a previous research work (Rainville, et al., 2006) where subjects were asked to recall an autobiographical episode that strongly evoked the target emotions. The same protocol already provided evidence-based results showing different and quite robust cerebral activity patterns (Damasio, et al., 2000). In our study the challenge is managing to distinguish between two base conditions (relax and stress) and four emotional states (rage, fear, happiness, sadness), specific areas of “Valence Arousal” space recording physiological signals, including SC signals.

7.1 Method

7.1.1 Subjects

35 normal subjects were voluntarily recruited from the student body of IULM University of Milan. Students were scheduled to come at the Behavior and Brain Lab for an interview where they had to let the researcher know whether they could recall two recent episodes where they felt each of the 4 target emotions: joy, sadness, rage and fear. If positive, the researchers asked them to recall verbally while a psychologist took notes about all the episodes. After the psychologist chose the most vivid and intense episodes between the two, they were scheduled for a second appointment to participate to the recording session. All the people who could not recall a vivid recent episode for each of the four emotions were asked not to participate in the research.

7.1.2 Device

SC signals were recorded continuously using Flexcomp Infinity™ encoder (Thought Technology Ltd.; Montreal, Canada) with a sampling rate of 2048 Hz, while subjects sitting; then it was resampled at 256 Hz. SC was recorded using two electrodes placed on different fingers of a hand (forefinger and ringfinger) using the exosomatic method.

7.1.3 Recording Session

It was not allowed for the subjects to drink coffee, tea or other stimulating substances on the recording day as well as the day before in order not to alter the sympathetic system. Once subjects came at the lab for the experiment, they were asked to fill in a consent form, and sit down. Then a researcher located all the sensors, and the recording started. After a *baseline* (relax) period of 3

minutes, the psychologist privately with the subject helped him to recall the episode he/she described in the interview while he/she is supposed to listen and focus on the emotion (*listening phase*). The duration of each of those is variable depending on the episode evoked. Once subject felt the emotion, the researcher asked to stay silent and try to focus intensely on the emotion without moving for 3 minutes (*focusing phase*). After the emotion recall, a rest of 3 minutes (*recovery time*) was provided before re-starting with the next emotion. The sequence of emotion recalled was randomly assigned for each subject in order not to bias the results. The recording sessions lasted approximately from 30 to 50 minutes.

In Figure 7-1 an example of SC signal with markers which identify the position of the *focusing phases*(the amplitude identifies the focused emotion: 2: Fear, 3: Happiness, 4: Rage, 5: Sadness. Baseline is identified by 1). The *listening phases* are identified by intervals of zero amplitude preceding the *focusing phases* (obtained by discarding initial 3 minutes – the *recovery time*).

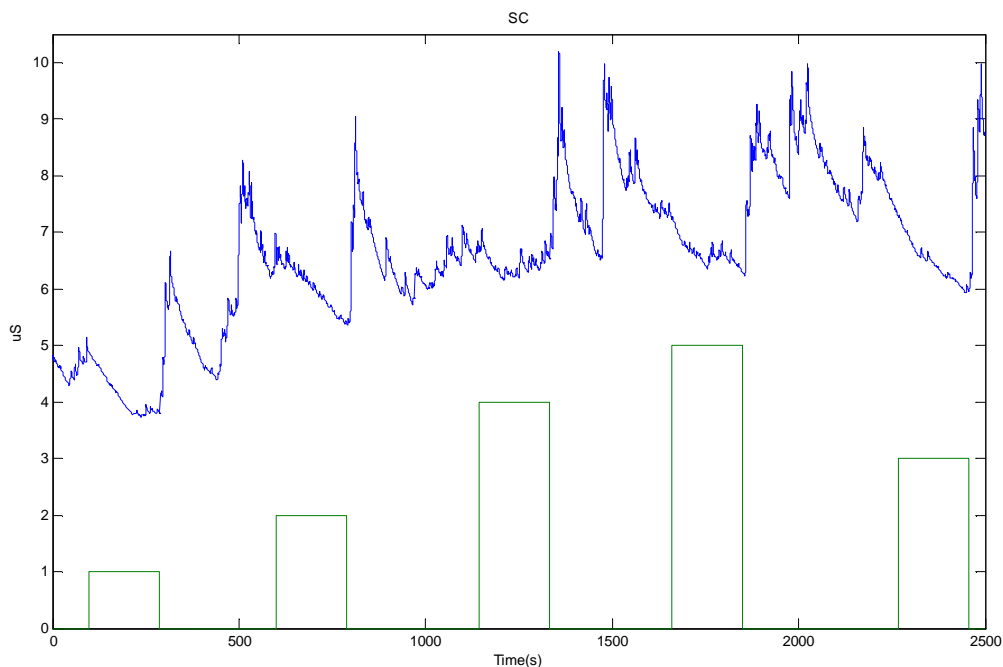


Figure 7-1: Example of SC signal with Markers

7.2 Elaboration

Before applying BC algorithm a normalization on SC signals is needed since it is clear by Figure 7-2 (top) that a wide subject inter variability exists. The normalization consists on detrending and dividing by the maximum variability range (max – min) of the signals to make them comparable. In result of the normalization procedure applied to 4 signals is depicted in Figure 7-2 (bottom).

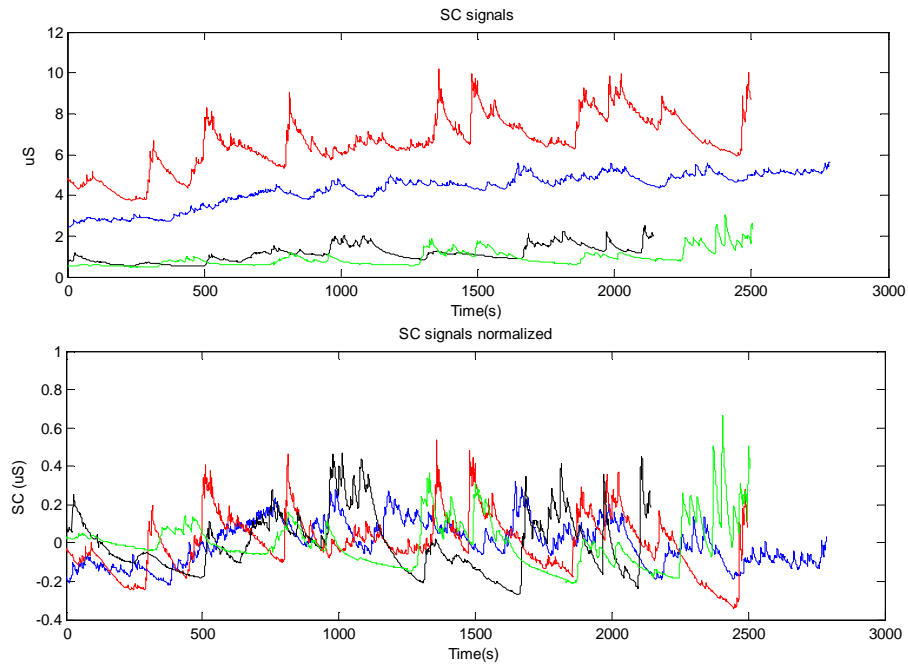


Figure 7-2: An example of BC algorithm output. SC signal with marker signal (top) and spike sequence(bottom)

Then BC algorithm with 0 for B_w and 0.2 for S_w because the S/N ratio was approximately estimated to be higher than 10^5 was run on signals. An example is depicted in Figure 7-3.

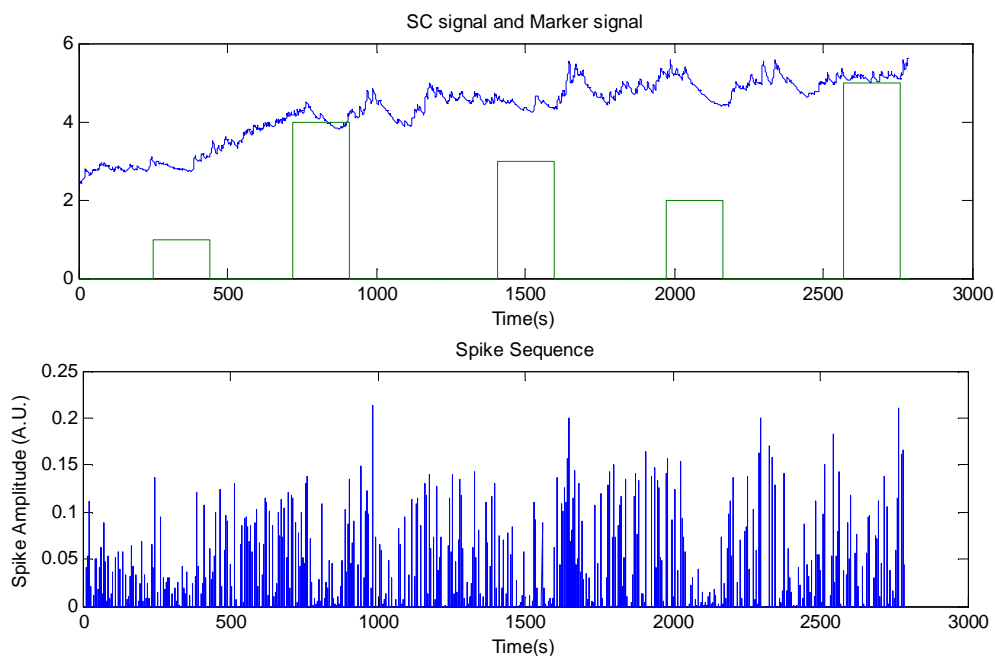


Figure 7-3: Output provided by BC algorithm

On the obtained spikes sequences we calculated the following parameters:

1. **Mean Spike Amplitude (MSA)**: index of the mean sympathetic activity (μS).
2. **Mean Spike Frequency (MSF)**: index of sympathetic activity (Number of spikes / s = Hz). During spontaneous skin conductance changes, augmented wave number and amplitude is interpreted as increased activity in the sympathetic nervous system.
3. **Area under “Integrated Activity Curve (IAC)” curve (AUC)**: AUC is the area underlying IAC. IAC provides a continuous index comprising frequency and amplitude information of spikes and is calculated as follow:

A window (WL, 2 seconds long) slides second by second over the spike sequence summing spike amplitudes within it; the result is strictly correlated to WL. In Figure 7-4 and Figure 7-5 an example of processing with WL=2 s.

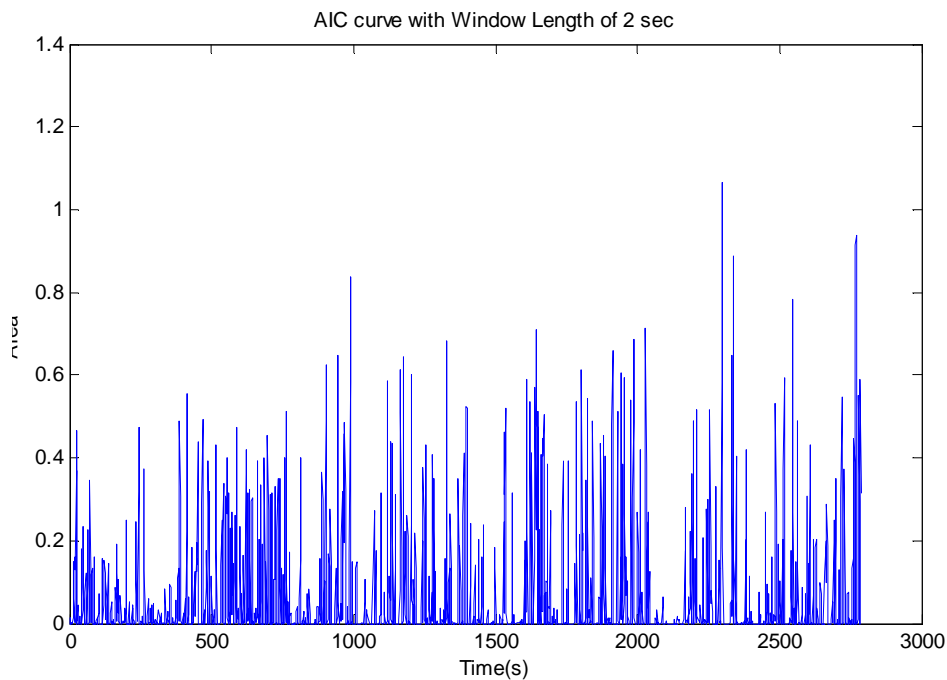


Figure 7-4: Integrated Activity Curve with WL of 2 seconds

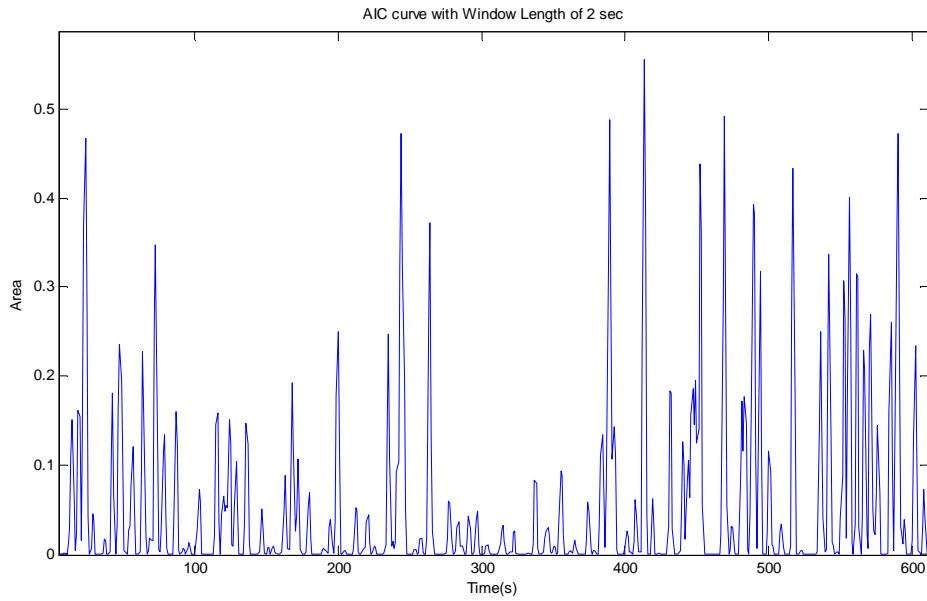


Figure 7-5: Zoom of a part of Figure 7-4

7.2.1 Tests

The 3 parameters were obtained for *listening phases* last minute (*List*), for each of the 3 minutes composing the *focusing phases* (*Foc1*, *Foc2* and *Foc3* respectively) and the central minute of *baseline* (*Bl*). To investigate whether existed statistical differences among phases an ANOVA one-way test was performed.

Moreover t-tests were performed between:

- *Bl* and successive *List*, *Foc1*, *Foc2*, *Foc3* for each emotion
- *List*, *Foc1*, *Foc2*, *Foc3* and each one with itself for the four emotions

Because of multiple t-tests are performed, the significance level was corrected with Bonferroni correction, passing from 0.05 to α calculated according to Equation 7 where in our case parameter n is the number of all considered t-test comparisons, precisely 16 (Baseline versus remaining phases) + $6 * 4 = 40$.

$$\alpha_{\text{Bonf}} = \frac{0.05}{n}$$

Equation 7: Bonferroni Correction

α_{Bonf} is 0.0013 which will be considered as new significant level.

7.3 Result

Figure 7-6, Figure 7-7 and Figure 7-8 depict the box and whisker plot of Mean Spike Amplitude, Mean Spike Frequency and AUC respectively. They show the median, first and fourth quartiles, minimum and maximum values and outliers for each phase of the parameter considered.

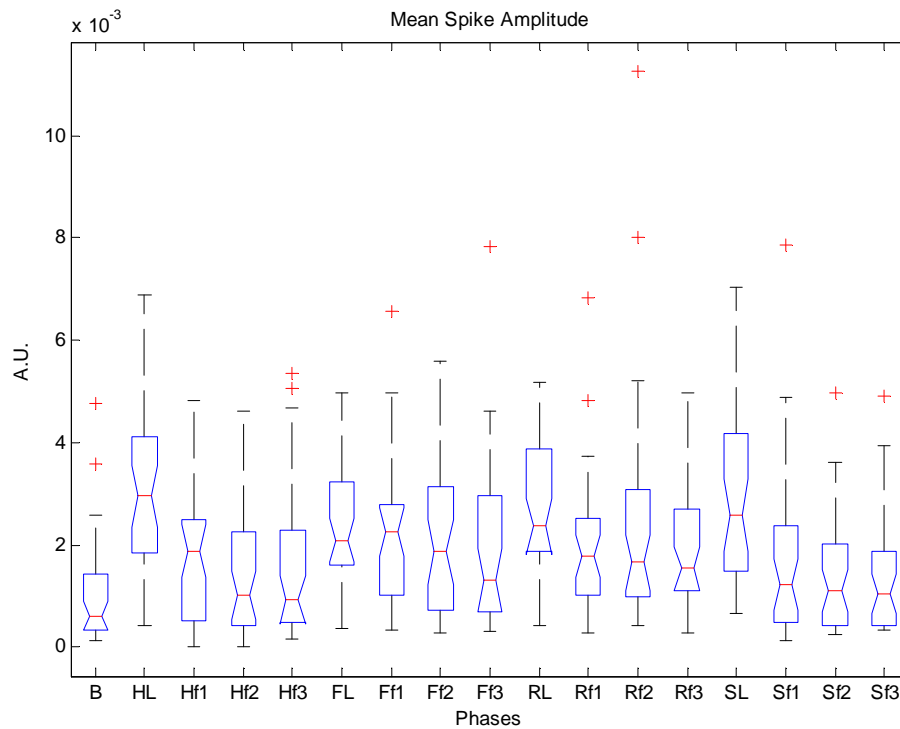


Figure 7-6: Box Plot of Mean Spike Amplitude for each phase where: B stands for Baseline , (H, F, R, S prefixes) indicate emotions, (L, f1,f2,f3) stand for the 4 phases

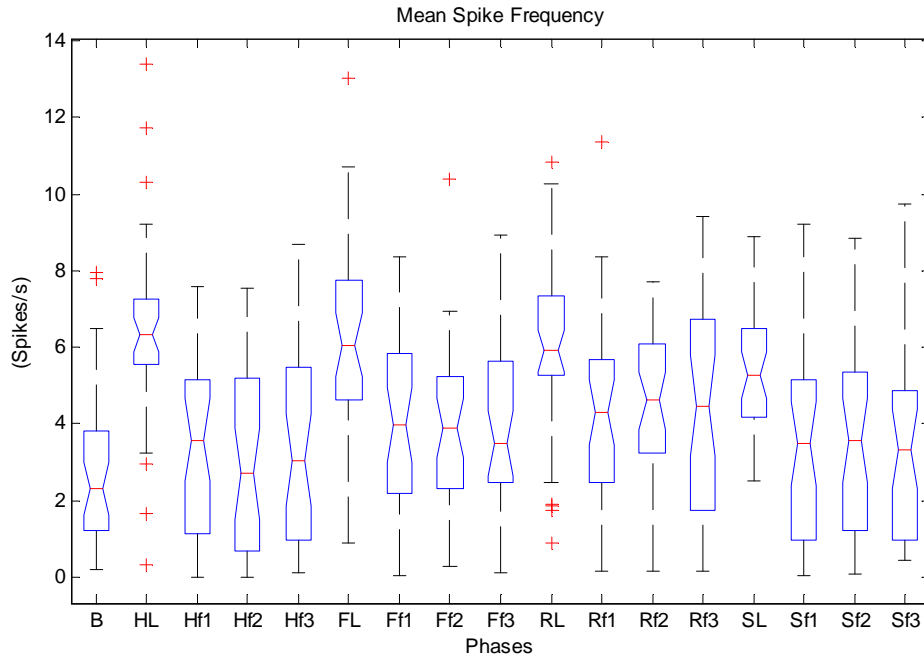


Figure 7-7: Box Plot of Mean Spike Frequency for each phase where: B stands for Baseline , (H, F, R, S prefixes) indicate emotions, (L, f1,f2,f3) stand for the 4 phases

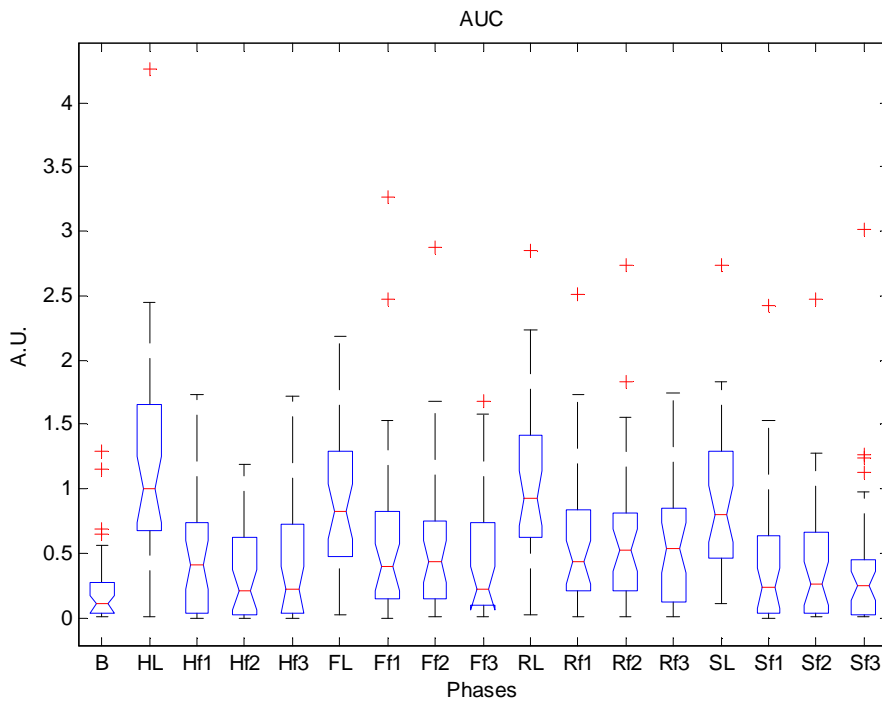


Figure 7-8: Box Plot of AUC for each phase where: B stands for Baseline , (H, F, R, S prefixes) indicate emotions, (L, f1,f2,f3) stand for the 4 phases

Table 7-1 reports ANOVA one-way results and Table 7-2 reports the p-values from the t-test comparing *Bl* with *List*, *Foc1*, *Foc2* and *Foc3*. Moreover the results from ANOVA test are reported in Table 7-2 (bottom) with values of F function, numerator and denominator.

ANOVA	P-Value	F (16,34)
M.S.Ampl.	9,442E-11 ^(*)	5,3916
AUC	2,22E-16 ^(*)	7,568
M. Spike Freq	2,22E-16 ^(*)	7,593

$$\alpha_{\text{Anova}}=0.05^{(*)}$$

Table 7-1: ANOVA results

T-Test	Bas_HappList	Bas_HappFoc1	Bas_HappFoc2	Bas_HappFoc3	Bas_FearList	Bas_FearFoc1	Bas_FearFoc2	Bas_FearFoc3
M.S.Ampl.	1,57*10 ⁻⁸ ^(*)	0,0010 ^(*)	0,0317	0,0036	1,9647*10 ⁻⁷ ^(*)	2,84*10 ⁻⁵ ^(*)	6,12*10 ⁻⁵ ^(*)	0,0019
AUC	1,12*10 ⁻⁷ ^(*)	5.3*10 ⁻⁴ ^(*)	0,0229	0,0044	9,2335*10 ⁻⁸ ^(*)	2,4*10 ⁻⁴ ^(*)	5,6*10 ⁻⁴ ^(*)	8,2*10 ⁻⁴ ^(*)
M Spike Freq	1,42*10 ⁻⁸ ^(*)	0,1020	0,2724	0,1329	2,5032*10 ⁻⁷ ^(*)	9,9*10 ⁻⁴ ^(*)	0,0120	0,0211

T-Test	Bas_RageList	Bas_RageFoc1	Bas_RageFoc2	Bas_RageFoc3	Bas_SadList	Bas_SadFoc1	Bas_SadFoc2	Bas_SadFoc3
M.S.Ampl.	2,34*10 ⁻⁹ ^(*)	8,87*10 ⁻⁶ ^(*)	0,0011 ^(*)	4,6*10 ⁻⁴ ^(*)	2,9387*10 ⁻⁸ ^(*)	0,0164	0,0249	0,0445
AUC	1,38*10 ⁻⁸ ^(*)	2,03*10 ⁻⁶ ^(*)	1,1*10 ⁻⁴ ^(*)	5,97*10 ⁻⁵ ^(*)	5,7321*10 ⁻⁹ ^(*)	0,0118	0,028	0,0875
M Spike Freq	1,47*10 ⁻⁸ ^(*)	9,6*10 ⁻⁴ ^(*)	1,6*10 ⁻⁴ ^(*)	5,6*10 ⁻⁴ ^(*)	8,3476*10 ⁻⁸ ^(*)	0,2111	0,1188	0,1391

$$\alpha_{\text{Bonf}}=0.0013^{(*)}$$

Table 7-2: T-Test results Baseline versus all remaining phases

Table 7-3, Table 7-4, Table 7-5, Table 7-6 report respectively the ANOVA and t-test results comparing *Listening phases (List)* among each other, *Focusing1 phases(Foc1)* among each other, *Focusing2 phases(Foc2)* among each other and *Focusing1 phases(Foc1)* among each others.

T-Test	HappList_FearList	HappList_RageList	HappList_SadList	FearList_RageList	FearList_SadList	RageList_SadList
M.S.Ampl.	0,0256	0,306	0,7444	0,1797	0,0702	0,5272
AUC	0,0551	0,1944	0,0906	0,2805	0,997	0,3366
M Spike Freq	0,571	0,3502	0,0104	0,6313	0,0517	0,074

 $\alpha_{\text{Bonf}}=0.0013^{(*)}$

Table 7-3: T-test results comparing *List phases* among each other

T-Test	HappFoc1_FearFoc1	HappFoc1_RageFoc1	Happfoc1_SadFoc1	FearFoc1_RageFoc1	FearFoc1_SadFoc1	RageFoc1_SadFoc1
M.S.Ampl.	0,382	0,4916	0,4263	0,8434	0,0369	0,0942
AUC	0,2765	0,432	0,4133	0,5469	0,0338	0,0573
M Spike Freq	0,1861	0,0922	0,6754	0,6183	0,0817	0,0242

 $\alpha_{\text{Bonf}}=0.0013^{(*)}$

Table 7-4: T-test results comparing *Foc1 phases* with each other

T-Test	HappFoc2_FearFoc2	HappFoc2_RageFoc2	Happfoc2_SadFoc2	FearFoc2_RageFoc2	FearFoc2_SadFoc2	RageFoc1_SadFoc2
M.S.Ampl.	0,0164	0,0224	0,6415	0,4101	0,0466	0,0324
AUC	0,0347	0,0079	0,4924	0,3211	0,1558	0,0381
M Spike Freq	0,08	0,0001 ^(*)	0,4753	0,1085	0,2985	0,0226

 $\alpha_{\text{Bonf}}=0.0013^{(*)}$

Table 7-5: T-test results comparing *Foc2 phases* with each other

T-Test	HappFoc3_FearFoc3	HappFoc3_RageFoc3	Happfoc3_SadFoc3	FearFoc3_RageFoc3	FearFoc3_SadFoc3	RageFoc3_SadFoc3
M.S.Ampl.	0,3218	0,2315	0,4752	0,9537	0,1109	0,0542
AUC	0,4973	0,1204	0,6656	0,3961	0,3608	0,134
M Spike Freq	0,2236	0,0205	0,9447	0,1485	0,419	0,0494

$\alpha_{\text{Bonf}}=0.0013$ (*)

Table 7-6: ANOVA and t-test results comparing *Foc3* phases among each other

T-Test	Bas_HappList	Bas_HappFoc1	Bas_HappFoc2	Bas_HappFoc3	Bas_FearList	Bas_FearFoc1	Bas_FearFoc2	Bas_FearFoc3
M.S.Ampl.	$1,57*10^{-8(*)}$	$0,0010^{(*)}$	0,0317	0,0036	$1,9647*10^{-7(*)}$	$2,84*10^{-5(*)}$	$6,12*10^{-5(*)}$	0,0019
AUC	$1,12*10^{-7(*)}$	$5,3*10^{-4(*)}$	0,0229	0,0044	$9,2335*10^{-8(*)}$	$2,4*10^{-4(*)}$	$5,6*10^{-4(*)}$	$8,2*10^{-4(*)}$
M Spike Freq	$1,42*10^{-8(*)}$	0,1020	0,2724	0,1329	$2,5032*10^{-7(*)}$	$9,9*10^{-4(*)}$	0,0120	0,0211

T-Test	Bas_RageList	Bas_RageFoc1	Bas_RageFoc2	Bas_RageFoc3	Bas_SadList	Bas_SadFoc1	Bas_SadFoc2	Bas_SadFoc3
M.S.Ampl.	$2,34*10^{-9(*)}$	$8,87*10^{-6(*)}$	$0,0011^{(*)}$	$4,6*10^{-4(*)}$	$2,9387*10^{-8(*)}$	0,0164	0,0249	0,0445
AUC	$1,38*10^{-8(*)}$	$2,03*10^{-6(*)}$	$1,1*10^{-4(*)}$	$5,97*10^{-5(*)}$	$5,7321*10^{-9(*)}$	0,0118	0,028	0,0875
M Spike Freq	$1,47*10^{-8(*)}$	$9,6*10^{-4(*)}$	$1,6*10^{-4(*)}$	$5,6*10^{-4(*)}$	$8,3476*10^{-8(*)}$	0,2111	0,1188	0,1391

$\alpha_{\text{Bonf}}=0.0013$ (*)

Table 7-2 reports significant differences between Baseline and Listening phases for all emotions, so it is demonstrated that the psychologist's goal was successfully reached managing to involve emotionally the subjects; moreover we can observe that Fear, Rage and only partially Happiness activate the subjects for longer time whereas Sadness is not significant for any of Focusing phases. Rage, Fear, Happiness and Sadness, in this order, are listed from the most activating to least activating emotion. Probably the reason involves innate survival instincts since rage and fear, opposed to sadness and happiness are more appropriate to promote subject adaptation to hostile environment so only focusing on memories involving those feelings increase the alertness level facilitating survival mechanisms. Only rage and fear create a more lasting alertness state in the subjects. Sadness tends to be the most short lasting emotion (being significant only Listening phase); the subject behave in this way probably due to psychological mechanisms that aims to avoid painful or stressful memories. Happiness is less activating than rage and fear but more than sadness: it may be that this emotion facilitates socialization being useful for human survival as well.

There are no significant difference between Listening and Focusing phases with themselves.

8 Conclusions

The surrogate SC signals are realistic enough to satisfy the aim of this investigation, making them even more realistic adding noise by setting S/N levels. We did not introduce motion artifacts or external artifacts as well as we did not modeled the spike generation mechanisms regulated by ANS. However, we judged this model enough to our goals.

BC algorithm developed at Boston MIT was proved to be more efficient in analyzing SC signals overtaking the state of the art Ledalab software. We have improved BC algorithm offering a criteria to properly tune it up; before this study S_w and B_w values were fixed and not chosen according to any precise and justified criteria. As demonstrated, to maximize performances the filter governed by B_w must not be applied whereas S_w parameter ranges between 0.1 and 0.9.

From the experimental protocol we obtained important findings highlighting psychological mechanisms in response to emotigenous stimuli, maybe linked to human innate survival instincts. It may be possible to improve the results combining SC signals with other physiological indexes (i.e. respiration or HRV). The reported findings can help to widen and enrich knowledge in psychology field as well as improve affecting computing area whose aim is to shorten distances between human and machines enabling them to perceive, interpret, process and simulate human feelings.

Definitely we tuned up and validated a powerful tool able to reflect sympathetic nervous system activity proposing a novel solution to SCRs overlap problem, faced by most of the most recent algorithms in literature.

References

- Ahlberg, J.H., Nilson, E.N. and Walsh, J.L. 1967.** *The theories of splines and their applications.* s.l. : New York: Academic., 1967.
- Akane, Sano and Picard, R.W.** Taxonomy of autonomic sleep patterns with electrodermal activity. Fellow, IEEE. : 33rd Annual International Conference of the IEEE EMBS. Boston.
- Alexander, D.M., et al. 2005.** *Separating individual skin conductance responses in a short interstimulus-interval paradigm.* 2005.
- Allen, J.A., Armstrong, J.E. and Roddie, I.C. 1973.** The regional distribution of emotional sweating in man. . s.l. : The Journal of Physiology, 235, 749–759., 1973.
- Asahina, M., et al. 2002.** Emotional Sweating response in a patient with bilateral amygdala damage. s.l. : International Journal of Psychophysiology, n°47, pp: 87-93, 2002.
- Benedek, M. and Kaernbach, C. 2010b.** [Online] 2010b. www.ledalab.de.
- . **2010b.** [Online] 2010b. <http://www.ledalab.de/>.
- . **2010a.** *A continuous measure of phasic electrodermal activity.* 2010a.
- Benedek, Mathias and Kaernbach, Christian. 2010.** *Decomposition of skin conductance data by means of nonnegative deconvolution.* s.l. : Psychophysiology, 47, 647–658, 2010.
- Boucsein, Wolfram. 2011.** *Electrodermal Activity.* Germany : Springer, 2011.
- . **1992.** *Electrodermal Activity.* s.l. : Plenum Press, 1992.
- Breault, C. and Ducharme, R. 1993.** *Effect of intertribal intervals on recovery and amplitude of electrodermal reactions.* s.l. : International Journal of Psychophysiology, 1993.
- Brown, C.C. 1967.** A proposed standard nomenclature for psychophysiological measures. s.l. : Psychophysiology, 4, 260–264., 1967.
- Bryant, R.A., et al.** Eye movement and electrodermal responses to threat stimuli in post-traumatic stress disorder. *Int J Psychophysiol* 1995;20(3):209-13.
- Butkevich, Kh. Yu., Spivak, Yu.G. and Semochkin, I.A. 1978.** *Vopr.Psikhol.* 1978.

References

- Damasio, Antonio R., et al. 2000.** *Subcortical and cortical brain activity during the feeling of self-generated emotions.* Department of Neurology (Division of Cognitive Neuroscience) and PET Imaging Center, University of Iowa College of Medicine, 200 Hawkins Drive, Iowa City, Iowa 52242, USA : Nature, 2000.
- Darrow, C.W. 1937.** The equation of the galvanic skin reflex curve: I. The dynamics of reaction in relation to excitation-background. s.l. : Journal of General Psychology, 16, 285–309, 1937.
- Davis, T., Love, B. C., & Maddox, W. T. and Davis. 2009.** *Anticipatory emotions in decision tasks: Covert markers of value or attentional processes?* 2009.
- Dawson, ME, Schell, AM and Filion, DL. 2001.** *The electrodermal system* . Cambridge : Cambridge University Press, 2001.
- Edelberg, R. and Muller, M. 1981.** *Prior activity as a determinant of electrodermal recovery rate.* s.l. : Psychophysiology, 1981.
- Edelberg, R. 1972.** *Electrical activity of the skin: Its measurement and uses in psychophysiology.* New York : Handbook of psychophysiology, 1972.
- . **1971.** *Electrical properties of skin.* 1971.
- . **1967.** *Electrical properties of the skin.* s.l. : Williams & Wilkins, 1967.
- . **1967.** *Electrical properties of the skin.* s.l. : Williams & Wilkins, 1967.
- . **1993.** *Electrodermal mechanisms: A critique of the two-effector hypothesis and a proposed replacement.* London : Progress in electrodermal research (pp. 7–30). London: Plenum., 1993.
- . **1973.** Mechanisms of electrodermal adaptations for locomotion, manipulation, or defense. *Progress in physiological psychology.* s.l. : In E. Stellar & J. M. Sprague (Eds.), 1973.
- Fahrenberg, J. 1988.** Psychophysiological processes. *Handbook of multivariate experimental psychology.* (pp. 867–914). : J. R. Nesselroade & R. B. Cattell, 1988.
- Féré, C. 1888.** Note sur les modifications de la résistance électrique sous l'influence des excitations sensorielles et des emotions. *Comptes Rendus des Séances de la Société de Biologie, n°5, pp: 217-219.* 1888.
- Fletcher, R.P., Venables, P.H. and Mitchell, D.A. 1982.** Estimation of half from quarter recovery time of SCR. s.l. : Psychophysiology, 19, 115–116., 1982.
- Foerster, F. 1984.** *Computerprogramme zur Biosignalanalyse.* Berlin : Springer., 1984.
- Fowles, D.C. 1986.** The eccrine system and electrodermal activity. *Psychophysiology: Systems, processes, and applications.* Amsterdam : s.n., 1986.
- Gladman, G. and Chiswick, M.L. 1990.** *Skin conductance and arousal in the newborn infant.* . s.l. : Arch Dis Child, 1990.
- Graham, FK. 1973.** *Habituation and dishabituation of responses innervated by the autonomic nervous system.* New York : Peeke HVS, Herz MJ, 1973.

References

- Grings, WW and Schell, AM. 1969.** *Magnitude of electrodermal response to a standard stimulus as a function of intensity and proximity of a prior stimulus.* s.l. : J Comp Physiology Psychology, 1969.
- Gutrech, J.A. 1994.** *Sympathetic skin response (review).* New York : Journal of Clinical Neurophysiology - Technique in psychophysiology, 1994.
- Hermann, L. and Luchsinger, B. 1878.** Über die Secretionsströme der Haut bei der Katze . 1878.
- Hermens, D., et al.** Sex differences in adult ADHD: a double dissociation in brain activity and autonomic arousal? *Psychol* 2004;66;221-33 .
- http://courses.washington.edu/bioen327/Labs/Lit_SkinStruct_Bensouillah_Ch01.pdf.** *Skin Structure.*
- Hunt, D.P. 1977.** *A mathematical model of a simple human galvanic skin response upon its rate topography.* s.l. : Bulletin of the Psychonomic Society, 10, 149–151, 1977.
- Hurley, H.J. and Shelley, W.B. 1960.** *The human Apocrine Sweat Gland in Health and Disease.* Springfield : CC Thomas , 1960.
- Ishchenko, A.N. and Shev'ev, P.P. 1989.** *Automated complex for multiparameter analysis of the galvanic skin response signal.* 23 (3): 113-117. : Biomedical Engineering, 1989.
- Janes, CL, et al. 1985.** *The effect of stimulus significance on skin-conductance recovery.* s.l. : Psychophysiology, 1985.
- Jänig, W., Sundlöf, G. and Wallin, B.G. 1983.** Discharge patterns of sympathetic neurons supplying skeletal muscle and skin in man and cat. . *Journal of the Autonomic Nervous System.* 1983.
- Kennedy, W.R., Wendelschafer-Crabb, G. and Brelje, T.C. 1994.** Innervation and vasculature of human sweat glands: an immunohistochemistry-laser scanning confocal fluorescence microscopy study . s.l. : Journal of Neuroscience, 1994.
- Kunimoto, M., et al. 1991.** Neuroeffector characteristics of sweat glands in the human hand activated by regular neural stimuli . s.l. : J Physiol;442:391–411., 1991.
- Kuno, Y. 1956.** Human Perspiration . 1956.
- Ledalab. *Ledalab.* [Online] www.ledalab.de.
- Lidberg, L. and Wallin, B. 1981.** *Sympathetic skin nerve discharges in relation to amplitude of skin resistance responses.* s.l. : Psychophysiology, 1981.
- Lim, C.L., et al. 1997.** *Decomposing skin conductance into tonic and phasic components.* s.l. : International Journal of Psychophysiology, 1997.
- Lim, C.L., et al. 1999.** *Dynamic of SCR, EEG, and ERP activity in an oddball paradigm with short interstimulus intervals.* s.l. : Psychophysiology, 1999.
- Luria, A.R. and Homskaya, E.D. 1970.** Frontal lobe and the regulation of arousal processes. [book auth.] New York: Appleton Century Crofts D. Mostofsky Editions. *Attention: Contemporary theory and research, pp: 303-330.* 1970.

References

- Lykken, David T. 1971.** Direct measurement of skin conductance: a proposal for standardization. 1971.
- Macefield, V.G. and Wallin, B.G. 1996.** The discharge behaviour of single sympathetic neurons supplying human sweat glands. 61:277–86. : J Autonomic Nervous Syst , 1996.
- Millington, P.F. and Wilkinson, R. 1983.** Skin. s.l. : Cambridge: University Press., 1983.
- Nagai, Y., et al. 2004.** Activity in ventromedial prefrontal cortex covaries with sympathetic skin conductance level: A physiological account of a “default mode” of brain function . s.l. : NeuroImage, 22, 243–251., 2004.
- Nasir, H.N. and Bechara, A.** Skin Conductance: A Psychophysiological Approach to the study of Decision Making. *Methods in Mind*. s.l. : Senio C., Russel T., Gazzaniga M.S., The MIT press.
- Neumann, E. and Blanton, R. 1970.** *The early history of electrodermal research*. s.l. : Psychophysiology 6, 453–475, 1970.
- Nicolaidis, S. and Sivadjan. 1972.** High-frequency pulsatile discharge of human sweat glands: myoepithelial mechanism. s.l. : J Appl Physiol 32:86-90,, 1972.
- Nishiyama, T., et al. 2001.** Irregular activation of individual sweat gland in human sole observed by a videomicroscopy. s.l. : Autonomic Neurosci: Basic Clin 2001;88:117–26., 2001.
- Ogawa, Tokuo and Sugeno, Junichi. 1993.** Pulsatile Sweating and Sympathetic Sudomotor Activity. *Japanese Journal of Physiology*. 1993.
- Polo, A., et al. 2000.** Painless fractures and thermoregulation disturbances in sensory-autonomic neuropathy: electrophysiological abnormalities and sural nerve biopsy. *Neuropediatrics* : 31:148-50, 2000.
- Rainville, Pierre, et al. 2006.** *Basic emotions are associated with distinct patterns of cardiorespiratory activity*. Canada : s.n., 2006.
- Rothman, S. 1954.** *Physiology and Biochemistry of the skin*. Chicago : University of Chicago Press, 1954.
- Sato, K. 1977.** The physiology, pharmacology, and biochemistry of the eccrine sweat gland. *Reviews of Physiology, Biochemistry and Pharmacology*. 1977.
- Schiefferdecker, P. 1917.** Die Hautdrüsen des Menschen und des Säugetieres, ihre biologische und rassenanatomische Bedeutung, sowie die musculus sexualis. s.l. : J Invest Dermatol, Biol Zentr 37, 1917.
- Schliack, H. and Schiffter, R. 1979.** Neurophysiologie und Pathophysiologie der Schweißsekretion. In E. Schwarz, H. W. Spier, & G. Stüttgen (Eds.), *Handbuch der Haut und Geschlechtskrankheiten*. Berlin : Springer, 1979.
- Schneider, R. L. 1987.** *A mathematical model of human skin conductance*. s.l. : Psychophysiology, 1987.
- Schoen, S.A., et al. July–September 2008.** Psychophysiology of children with autism spectrum disorder. Volume 2, Issue 3 : Pages 417–429, July–September 2008.
- Shields, S.A., et al. 1987.** Ismediation of sweating cholinergic, adrenergic, or both? A comment on the literature. s.l. : Psychophysiology, 24, 312–319., 1987.

Skin Structure.

Sokolov, E.N. 1960. Neuronal models in the orienting reflex. *The central nervous system and behavior*. s.l. : In M. A. Brazier (Ed.), 1960.

Storm, H., et al. 2000. *The development of a software program for analyzing spontaneous and externally elicited skin conductance changes in infants and adults*. s.l. : Clinical Neurophysiology 111 (2000), 2000.

Tarchanoff, J. 1889. Décharges électriques dans la peau de l'homme sous l'influence de l'excitation des organes des sensés et de différentes formes d'activité psychique. s.l. : Comptes Rendus des Seances de la Société de Biologie, n°41, pp : 447-451, 1889.

Thom, E. 1988. *Die Hamburger EDA-Auswertung. Elektrodermale Aktivität. Grundlagen, Methoden und Anwendungen (pp. 501–514)*. Berlin : Springer, 1988. Appendix in W. Boucsein..

Thomas, P.E. and Korr, I.M. 1957. Relationship between sweat gland activity and electrical resistance of the skin. s.l. : Journal of Applied Physiology, 10, 505–510., 1957.

Tranel, D. and Damasio, H. 1994. Neuroanatomical correlates of electrodermal skin conductance response. *Psychophysiology*, 31, 427–438. 1994.

Venables, P.H. and Christie, M.J. 1980. *Electrodermal activity*. New York: Wiley. : Techniques in psychophysiology, 1980. In I. Martin & P. H. Venables .

—. 1973. Mechanisms, Instrumentation, Recording Techniques and Quantification of Responses. *Electrodermal Activity in Psychological Research*. New York and London : pp: 1-109. Academic Press, 1973.

Wallin, BG. 1981. *Sympathetic nerve activity underlying electrodermal and cardiovascular reactions in man*. s.l. : Psychophysiology , 1981.

Wang, G.H. 1964. The neural control of sweating . University of Washington : s.n., 1964.

Weiner and Hellmann. 1960. The sweat glands. 1960.

Wikipedia. Inverse Gaussian. *Wikipedia.com*. [Online]

Williams, L.M., Brown, K.J. and Das, P., Boucsein, W., Sokolov, E. N., Brammer, M. J., Olivieri, G., Peduto, A., & Gordon, E. 2004. *The dynamics of cortico-amygdala and automatic activity over the experimental time course of fear perception*. s.l. : Brain Research. Cognitive Brain Research, 21, 114–123., 2004.

Williams, L.M., et al. 2000. “The Neural Correlates of Orienting: An Integration of fMRI and Skin Conductance Orienting. s.l. : Brain Imaging, v.11, n°13, pp: 3011-3015 , 2000.

Williams, L.M., et al. 2004. Dysregulation of arousal and amigdala-prefrontal systems in paranoid schizophrenia. 161(3):480-9. : Am J Psychiatry, 2004.

References